



Calhoun: The NPS Institutional Archive
DSpace Repository

Theses and Dissertations

1. Thesis and Dissertation Collection, all items

1969-10

An investigation of a transonic turbine test rig.

Esdaile, Stewart Gary

Monterey, California. U.S. Naval Postgraduate School

<https://hdl.handle.net/10945/12496>

Copyright is reserved by the copyright owner

Downloaded from NPS Archive: Calhoun



Calhoun is the Naval Postgraduate School's public access digital repository for research materials and institutional publications created by the NPS community. Calhoun is named for Professor of Mathematics Guy K. Calhoun, NPS's first appointed -- and published -- scholarly author.

Dudley Knox Library / Naval Postgraduate School
411 Dyer Road / 1 University Circle
Monterey, California USA 93943

<http://www.nps.edu/library>

NPS ARCHIVE
1969
ESDAILE, S.

AN INVESTIGATION OF A TRANSONIC
TURBINE TEST RIG

Stewart Gary Esdaile

United States
Naval Postgraduate School



THESIS

An Investigation of a Transonic

Turbine Test Rig

by

Stewart Gary Esdaile

October 1969

This document has been approved for public release and sale; its distribution is unlimited.

T133763



An Investigation of a Transonic
Turbine Test Rig

by

Stewart Gary Esdaile
Captain, Canadian Armed Forces
B.Eng., Royal Military College, 1964

Submitted in partial fulfillment of the
requirements for the degree of

MASTER OF SCIENCE IN AERONAUTICAL ENGINEERING

from the

NAVAL POSTGRADUATE SCHOOL
October 1969

NPS ARCHIVE
1969
ESDAILE, S.

~~4-11-69~~
ABSTRACT

The Transonic Turbine Test Rig installed in the Turbo-Propulsion Laboratory at the Naval Postgraduate School was designed such that losses in nozzles and rotor blading and overall performance characteristics can be determined for operation at several combinations of blade configurations, pressure ratios and speeds. This study relates the empirical data for stator loss coefficients to those determined for the converging-nozzle stator presently installed, and discusses reasons for some of the discrepancies. Also discussed are results of the flow nozzle calibration, locked rotor data, and temperature and inlet swirl effects. A method is proposed to reduce these effects for future work on the Turbine Test Rig.

TABLE OF CONTENTS

I.	INTRODUCTION -----	13
II.	EQUIPMENT MODIFICATIONS -----	15
III.	FLOW RATE DETERMINATION -----	17
	A. Nozzle Calibration -----	17
	B. Turbine Flow Rate -----	18
IV.	ANALYSIS AND DATA REDUCTION -----	19
	A. General -----	19
	B. Description of Method 1 -----	22
	C. Description of Method 2 -----	24
V.	NATURE OF PROBLEM -----	27
VI.	DESCRIPTION OF TESTS -----	30
VII.	RESULTS AND ANALYSIS OF TESTS -----	34
VIII.	CONCLUSIONS AND RECOMMENDATIONS -----	44
APPENDIX A	Prediction of Stator Discharge Angle and Stator Loss Coefficient -----	79
APPENDIX B	Prediction of Torque on Closure Plate and Shroud -----	88
APPENDIX C	Prediction of Stator Discharge Pressure Distribution -----	90
APPENDIX D	Computer Output (Run 15) -----	95
	Computer Program FLOCAL -----	106
	Computer Program TTTR -----	109

LIST OF TABLES

I.	PREDICTED AND EXPERIMENTAL VALUES OF STATOR LOSS COEFFICIENT -----	27
II.	SUMMARY OF RUNS -----	31
III.	PREDICTION OF STATOR DISCHARGE ANGLE -----	82
IV.	LOSS COEFFICIENT BY METHOD OF AINLEY -----	83
V.	LOSS COEFFICIENT BY METHOD OF TRAUPEL -----	85
VI.	LOSS COEFFICIENT BY METHOD OF SODERBERG -----	87

LIST OF FIGURES

Figure	Page
1. Piping Installation, Transonic Turbine Test Rig -----	48
2. Transonic Turbine Test Rig -----	49
3. Turbine Blading Arrangement -----	50
4. Floating Stator Assembly -----	51
5. Stator Torque Capsule Support Assembly -----	52
6. Turbine and Shroud Details -----	53
7. Mean Radius Blade Profile, Converging Nozzles -----	54
8. Mean Radius Blade Profile, Circular Arc, Sharp Leading Edge Rotor -----	55
9. Honeycomb Flow Straightener -----	56
10. Stator Roller Bearing Supports -----	57
11. Nozzle Calibration Coefficient -----	58
12. Thermodynamic Process for an Axial Turbomachine -----	59
13. Velocity Diagram of a Turbine Stage -----	60
14. Total-Static Turbine Efficiency -----	61
15. Referred Stator Axial Force versus Referred RPM -----	62
16. Referred Stator Torque versus Referred RPM -----	63
17. Referred Stator Torque versus Stator Pressure Ratio -----	64
18. Flow Function versus Stator Pressure Ratio -----	65
19. Referred Velocities versus Stator Pressure Ratio -----	66
20. Stator Loss Coefficient versus Stator Pressure Ratio -----	67
21. Referred Axial Force versus Stator Pressure Ratio with Locked Rotor -----	68
22. Referred Stator Torque versus Stator Pressure Ratio with Locked Rotor -----	69
23. Referred Flow Rate versus Stator Pressure Ratio with Locked Rotor -----	70

24.	Flow Function versus Stator Pressure Ratio with Locked Rotor -----	71
25.	Stator Pressure Ratio versus Overall Pressure Ratio with Locked Rotor -----	72
26.	Referred Velocities versus Stator Pressure Ratio with Locked Rotor -----	73
27.	Stator Loss Coefficient versus Stator Pressure Ratio with Locked Rotor -----	74
28.	Temperature Increase of Capsule Support versus Referred Flow Rate with Honeycomb Installed -----	75
29.	Predicted Error in Stator Torque due to Temperature Effect on Capsule Support -----	76
30.	Referred Stator Torque versus Stator Pressure Ratio with Honeycomb Installed -----	77
31.	Flow Exit Angle From Honeycomb versus Referred Flow Rate -----	78
32.	Predicted Velocity Profiles at Stator Discharge -----	93

TABLE OF SYMBOLS

Latin

A	Cross-sectional area (in^2)
a	Speed of sound (ft/sec)
b	Blade width (in)
C	Conversion factor, $2g_c J C_p$ ($\text{ft}^2/\text{sec}^2 \text{ } ^\circ\text{R}$)
C_n	Nozzle discharge coefficient
C_p	Specific heat at constant pressure (Btu/lbm. $^\circ\text{R}$)
d	Throat diameter (in)
F	Force (lbf)
g_c	Gravitational constant ($32.174 \text{ lbm-ft/lbf-sec}^2$)
h	Blade height (in)
h_w	Differential pressure across flow nozzle (in H_2O)
J	Joules constant ($778.16 \text{ ft-lbf/Btu}$)
K_t	Area reduction factor
K_{is}	Isentropic head coefficient (dimensionless)
M	Mach number (dimensionless)
M	Moment (ft-lbf)
N	Rotational speed (rpm)
P_T	Total pressure (psia)
P	Static pressure (psia)
R_g	Gas constant (ft-lbf/lbm- $^\circ\text{R}$)
Re	Reynolds Number (dimensionless)
R_m	Mean radius (in)
r	Radius (in)
s	Distance between blades (in)

T_T	Total temperature ($^{\circ}R$)
T	Static temperature ($^{\circ}R$)
t	Trailing edge thickness of blade (in)
U	Peripheral velocity (ft/sec)
V	Absolute velocity (ft/sec)
W	Relative velocity (ft/sec)
\dot{w}	Flow rate (lbm/sec)
Z	Number of blades

Greek

α	Absolute flow angle (degrees)
β	Relative flow angle (degrees)
γ	Ratio of specific heats (dimensionless)
ϵ	Correction factor for pressure distribution
ζ	Loss coefficient (dimensionless)
η	Efficiency (dimensionless)
ξ	Area restriction factor (dimensionless)
ϕ	Flow function (dimensionless)
ω	Angular velocity (radians/sec)

Subscripts

a	Axial direction
av	Average
ax	Annulus exit area
C	Continuity analysis
h	Hub
is	Isentropic
m	Mean streamline

M Momentum analysis
n Flow nozzle properties
ref Referred value
s Stator
t Tip
T Turbine
th Throat
u Peripheral or tangential direction
o Stator entrance properties
1 Stator discharge properties
2 Rotor discharge properties

I. INTRODUCTION

Much of the design and analysis of modern turbines is based on the experience of the designer and his use of empirical data available in the literature. As a result, many investigations of test turbines are being carried out in an effort to more fully explain and mathematically model the flow phenomena in stationary and rotating channels. Present methods for design of axial flow machines base calculations on a reference diameter, usually taken as the mean of the hub and tip. A major simplification is then made by assuming that at any point in a cross-section, such parameters as total pressure and temperature and axial velocity have the same values as at the reference diameter. The overall characteristics of a stage are then determined, but depend on how accurately flow discharge angles and loss coefficients are known. Thus, it is extremely important to be able to predict these values as functions of blade geometry, Mach number and certain other flow parameters. Such a method as just described is conventionally known as a "One-Dimensional Analysis".

The Transonic Turbine Test Rig (TTTR) located at the Turbopropulsion Laboratory is a particularly desirable test machine because it permits evaluation of performance at many combinations of operating conditions and configurations. One of the most important features of the TTTR is that it enables one to evaluate flow angles and loss coefficients using momentum and moment of momentum equations, without making extensive flow surveys which cause an upset of the true flow conditions. The empirical methods available for prediction of flow angles and loss coefficients yield results varying from unreasonably

low values to one so conservative it would be unlikely the machine would operate. Results from previous runs on the TTTR showed the latter trend in loss coefficients, although the TTTR had a reasonable overall performance.

This thesis investigates the methods by which the loss coefficients are determined for the TTTR and relates these coefficients to those predicted by the literature. It then describes the investigation carried out to explain the apparent discrepancies, and examines the effect of some of the more important parameters used to evaluate the loss coefficient.

The author would like to express his appreciation for the competent assistance provided by Mr. Jim Hammer and members of the Turbo-propulsion Laboratory. Special thanks are extended to Dr. M. H. Vavra for his guidance and advice during the investigation.

II. EQUIPMENT MODIFICATIONS

The TTTR instrumentation has been described extensively by Commons [Ref. 4] and Lenzini [Ref. 6]. Discussion here will be limited to recent modifications made to the TTTR.

Fig. 1 shows the piping and valve location in the Turbine test cell. Fig. 2 shows a cross-section of the floating stator and support assembly, while Fig. 3 shows a more detailed cross-section of the stator plenum and hub area. The closure plate assembly shown in Fig. 3 was instrumented with additional strain gauges on the flexures, and the back face towards the rotor had three static pressure taps installed at known radii. Results of these pressure readings and closure plate torque calibration are discussed later.

Fig. 4 shows the floating stator assembly with the locations of the axial force and torque capsule supports and Fig. 5 shows a more detailed view of the torque capsule support assembly. The capsule support assembly was moved from the previous location between the overhead support and plenum casing to its position at the upstream end of the stator in an attempt to reduce both the temperature effect on the capsule and the errors induced by differential thermal expansion.

Fig. 6 shows the stator exit and shroud area. Two additional pressure taps, P13 and P14 were installed, with the hope of correlating the stator discharge tip pressure to the shroud pressure at the same plane. In addition, the machine was completely dismantled and cleaned, and new pressure lines were installed in many cases. The pressure lines were connected to a mercury manometer board in a

logical sequence, extending from the nozzle to the plenum assembly and along the shroud to the rotor discharge, so that the pressure distribution through the machine could be readily observed.

Fig. 7 shows the converging nozzles presently installed in the TTR and Fig. 8 shows the circular-arc, sharp leading-edge rotor used.

III. FLOW RATE DETERMINATION

A. NOZZLE CALIBRATION

Previous nozzle calibration techniques have been described by Naviaux¹ and Lenzini [Ref. 6]. It was shown that the nozzle coefficient was a function of nozzle Reynolds number. However, former results for nozzle coefficients were determined as a function of the Reynolds number based on the conditions of the ASME standard calibrating orifice, rather than on the flow nozzle. As a result, it was decided to repeat the nozzle calibration to obtain a new relationship, and to determine if any deterioration of the nozzle had taken place.

The program for the data reduction is given in Appendix D, program FLOCAL. The method used is similar to that given by Williams², which was found to be more suitable for computer computations. The basic equation is given in the ASME Power Test Code³ and values of the constants are taken from Stearns.⁴ Tests were carried out at nozzle supply pressures of 26, 29, 34 and 39 psia over a range of Reynolds numbers from 2×10^5 to 12×10^5 . Fig. 11 shows the results of these

¹Naviaux, J. C., "Transonic Turbine Test Rig Exhauster System Tests and Tests of a Reaction Turbine, "Naval Postgraduate School Thesis, December, 1966.

²Williams, D. D., "Determination of Performance Parameters of a Dual-Discharge Radial Turbine, "Naval Postgraduate School Thesis, December, 1968.

³Flow Measurement, Chapt. 4, Part 5, Supplement to ASME Power Test Codes, ASME, New York, N. Y., 1959, p. 57ff.

⁴Stearns, R. F., et al., Flow Measurement With Orifice Meters. New York: D. van Norstrand Company, 1951. pg. 65-212.

tests, with nozzle coefficient plotted as a function of Reynolds number. The curve differs from that given by Lenzini [Ref. 6], being higher by 2 to 3 percent. The curve also shows a maximum coefficient occurring at a Reynolds number of 6×10^5 and then decreasing as Reynolds number is increased. It is suspected that this increasing trend of nozzle coefficient each time a calibration is performed indicates some deterioration of the nozzle.

An analytical curve for the nozzle coefficient was obtained by using a least-squares polynomial curve fit. A fourth-order polynomial was chosen as the best fit to the data, namely:

$$C_n = 9.5208828 \times 10^{-1} + 4.4891640 \times 10^{-7} \text{ Re} - 7.5810743 \times 10^{-13} \text{ Re}^2 + 5.5023778 \times 10^{-19} \text{ Re}^3 - 1.4571314 \times 10^{-25} \text{ Re}^4$$

The maximum error between the analytical curve and the actual data points for a range of Reynolds numbers between 4×10^5 and 12×10^5 is 0.2 percent.

B. TURBINE FLOW RATE

The program to obtain the turbine flow rate is given in subroutine FLORAT of program TTTR, and employs a procedure similar to that described in section A. The labyrinth leak rate uses a formula determined by Lenzini [Ref. 6] which is a function of plenum pressure ratio and temperature. The labyrinth leak rate was found to be only 2 percent of the total flow rate. The recalibration of the nozzle and improved flow rate determination resulted in referred turbine flow rates which were 3 percent higher than those previously used.

IV. ANALYSIS AND DATA REDUCTION

A. GENERAL

The basic equations for a one-dimensional flow analysis of the TTTR are well known and have been described in detail by Commons [Ref. 4], Lenzini [Ref. 6] and Messegee [Ref. 7]. The reference diameter referred to previously is twice the mean radius:

$$R_m = \frac{R_{\text{hub}} + R_{\text{tip}}}{2}$$

The data for the TTTR are reduced by program TTTR given in Appendix D, which also gives the results of Run 15. Fig. 12 shows the thermodynamic process for an axial turbomachine and the stator loss coefficient is designated ζ_s . Fig. 13 shows the associated velocity diagram for a turbine stage.

It is of interest here to summarize the assumptions made in using the one-dimensional analysis, as they will have a large bearing on the accuracy of the results. These assumptions are:

1. Adiabatic, steady flow, so that the absolute and relative enthalpies are constant respectively along any streamline.
2. Cylindrical stream surfaces, so there is no bending of the stream surface, or radial component of velocity.
3. Uniform conditions ahead of the stator so there is no total pressure or total temperature gradient in the radial direction.
4. Completely radial flow into the plenum, and axial flow into the stator with no tangential velocity component.
5. Shear stresses are negligible on the annulus and shroud, and symmetrical wakes occur at the trailing edges of the blades.

The validity of these assumptions will be discussed later and where invalid assumptions were found to exist their influence on the loss coefficient will be discussed.

When analysing the reduced data, nearly all variables were plotted as functions of the stator discharge pressure ratio P_{T0}/P_1 . The following discussion will show why P_{T0}/P_1 is an important parameter. From the equation of momentum

$$M = \frac{\dot{w}_T}{g_c} RV_u$$

and using

$$\phi = \frac{\dot{w}_T \sqrt{R_g/g_c T_{T0}}}{P_{T0} A_{ths}} = \left(\frac{P_1}{P_{T0}} \right)^{\frac{1}{n}} \sqrt{\frac{2\gamma}{\gamma-1} \left[1 - \left(\frac{P_1}{P_{T0}} \right)^{\frac{n-1}{n}} \right]}$$

where

$$n = \frac{\gamma}{1 + \zeta_\rho (\gamma - 1)}$$

and

$$\zeta_\rho = \frac{P_{T0} - P_{T1}}{P_{T0} - P_1}$$

hence

$$\phi = f_1 \left(\frac{P_{T0}}{P_1}, n, \gamma \right)$$

Thus

$$M = \frac{P_{T0} A_{ths} \phi}{g_c \sqrt{R_g/g_c T_{T0}}} RV_u$$

or

$$\frac{M}{P_{T0}} = M_{ref} = \frac{V_u}{\sqrt{T_{T0}}} f_1 \left(\frac{P_{T0}}{P_1}, n, \gamma \right)$$

Now

$$V_u^2 = V^2 \sin^2 \alpha = C (T_{T0} - T_1) \sin^2 \alpha$$

or

$$V_u^2 = C T_{T0} \left[1 - \left(\frac{P_1}{P_{T0}} \right)^{\frac{n-1}{n}} \right] \sin^2 \alpha$$

and

$$\frac{V_u}{\sqrt{T_{T0}}} = \sqrt{C} \left[1 - \left(\frac{P_1}{P_{T0}} \right)^{\frac{n-1}{n}} \right]^{\frac{1}{2}} \sin \alpha = f_2 \left(\frac{P_{T0}}{P_1}, n, \gamma \right)$$

Hence

$$M_{ref} = f_3 \left(\frac{P_{T0}}{P_1}, n, \gamma, \alpha \right)$$

For an ideal gas γ is constant, and for small pressure ratios n is nearly a constant. Thus, if it is assumed that the stator discharge angle is constant:

$$M_{ref} = f_4 \left(\frac{P_{T0}}{P_1} \right)$$

and

$$\phi = f_1 \left(\frac{P_{T0}}{P_1} \right)$$

and

$$\frac{V_u}{\sqrt{T_{T0}}} = f_2 \left(\frac{P_{T0}}{P_1} \right)$$

Using the loss coefficient as defined by Vavra [Ref. 8]:

$$\begin{aligned} \zeta_s &= 1 - \phi^2 = 1 - \left(\frac{V_1}{V_{lis}} \right)^2 = \frac{T_1 - T_{lis}}{T_{T0} - T_{lis}} = \frac{T_1/T_{T0} - T_{lis}/T_{T0}}{1 - T_{lis}/T_{T0}} \\ &= \frac{\left(\frac{P_1}{P_{T0}} \right)^{\frac{n-1}{n}} - \left(\frac{P_1}{P_{T0}} \right)^{\frac{\gamma-1}{\gamma}}}{1 - \left(\frac{P_1}{P_{T0}} \right)^{\frac{\gamma-1}{\gamma}}} = f_s \left(\frac{P_{T0}}{P_1}, n, \gamma \right) \end{aligned}$$

And, consistent with the above assumptions for n and γ ,

$$\zeta_s = f_5 \left(\frac{P_{T0}}{P_1} \right)$$

B. DESCRIPTION OF METHOD 1

It is possible to solve for the stator discharge properties by satisfying continuity at the throat plane and the exit plane, provided certain parameters are accurately known and some assumptions are made.

At the exit plane, from continuity:

$$\dot{w}_T = \rho_1 V_{a1} A_1$$

From the perfect gas relationship

$$\rho_1 = \frac{P_1}{R_g T_1}$$

Thus

$$V_{a1} = \frac{\dot{w}_T R_g T_1}{P_1 A_1} \quad (1)$$

However T_1 is not known until V_1 is determined. If one assumes that the same pressure and temperature acting at the exit also exist across the throat plane, then continuity may be applied at the throat:

$$\dot{w}_T = \rho_1 V_1 A_{ths}$$

Then using

$$\rho_1 = \frac{P_1}{R_g T_1} \quad \text{and} \quad T_1 = T_{T0} - \frac{V_1^2}{C}$$

$$V_1 = \frac{\dot{w}_T}{P_1 A_{ths}} = \frac{\dot{w}_T R_g T_1}{P_1 A_{ths}} = \frac{\dot{w}_T R_g}{P_1 A_{ths}} \left(T_{T0} - \frac{V_1^2}{C} \right)$$

or

$$V_1^2 + \frac{C P_1 A_{ths}}{\dot{w}_T R_g} V_1 = \frac{\dot{w}_T R_g}{P_1 A_{ths}} T_{T0}$$

Let

$$C_2 = \frac{C P_1 A_{ths}}{\dot{w}_T R_g}$$

Thus

$$V_1^2 + C_2 V_1 = C T_{T0}$$

And completing the square:

$$V_1^2 + C_2 V_1 + \left(\frac{C_2}{2}\right)^2 = \left(V_1 + \frac{C_2}{2}\right)^2 = C T_{T0} + \left(\frac{C_2}{2}\right)^2$$

Hence

$$V_1 = \sqrt{C T_{T0} + \left(\frac{C_2}{2}\right)^2} - \left(\frac{C_2}{2}\right) \quad (2)$$

and

$$T_1 = T_{T0} - \frac{V_1^2}{C} \quad (3)$$

Once V_{al} is determined from (1),

$$\alpha_1 = \cos^{-1}\left(\frac{V_{al}}{V_1}\right) = \cos^{-1}\left(\frac{A_{ths}}{A_1}\right) \quad \text{and} \quad V_{ul} = V_1 \sin \alpha_1$$

and all quantities are available to determine ζ_s .

It is important to examine in detail the assumptions made in arriving at ζ_s by continuity only, which are:

1. The same pressure P_1 and temperature T_1 exist at the throat and exit plane.
2. There is no change of V_1 from the throat to the exit plane.
3. The correct pressure distribution for P_1 is accurately known.
4. The areas A_{ths} and A_1 are known exactly.
5. There is one-dimensional or uniform flow at both the throat and exit plane, which implies no boundary layer restriction.

In the data reduction, P_1 was taken as the mean of the measured hub and tip pressures, and A_1 was the annulus exit area reduced by a factor K_t to account for the trailing edge thickness.

C. DESCRIPTION OF METHOD 2.

In this method both continuity and momentum are applied, where the tangential velocity is determined from the momentum equation, while the axial velocity is determined from knowledge of the axial forces acting on the stator and by applying continuity at the stator exit. From angular momentum:

$$V_{ul} = \frac{M g_c}{\dot{w}_T R_{ml}} \quad (4)$$

At the stator exit plane, a parabolic pressure distribution is assumed to exist, which is expressed by equation 12 of Lenzini [Ref. 6] and is repeated here:

$$P_{lav} = \frac{P_{hub}}{3} \left[\frac{(1 + \epsilon) R_{tip}^2 + R_{tip} R_{hub} - (2 + \epsilon) R_{hub}^2}{(R_{tip}^2 - R_{hub}^2)} \right] + \frac{P_{tip}}{3} \left[\frac{(2 + \epsilon) R_{tip}^2 - R_{tip} R_{hub} - (1 + \epsilon) R_{hub}^2}{(R_{tip}^2 - R_{hub}^2)} \right] \quad (5)$$

The value of ϵ determines the shape of the parabola. A value for ϵ is first assumed and with this first approximation for P_{lav} , the force balance equation may be solved for V_{al} ,

$$V_{alM} = \frac{g_c}{\dot{w}_T} \left(R - P_{lav} A_{axs} \right) \quad (6)$$

where R = the algebraic sum of the measured forces and the pressure forces acting on the stator. Thus V_{alM} is a direct function of the value of ϵ , or the shape of the pressure distribution. Continuity is then written for the exit plane as in Method 1, employing the perfect

gas relations, to obtain:

$$V_{alC} = \frac{\dot{w}_T R_g}{P_1 A_1} \left(T_{T0} - \frac{V_1^2}{C} \right) = \frac{\dot{w}_T R_g}{P_1 A_1} \left[T_{T0} - \frac{1}{C} \left(V_{alC}^2 + V_{ul}^2 \right) \right]$$

Let

$$C_1 = \frac{\dot{w}_T R_g}{P_1 A_1}$$

Then

$$V_{alC} = C_1 T_{T0} - \frac{C_1}{C} V_{alC}^2 - \frac{C_1}{C} V_{ul}^2$$

or

$$V_{alC}^2 + \frac{C}{C_1} V_{alC} = C T_{T0} - V_{ul}^2$$

and completing the square:

$$V_{alC}^2 + \frac{C}{C_1} V_{alC} + \left(\frac{C}{2C_1} \right)^2 = \left(V_{alC} + \frac{C}{2C_1} \right)^2 = C T_{T0} - V_{ul}^2 + \left(\frac{C}{2C_1} \right)^2$$

or

$$V_{alC} = \sqrt{C T_{T0} - V_{ul}^2 + \left(\frac{C}{2C_1} \right)^2} - \left(\frac{C}{2C_1} \right) \quad (7)$$

Equations (6) and (7) are compared and the value of ϵ is changed appropriately until the two methods produce the same value of V_{al} . In summary then, the steps are:

1. Assume an initial value of ϵ and determine P_{lav} from equation (5).
2. Solve for V_{ul} from equation (4).
3. Solve for V_{alM} from equation (6).
4. Solve for V_{alC} from equation (7).
5. Compare the two values of V_{al} and vary ϵ until the two values of V_{al} become equal.
6. Compute ζ_s .

The assumptions made using this method are as follows:

1. The stator torque can be measured accurately, yielding a correct value of V_{ul} .
2. The correct pressure distribution for P_1 is known accurately, or conversely the iterated value of ϵ will yield the correct pressure distribution.
3. The correct axial force is being recorded.
4. The area A_1 is known exactly.
5. There is one-dimensional or uniform flow in the nozzles, so, no boundary layer correction factor is required.

As in Method 1, the area A_1 was reduced by the same factor K_t to account for the effect of trailing edge thickness.

If the assumptions for both methods are met, then either method should result in essentially the same values for V_{al} , V_{ul} , α , and ζ_s , respectively.

V. NATURE OF PROBLEM

A survey of previous results has shown that ζ_s has ranged from negative values to as high as 0.30. The result of this has produced stator or rotor efficiencies of over one-hundred percent, but the overall machine had a total-static efficiency in the order of eighty percent at the design point. The conclusion reached was that the determination of overall performance was correct, but that some error existed, either in the theory of calculating stator loss coefficients or in measuring the properties necessary to arrive at the loss coefficient.

Appendix A presents several methods by which the stator discharge angle and stator loss coefficients may be predicted. In addition, a curve fit of data is given by Vavra [Ref. 8]. A summary of these values and some representative ones from previous work by Lenzini [Ref. 6] are presented in Table I below.

TABLE I
Predicted and Experimental Values of ζ_s

	Source	ζ_s
Predicted Values	Ainley	0.0756
	Traupel	0.1545
	Soderberg	0.1022
	Vavra	0.1400
Experimental	Lenzini	-0.0100 to 0.3000

Since previous work by Lenzini [Ref. 6] indicated that the overall total-static turbine efficiency was about eighty percent, it was concluded that many of the above values were too high, and that an average value for the loss coefficient ζ_s of 0.08 would be more in order. The problem then became one of determining where the error in computing the loss coefficient was occurring and to reduce the error as much as possible.

In order to determine the error, it was assumed that the theory to calculate ζ_s was correct and that the error arose from invalid assumptions and incorrect measurements of some variables. If a value for ζ_s is assumed, certain parameters can be calculated and plotted as a function of P_{T0}/P_1 , and then actual measurements could be compared against these predicted values. Thus, based on the definition of ζ_s , several important relationships could be developed:

$$\zeta_s = \frac{T_1 - T_{1is}}{T_{T0} - T_{1is}} = \frac{(T_{T0} - v_1^2/C) - T_{T0} \left(P_1/P_{T0}\right)^{\frac{\gamma-1}{\gamma}}}{T_{T0} - T_{T0} \left(P_1/P_{T0}\right)^{\frac{\gamma-1}{\gamma}}}$$

$$\text{Let } X = \left(P_1/P_{T0}\right)^{\frac{\gamma-1}{\gamma}}$$

Hence

$$\zeta_s = \frac{(1 - v_1^2/CT_{T0}) - X}{1 - X} = 1 - \frac{v_1^2/CT_{T0}}{(1 - X)}$$

$$\text{and using } C_p = \frac{\gamma}{\gamma-1} \frac{R}{J}$$

$$\frac{v_1}{a_{T0}} = \sqrt{\frac{2}{\gamma-1} (1 - \zeta_s)(1 - X)} \quad (8)$$

With the chosen value of $\zeta_s = 0.08$ and $\gamma = 1.4$,

$$\frac{V_1}{a_{T0}} = 2.1450 (1 - X)^{\frac{1}{2}} \quad (9)$$

and

$$\frac{T_1}{T_{T0}} = 1 - \frac{\gamma - 1}{2} \left(\frac{V_1}{a_{T0}} \right)^2 \quad (10)$$

From

$$\dot{w}_T = \rho_1 V_1 A_{ths} = P_{T0} \left(\frac{P_1}{P_{T0}} \right) \left(\frac{T_{T0}}{T_1} \right) \frac{A_{ths}}{R_g T_{T0}} \frac{V_1}{\sqrt{\gamma g_c R_g T_{T0}}} \sqrt{\gamma g_c R_g T_{T0}}$$

$$\frac{\dot{w}_T R_g T_{T0}}{P_{T0} A_{ths} \sqrt{\gamma g_c R_g T_{T0}}} = \frac{\dot{w}_T \sqrt{R_g / g_c T_{T0}}}{\sqrt{\gamma} P_{T0} A_{ths}} = \left(\frac{P_1}{P_{T0}} \right) \left(\frac{1}{T_1 / T_{T0}} \right) \left(\frac{V_1}{a_{T0}} \right)$$

or

$$\phi = \sqrt{\gamma} \left(\frac{P_1}{P_{T0}} \right) \left(\frac{1}{T_1 / T_{T0}} \right) \left(\frac{V_1}{a_{T0}} \right) \quad (11)$$

$$\text{Then } M = \frac{\dot{w}_T}{g_c} R_{m1} V_{u1} = \frac{\phi A_{ths} P_{T0} R_{m1} V_{u1}}{g_c \sqrt{R_g / g_c T_{T0}}}$$

or

$$\frac{M}{P_{T0}} = M_{ref} = \sqrt{\gamma} A_{ths} R_{m1} \phi \left(\frac{V_{u1}}{a_{T0}} \right) \quad (12)$$

VI. DESCRIPTION OF TESTS

A new electrical read-out system was employed for the strain-gauges on the closure plate. It was decided to calibrate both the closure-plate axial force and torque with the closure-plate mounted on the stator, rather than using the previous method of calibrating away from the TTTR and then possibly destroying the calibration during the installation in the stator casing.

A summary of the operating runs is listed in Table II. The first series of runs was carried out at pressure ratios of 1.5 and 2.0 over the full range of RPM allowable by the torque capacity of the air dynamometer. The configuration was unhooded with rotor axial clearances of 0.250 in. and 0.500 in. Several pressure leaks developed on nearly every run, and only Run 8 was considered sufficiently trouble-free to be used for analysis.

Once the high loss coefficients were confirmed to exist from the data of Run 8 and reduction by Method 1 and Method 2, it was decided to attempt some locked rotor tests at axial clearances of 0.250 in. and 0.500 in. and 2.000 in. to determine the conditions at zero RPM and a pressure ratio of 1.5. Few problems were incurred during this series of tests, and data points could be repeated to within 1 percent or better. During the last run however, several pressure lines were torn loose, which required extensive repairs before any further runs could be made.

During the runs up to and including Run 14, the standard method of operation had been to leave the inlet valve of Tank 1 full open and gradually open the turbine inlet valve to increase the pressure ratio.

TABLE II

Summary of Runs

Run	Configuration	Purpose
1 - 4	ASME Standard Pipe and Orifice Installed P _{noz} varied	To determine nozzle calibration coefficient.
5 6	Rotor removed Rotor removed	Closure plate axial and torque calibration
7 8 9 10 11	Operating, PR = 2.0, AX = 0.250" Operating, PR = 1.5, AX = 0.250" Operating, PR = 1.5, AX = 0.500" Operating, PR = 2.0, AX = 0.500" Operating, PR = 2.0, AX = 0.500"	To check the system after modifications and determine operating data
12 13 14	Locked Rotor, AX = 0.500" Locked Rotor, AX = 2.000" Locked Rotor, AX = 0.250"	To examine the system operation at zero RPM and various clearances.
15	Operating, PR = 1.5, AX = 0.250"	To confirm previous results
16 17 18 19	Honeycomb, flexures installed Honeycomb, flexures removed Honeycomb, flexures installed Honeycomb, flexures removed	To determine the effects of the torque flexures and various turbine inlet valve openings.
20 21	Nozzles installed, rotor removed, flexures removed Nozzles installed, rotor removed, flexures installed	To determine the effects of torque flexures and inlet valve openings with no rotor influence.

As a result, a pressure drop in the order of 50 in. of mercury was occurring across the turbine inlet valve. Also, it was noticed that after shutting off the flow to the stator, there were residual values of stator axial force and torque in the order of 1.0 and 5.0 percent respectively, which gradually dropped to zero after some time.

In an effort to examine the validity of the assumption of no inlet tangential velocity ahead of the stator, the stator was removed and the honeycomb flow straightener shown in Fig. 9 was installed. Also, during the next series of tests, the method of operation was changed and a further modification was employed. For Run 16, the honeycomb was installed and the turbine valve operated as before. Because a residual torque reading was again observed, it was decided to remove the stator torque flexures which take up some of the torque and transmit the axial force to the cradle assembly. A system of roller bearings was installed between the cradle assembly and stator plenum casing in place of the torque flexures, as shown in Fig. 10. Also, a thrust collar was fastened on the stator support shaft and allowed to press against the support bearing, as a means of transmitting the stator axial force to the cradle assembly. The next series of runs was performed by either gradually opening the turbine valve to obtain the desired pressure ratio, or fully opening the valve and adjusting the pressure ratio by slowly closing a dump valve in the delivery line near the Allis-Chalmers compressor. It was possible to obtain similar flow rates as used during all previous tests, but because of the much less restricted flow, considerably smaller pressure ratios were required.

Prior to Run 16, a thermocouple was installed on the torque capsule support assembly, and during the next series of tests the temperature of the assembly was monitored. Also, the discharge temperature from the Allis-Chalmers compressor was varied from 90° to 130° F to provide a sufficient temperature gradient at the stator in order to examine the effects of differential thermal expansion. During Run 17, the flow exit angle from the honeycomb was measured using a 5-hole probe, to find out whether the flow leaving the honeycomb straightener was truly axial as desired.

Once an improved method of operation was determined, a final series of tests was performed with stator nozzles reinstalled, but the rotor removed to eliminate any influence it might have. The same procedure was adopted as above, with the flexures installed and the turbine valve operated either fully open or partly open, and then the flexures were removed and the roller bearing supports installed, and the valve operated either fully open or partly open.

VII. RESULTS AND ANALYSIS OF TESTS

Fig. 14 shows the total-static turbine efficiency as a function of isentropic head coefficient. It is seen that a maximum efficiency of 79.6 percent occurs at a k_{is} of 4.2. Previous results for these operating conditions quoted a maximum efficiency of 83 percent at the same k_{is} . However, the efficiency is directly proportional to the dynamometer torque M_d and inversely proportional to the flow rate \dot{w}_T for given inlet conditions and speed N . Since the calculated flow rate is now considered to be in the order of 3.0 percent higher because of the corrected nozzle coefficient, this would account for the difference, and it was therefore concluded that the correct results were being obtained.

Fig. 15 shows the referred stator axial force as a function of referred RPM. It can be seen that there is some non-linearity when the curve is continued to the locked rotor condition, which can be accounted for by the changing pressure distribution around the shroud with the rotor locked.

Fig. 16 shows the referred stator torque as a function of referred speed. There is good linearity to the locked rotor condition, indicating the locked rotor torque is in the range of its expected value. When the referred torque is plotted as a function of stator pressure ratio, as shown in Fig. 17, there is a difference between the results of Method 1 and Method 2 and a considerable difference between the actual and the predicted value for the assumed $\zeta_s = 0.08$. The difference between the methods is due to the resulting higher pressure of P_1 by Method 2. It can be concluded however, that the torque

measurements at a pressure ratio of 1.45 are about 8 percent too high. It will be discussed later how this can occur.

Fig. 18 shows the flow function ϕ plotted against the stator pressure ratio. The curve extends well to the locked rotor condition. The reference curve shows that the actual ϕ is more in error at the lower than at the higher pressure ratios when using Method 1. The difference between the curves of Method 1 and Method 2, as discussed previously, is due to the higher P_1 by Method 2. Although ϕ is a function of both \dot{w}_T and A_{ths} for fixed inlet conditions, it was concluded that A_{ths} was in error. Build-up of dirt deposits on the blades and the presence of an increasingly thick boundary layer at higher pressure ratios would result in a lower effective throat area than was used.

Fig. 19 shows the dimensionless velocity ratios V_{al}/a_{T0} and V_{ul}/a_{T0} as functions of the stator pressure ratio. In both cases the curves extend smoothly to the locked rotor condition, and there is generally good agreement between the two data reduction methods. It can be seen that both V_{al}/a_{T0} and V_{ul}/a_{T0} are lower than the calculated values for an assumed $\zeta_s = 0.08$. When using Method 1, V_{al} is determined from equation (1), and a low value of V_{al} could be due to a high value of pressure P_1 or the reduction factor K_t . When using Method 2, V_{al} is determined by varying ϵ until equations (6) and (7) agree, which means in effect that P_1 is varied. Method 2 implicitly assumes that V_{ul} is correct. Examination of the behaviour of equations (6) and (7) when reducing the data revealed that equation (7) generally produced a lower V_{al} than equation (6), and its value changed very little during the iteration. The strongest variables

in equation (7) are P_1 and K_t , and a low value of V_{a1} would be due to high values of P_1 and K_t , which is in agreement with the previous conclusion for Method 1. The magnitude of V_{u1} has little effect on V_{a1} in equation (7). Since V_{a1} by equation (6) is generally higher than by equation (7), and because changing P_{1av} causes equation (6) to change more rapidly than equation (7), the iteration scheme forces P_1 higher in order to reduce the net stator force and thus reduce V_{a1} in equation (6). The increase in P_1 causes only a slight reduction in V_{a1} by equation (7). If the initial value for P_1 with $\epsilon = 0$ were too high then the above undesirable situation would occur, and the net result would be too high a value of P_1 and too low a value of V_{a1} . A desirable condition would occur if the initial value of V_{a1} by equation (7) were higher than that by equation (6), since the iteration scheme would then reduce P_1 causing a higher resultant V_{a1} . Previous work by Commons [Ref. 4] indicated that the stator hub pressure and the stator tip pressure measured with the arrangement of Fig. 6 were 5 percent higher and 5 percent lower, respectively, than the pressures obtained by flow surveys after the stator. The overall effect of these errors would produce a higher initial P_1 than the correct value, which is consistent with the previous conclusion for the low value of V_{a1} . Examination of the results from Run 15 given in Appendix D shows that the hub pressure acting on the hub area produces the largest effect on the net force in equation (6). As a consequence, a slightly low value of P_{hub} would result in the undesirable condition of a higher value of V_{a1} by equation (6) than by equation (7).

When using Method 1, the low value of V_{u1}/a_{T0} in relation to the calculated curve for an assumed $\zeta_s = 0.08$ would be due to the low values of V_{a1} and V_1 caused by an erroneously high pressure P_1 . This supports the previous argument where it was stated that high values of P_1 could be causing the errors. Using Method 2, equation (4) shows that the low value of V_{u1} could be caused by a low stator torque reading. However, that condition would conflict with the conclusion from Fig. 17 which shows the torque to be reading about 8.0 percent high. A reduction in the stator torque would result in a further deviation of V_{u1} from the calculated curve for $\zeta_s = 0.08$, and an increase in the mean loss coefficient. This situation can be resolved only by concluding that the angle of 75.9° chosen to calculate the velocity components from equation (9) was too high. A reduction in the chosen flow angle would result in a higher V_{a1} and lower V_{u1} for a given V_1 .

Fig. 20 shows the stator loss coefficients calculated by the two methods as a function of stator pressure ratio. It can be seen that the losses obtained by either method are at least 50 percent higher than the predicted value. The higher loss coefficient by Method 2 is due to the higher pressures resulting from Method 2 and the fact that constant pressure lines diverge. Fig. 20 also shows that the loss coefficients determined by both methods decrease slightly as the stator pressure ratio and the flow rate increases. Such a condition is opposite to that expected, since at higher pressure ratios an increased possibility of separation exists, and a thicker boundary layer with greater secondary losses should occur. The apparent reduction of the loss coefficient as the stator pressure ratio increases is likely due to an unexpected flow condition at higher flow rates. It will be shown later that at higher flow rates a changing inlet flow condition does occur.

Fig. 21 shows the referred stator axial force as a function of stator pressure ratio for three axial clearances of 0.250 in. 0.500 in. and 2.000 in. It can be seen that at a clearance of 0.500 in. a more negative axial force occurs than at 0.250 in. or 2.000 in. It is suspected that the presence of the locked rotor at various axial clearances causes a changing pressure distribution on the shroud, and thus the rotor axial clearance has a large effect on the stator axial force and the shroud pressure distribution.

Fig. 22 shows the referred stator torque as a function of the stator pressure ratio. The same reversal of trend occurs when the axial clearance is increased, confirming the fact that the presence of the rotor influences conditions upstream. The locked rotor results shown in Fig. 22 at the three different axial clearances further supports the previous conclusion from Fig. 17, namely that the stator torque is reading high.

Fig. 23 shows the referred flow rate as a function of stator pressure ratio for the three axial clearances at the locked rotor configuration. It can be seen that there is good agreement at each of the three axial clearances, so the changing torque with clearance is not due to a different flow rate. Fig. 23 also shows that the flow rate approaches a maximum as the pressure ratio nears the critical value, but that choking does not occur.

Fig. 24 shows the flow function Φ with changing stator pressure ratio for the locked rotor condition. As in Fig. 23 there is no effect of clearance on flow rate. However, the same trend of a lower flow function than desirable is occurring, which confirms the results of Fig. 18.

Fig. 25 shows the stator discharge pressure ratio as a function of the overall pressure ratio P_{T0}/P_2 . It can be seen there is a linear relationship between stator pressure ratio and overall pressure ratio. Fig. 25 also shows the increasing difference between Method 1 and Method 2 as the overall pressure ratio is increased.

Fig. 26 shows the referred velocities as a function of stator pressure ratio for the locked rotor configuration. The same trend in V_{a1} occurs with the locked rotor results as was noticed in Fig. 19 when the rotor was unlocked, confirming the conclusion that some error exists in the pressure P_1 and the reduction factor K_t . However, Method 2 results in a tangential velocity component which is greater than the calculated value for the assumed $\zeta_s = 0.08$. It can therefore be concluded that the increased value of V_{u1}/a_{T0} is directly due to an error in the stator torque measurement and that the high torque reading is caused by some combination of temperature effect on the assembly and an inlet swirl at the stator plenum.

Fig. 27 shows the stator loss coefficient as a function of stator pressure ratio for the locked rotor condition. Equation (8) gives the relationship between the pressure ratio, exit velocity and stator loss coefficient, and it can be seen that for a given pressure ratio a low velocity will result in a high loss coefficient, and conversely, if the velocity were too high, the loss coefficient could become negative. When using Method 1 the loss coefficient is a unique function of the throat pressure and area where the throat pressure was assumed to be the same as that existing at the exit plane. Behaviour of equation (2) shows that a low velocity will result if a combination of

the pressure and throat area is too large. It has been previously shown that the throat area appears to be too large and Figures 20 and 27 show that at low pressure ratios the throat pressure must be high also. Appendix C gives a predicted pressure distribution at the exit plane, and it can be seen that a parabolic, rather than a linear variation would be more in order, resulting in a slightly higher P_1 than the linear variation from hub to tip would predict. From this it may be concluded that assumption 1 of Section 4.B, namely that equal pressures exist at the throat and exit plane would be in error. As the stator discharge pressure ratio increases the loss coefficient decreases somewhat, indicating that the pressure at the throat and exit plane are more nearly equal. When using Method 2, an erroneously high stator torque reading will produce a high tangential velocity component resulting in a higher net velocity than should exist for a given pressure ratio. It should be noticed that the loss coefficient by Method 2 increases with increasing pressure ratio even though the stator torque is high. This indicates that the error in hub pressure P_{hub} and exit pressure P_1 have a stronger effect than does the stator moment and it was concluded earlier from the analysis of Fig. 19 that P_1 was indeed too high.

Fig. 28 shows the measured temperature of the torque capsule support assembly as the flow rate is increased, and Fig. 29 shows the results of the temperature analysis on the cradle assembly. It can be seen that as the cradle assembly heats up, a positive error occurs in the stator torque reading, indicating that the reading becomes too high as the inlet temperature increases. The reason for the increasing torque error is the unequal expansion of the capsule support assembly

and the connectors between the point of action of the torque arm and the upper end of capsule support. The stator torque flexures prevent free rotation of the stator as the capsule assembly grows due to thermal expansion. The two steel rods and the Invar ring of the torque capsule do not expand by an equal amount in the opposite direction to cancel the thermal expansion of the capsule support. The differential thermal expansion causes an additional tensile force on the capsule and a higher apparent torque reading. Additional analysis showed that it would be impractical to compensate for this thermal expansion by making the support assembly of the same type of material as the capsule ring and steel attachments, since the compensation would be possible only for a fixed temperature. In addition it would be impractical to thermally shield or cool the assembly as was done with the dynamometer capsule, since this set-up would present severe complications if the turbine were operated inside the closed hood. Thus the only practical way to eliminate the thermal effect on the capsule support assembly was to give the stator freedom to rotate so that no additional tension could be applied to the capsule. A solution was accomplished by removing the torque flexures and installing roller bearing supports to maintain the stator alignment, and a thrust collar was fastened to the stator support shaft and allowed to press against the support bearing as a means of transmitting the stator axial force to the cradle assembly.

Fig. 30 shows the referred stator torques obtained with the honeycomb flow straightener replacing the guide vanes. Test data are shown at different openings of the turbine inlet valve and the tests were carried out with the torque flexures installed or removed. If the

flow after the honeycomb were axial, and if the flow entered the stator assembly with no whirl components, the stator torque would be zero for any pressure ratio. Fig. 30 shows that the stator torque was only zero at zero flow rate, and increased with increasing pressure ratio. From the results of Fig. 30 it can be concluded that temperature effects caused by the presence of the torque flexures and throttling the flow by partly closing the turbine inlet valve influence the stator torque readings. With the turbine valve full open less torque occurs when the flexures are removed, indicating that the temperature effect due to the flexures has been reduced. When the pressure ratio is set with the turbine valve partly closed a considerably larger torque occurs and it is again higher if the torque flexures are installed. Since an increasing torque with increasing pressure ratio still occurs when the turbine valve is full open and the torque flexures are removed, it can be concluded that either the honeycomb is not truly axial or the flow still enters the stator plenum with a small whirl component.

Fig. 31 shows the flow angles measured after the honeycomb straightener. It can be seen that the velocity after the honeycomb has a tangential component which increases with increasing flow rate. From Figures 30 and 31 it can be concluded that the partly opened turbine valve causes whirl components in the delivery pipe, and the flow enters the stator assembly with a tangential velocity. Hence, assumption 4 of Section 4.a, namely, that the flow into the plenum is radial and no whirl component exists ahead of the stator is not satisfied with the present installation. Because the honeycomb has openings of about 1/8 inch it is apparently not capable of completely turning the

flow into the axial direction. It was found also that the stator blockage factor ξ through the honeycomb is about 0.72, where ξ represents the ratio of the actual flow area and that necessary to pass the flow if the expansion were isentropic. Because of the low values of ξ it can be concluded there must exist large whirl components ahead of the honeycomb causing flow separation at the inlet and large losses.

VIII. CONCLUSIONS AND RECOMMENDATIONS

From the preceding analysis, it can be concluded that the stator torque reading is about 8 percent too high, and that this error is due to a combination of the temperature effect on the capsule support assembly and an inlet swirl caused by the turbine inlet valve and piping. It is recommended that the turbine be operated with the turbine inlet valve full open at all times, and that the pressure ratio be set by closing a dump valve near the air supply.

During the last series of runs with the stator nozzles installed and the rotor removed, inconsistent and residual values of stator axial force occurred when the torque flexures were removed and the roller bearings installed. This was due to the mechanical friction inherent in the present system. It is felt that a better system should be designed which would allow the stator to rotate and move axially without restraints. This would make the stator a truly free-floating assembly and eliminate the influence of temperature on the measurement of the stator torque. Such a system would require the use of ball-bearings mounted in such a way that they would allow both rotation and axial movement of the stator and thermal expansion or contraction of the casing, but maintain the stator axial alignment.

The analysis of the cradle assembly showed also that thermal effects occur in the horizontal direction which affect the capsule measuring the stator axial force. This problem could be eliminated by constructing a cradle support assembly similar to that used for the torque measurement but made of aluminum. Proper installation of this cradle would allow its growth or contraction to be in the same

direction as the horizontal members of the stator cradle, thus compensating for thermal effects on these members.

It is suggested that a honeycomb flow straightener and series of screens be installed in the delivery pipe just ahead of the inlet to the stator plenum chamber, and that the conical screen presently installed in the plenum chamber be removed. This should produce a more uniform flow into the plenum and eliminate the tangential component, while removal of the conical screen should eliminate some of the existing total pressure gradient at the entrance to the stator nozzles.

From the analysis of the pressure effects on the loss coefficient it can be concluded that extensive flow surveys should be done at different operating conditions to accurately determine the pressure distribution at the stator discharge. Means must then be found to ensure that accurate hub and tip pressures can be recorded since they have a large effect on the loss coefficient. It was shown that the assumption of stator exit pressure also acting at the throat plane was erroneous and the assumption could be eliminated if the throat hub and tip pressure taps were accurately located at the throat plane. At present there is up to a 5 percent error between the four sets of taps. The flow surveys must be carried out with probes which properly compensate for Mach number effect, depth of immersion and pitch angle. Very useful information could be gained by using a hot wire anemometer probe to accurately determine velocity profiles and magnitudes in the stator area at different operating conditions.

Results of the prediction of closure plate torque and shroud torque given in Appendix B show these values never exceed 0.1 percent of the

stator torque reading. This amount is considered negligible and thus the closure plate torque webs, strain gauges and wires could be removed. This would eliminate the congestion in the hub area and allow the closure plate greater freedom of movement, since some friction might be caused by the presently installed equipment. The predicted torque as a function of pressure ratio and speed agreed very well with the strain gauge readings and so it is concluded the closure plate and shroud torques could be accounted for during the data reduction by using an empirical formula. Results of the forces on the closure plate due to the pressure distribution on the face agreed to within 1.0 percent of the strain gauge reading. Considerable effort was required to numerically integrate the pressure over the face area, and since measurement of the closure plate axial force by the strain gauges was much quicker and produced comparable results, it is recommended the closure plate pressure lines be removed.

It can be concluded that several of the assumptions utilized to solve the equations for a one-dimensional analysis were not valid, and that ignoring their effects can produce very poor results. Appendix C shows that cylindrical stream surfaces cannot exist, and a radial component of velocity must be taken into account. Flow surveys made by Commons [Ref. 4] show that there is a variation of the total pressure at the stator entrance and thus a radial entropy gradient exists. The results of this investigation have shown that the flow is not completely radial into the plenum or axial into the stator and that a tangential component of velocity does exist. However,

these unsatisfactory conditions can be reduced by incorporating the equipment modifications suggested.



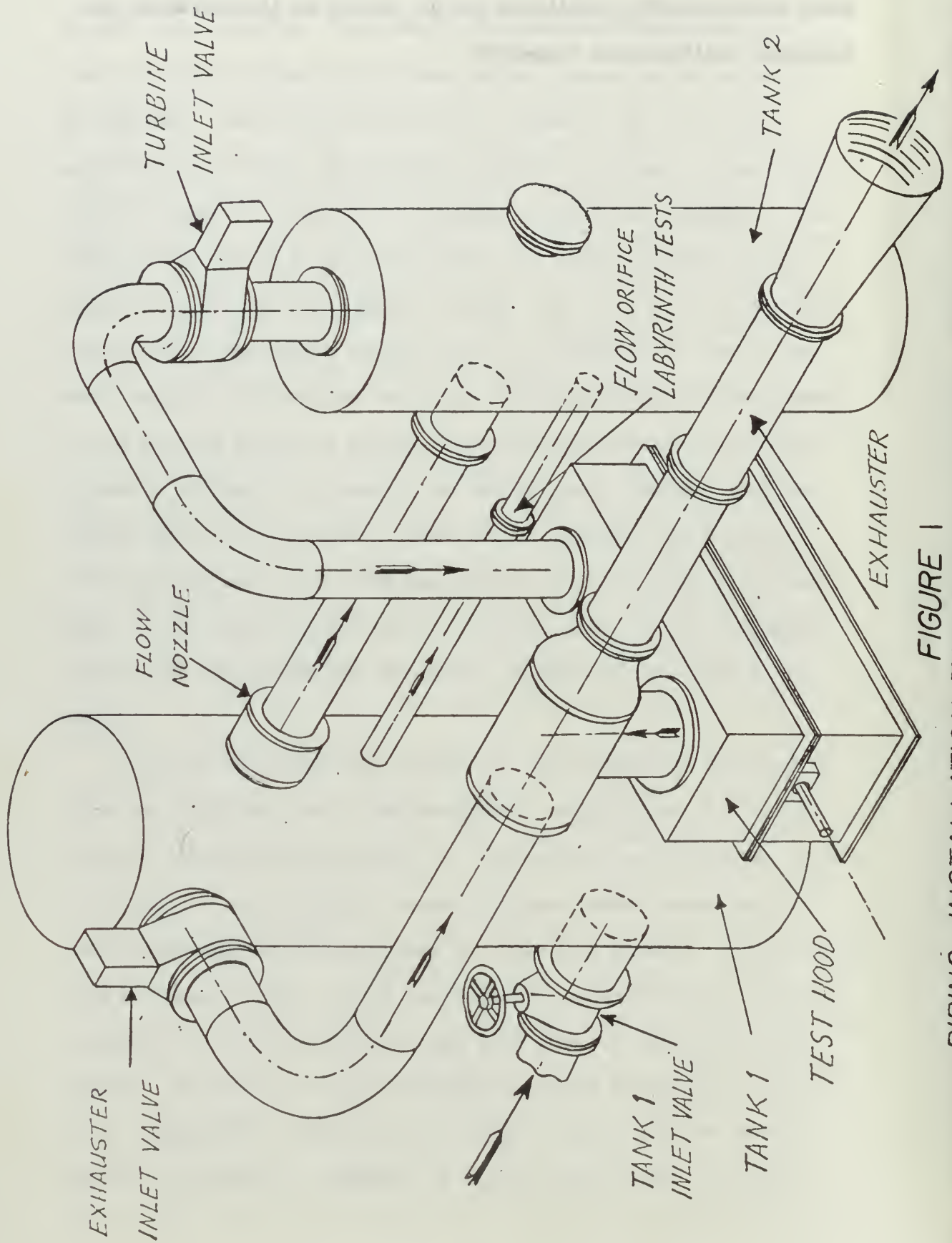


FIGURE 1
 PIPING INSTALLATION, TRANSONIC TURBINE TEST RIG

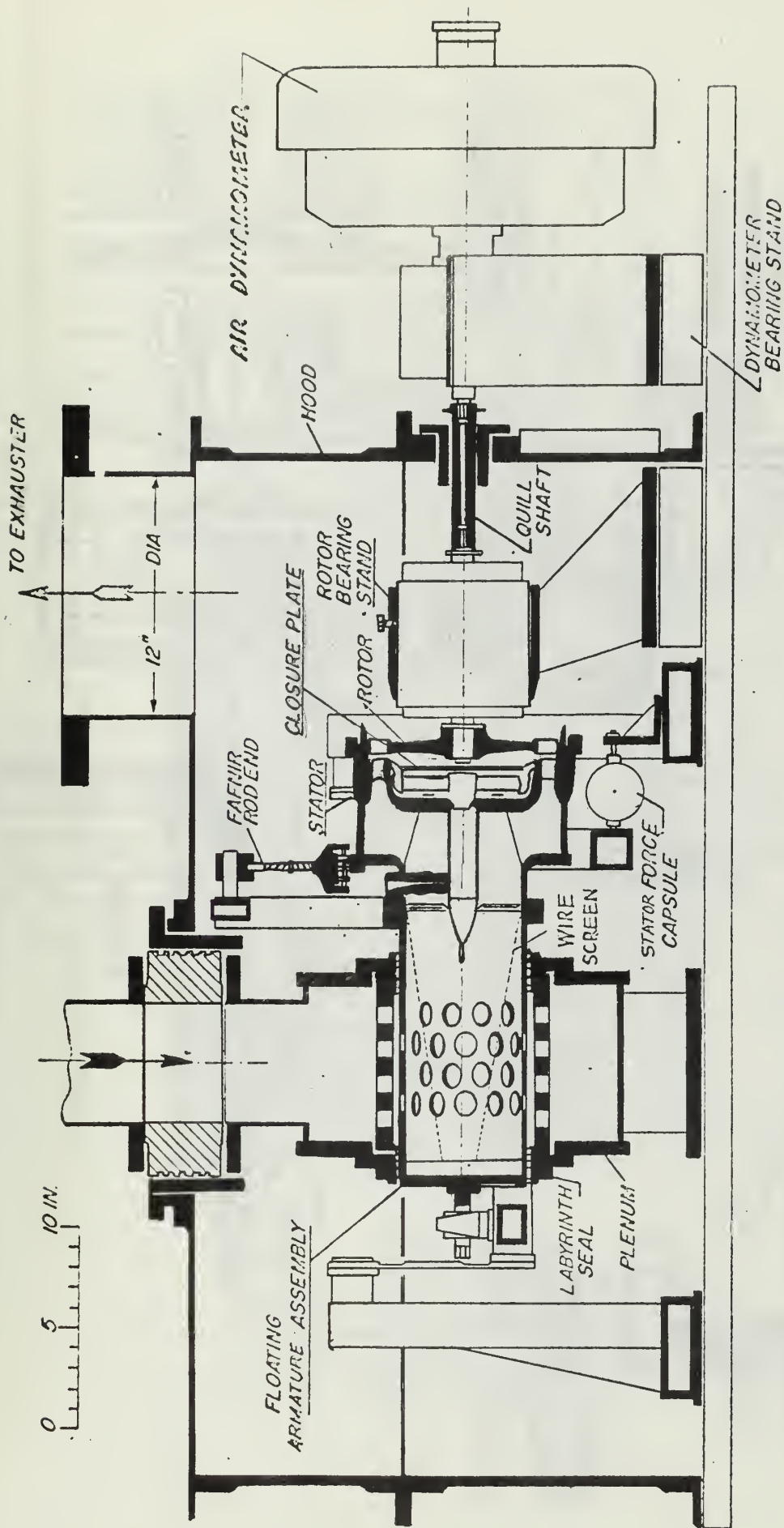


FIGURE 2
TRANSONIC TURBINE TEST RIG

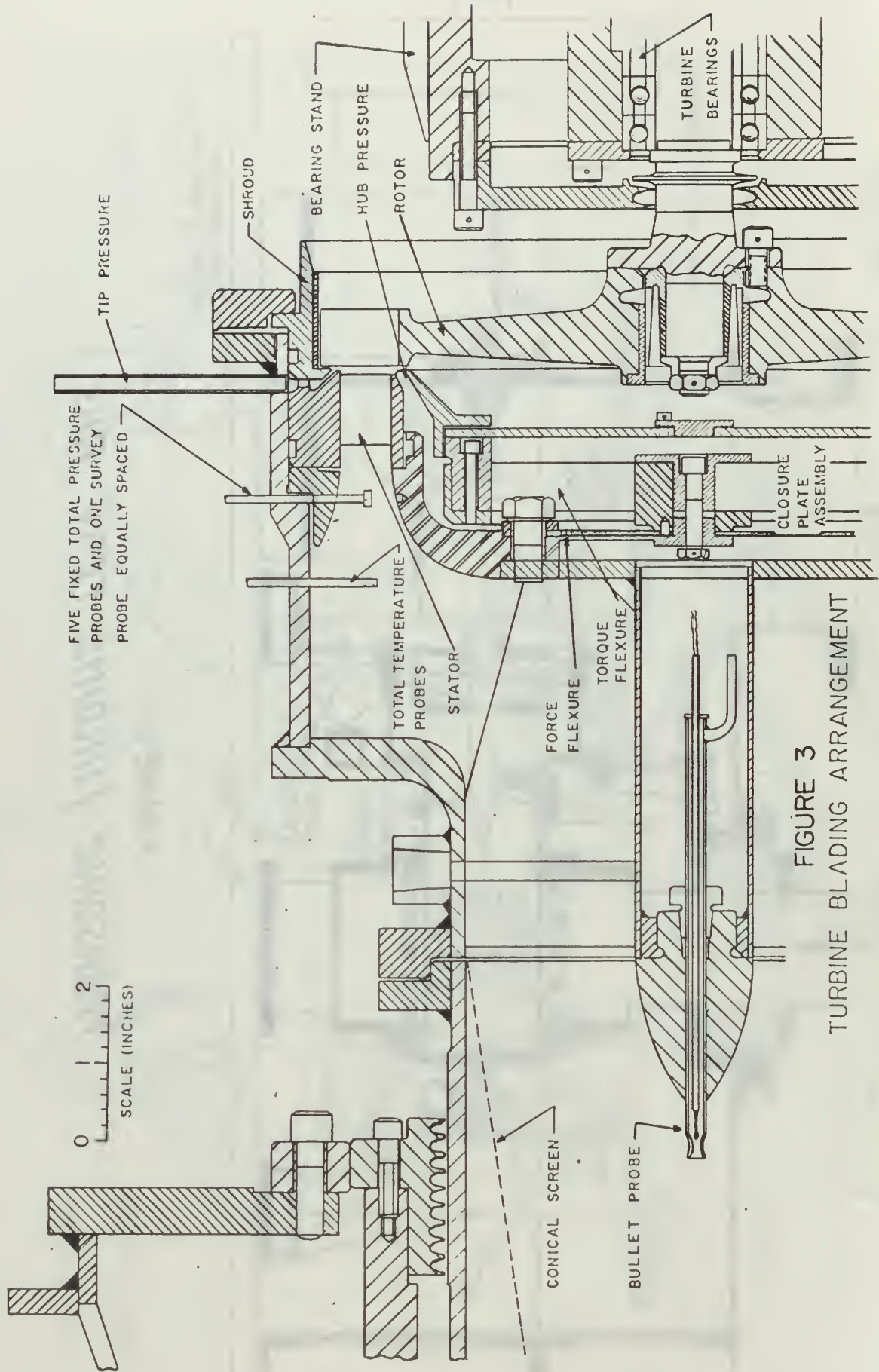


FIGURE 3
TURBINE BLADING ARRANGEMENT

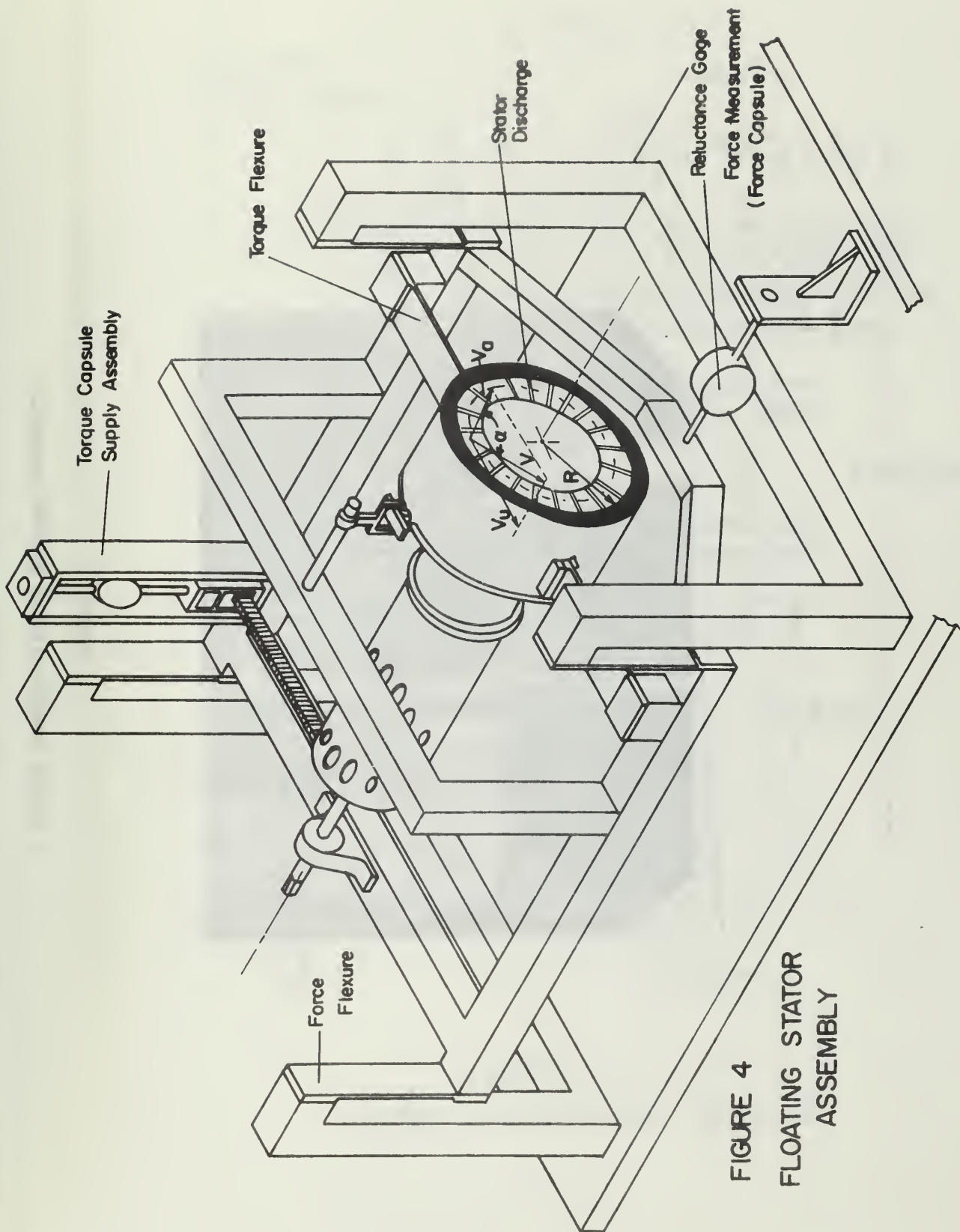


FIGURE 4
 FLOATING STATOR
 ASSEMBLY



FIGURE 5
STATOR TORQUE CAPSULE SUPPORT ASSEMBLY

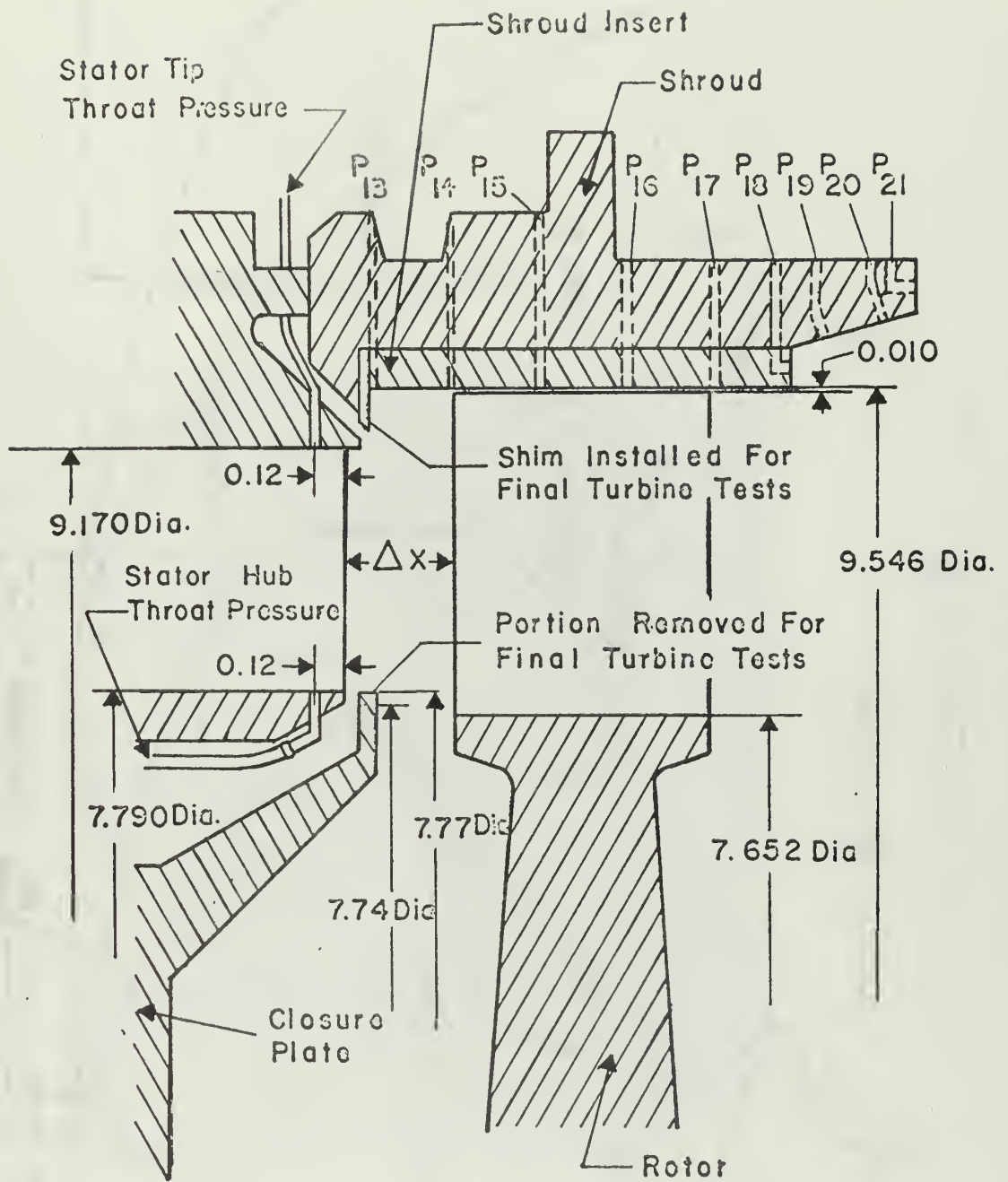


FIGURE 6
 TURBINE AND SHROUD DETAILS

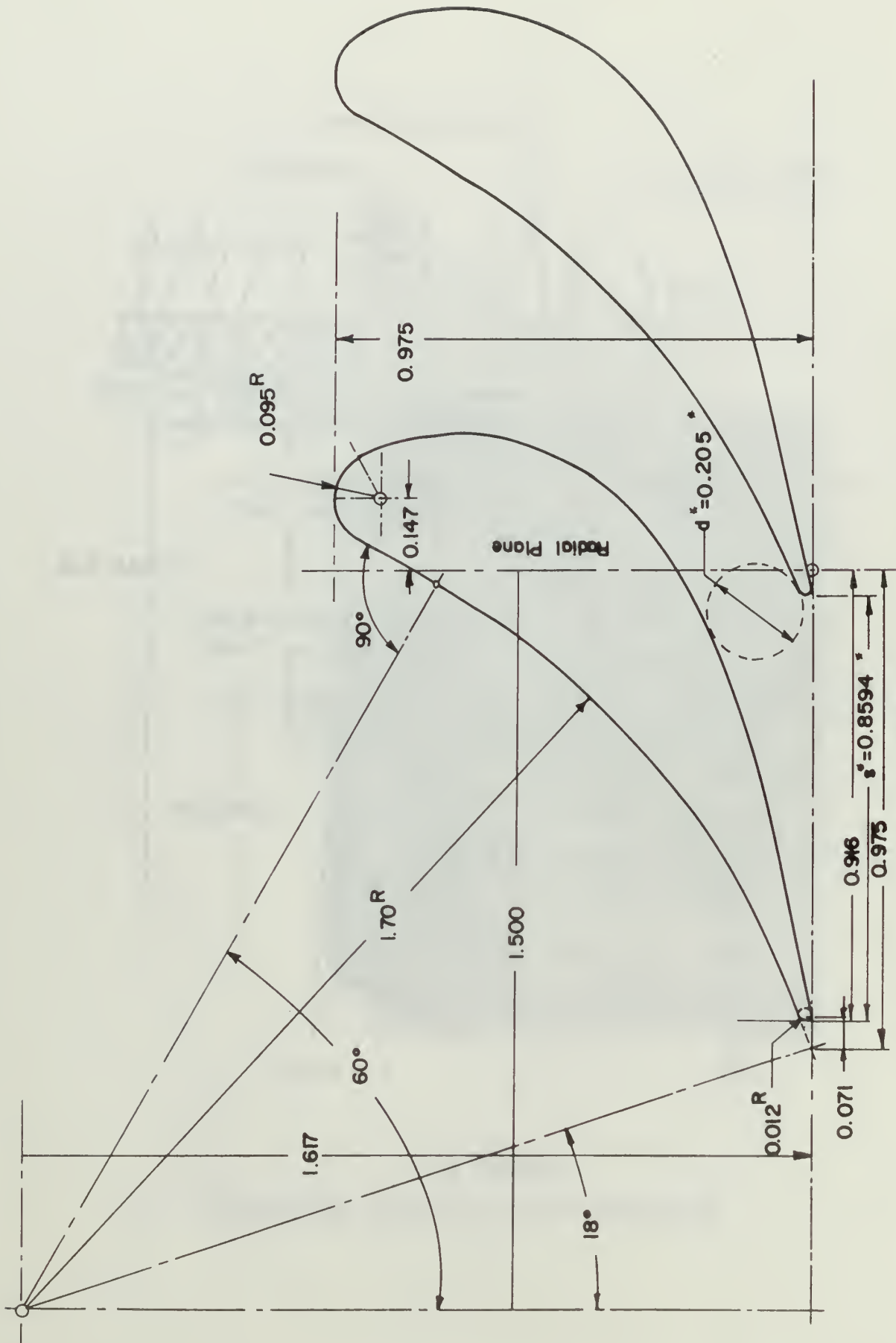


FIGURE 7
 MEAN RADIUS BLADE PROFILE CONVERGING NOZZLES

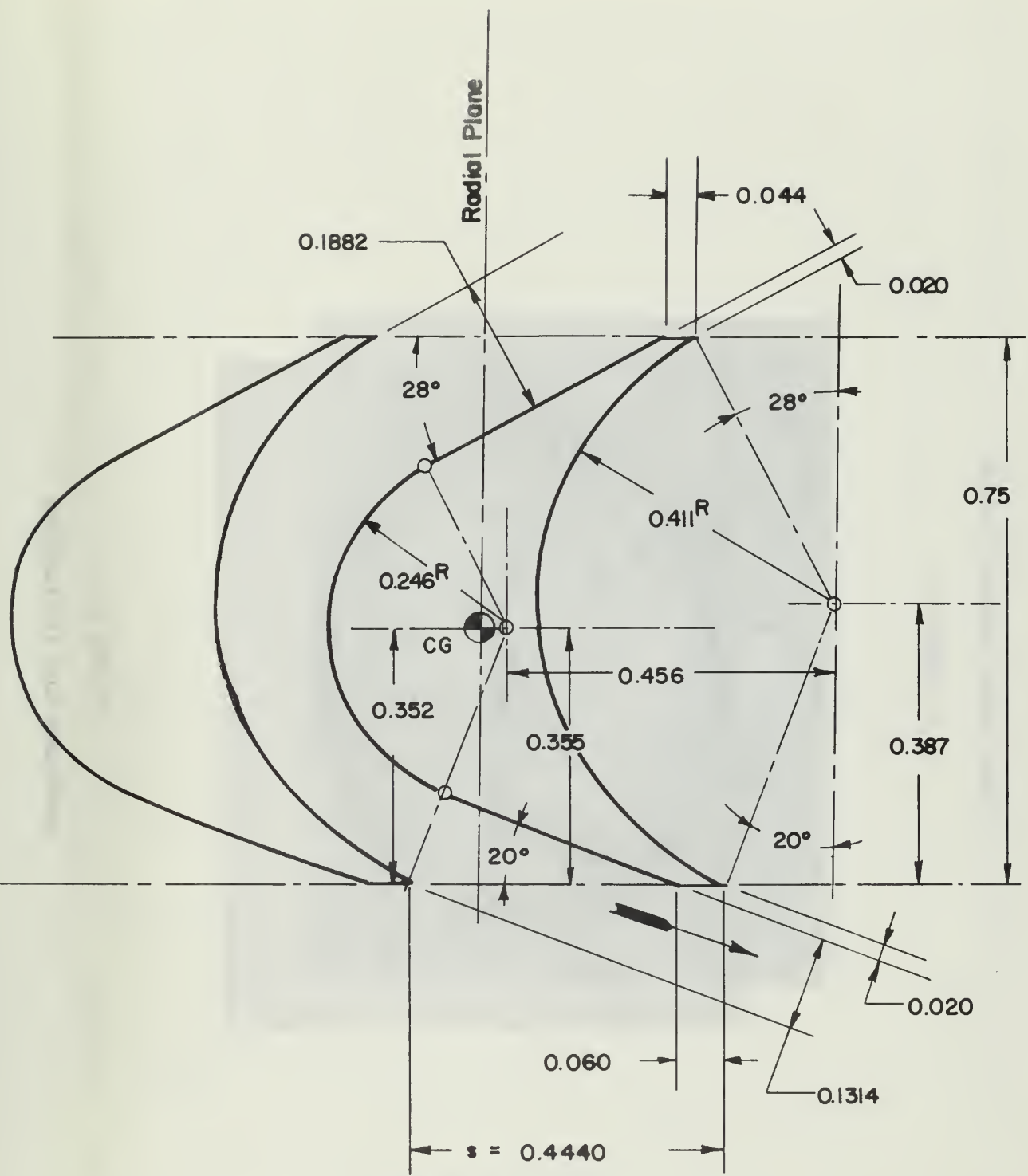


FIGURE 8
 MEAN RADIUS BLADE PROFILE
 CIRCULAR ARC
 SHARP LEADING EDGE ROTOR

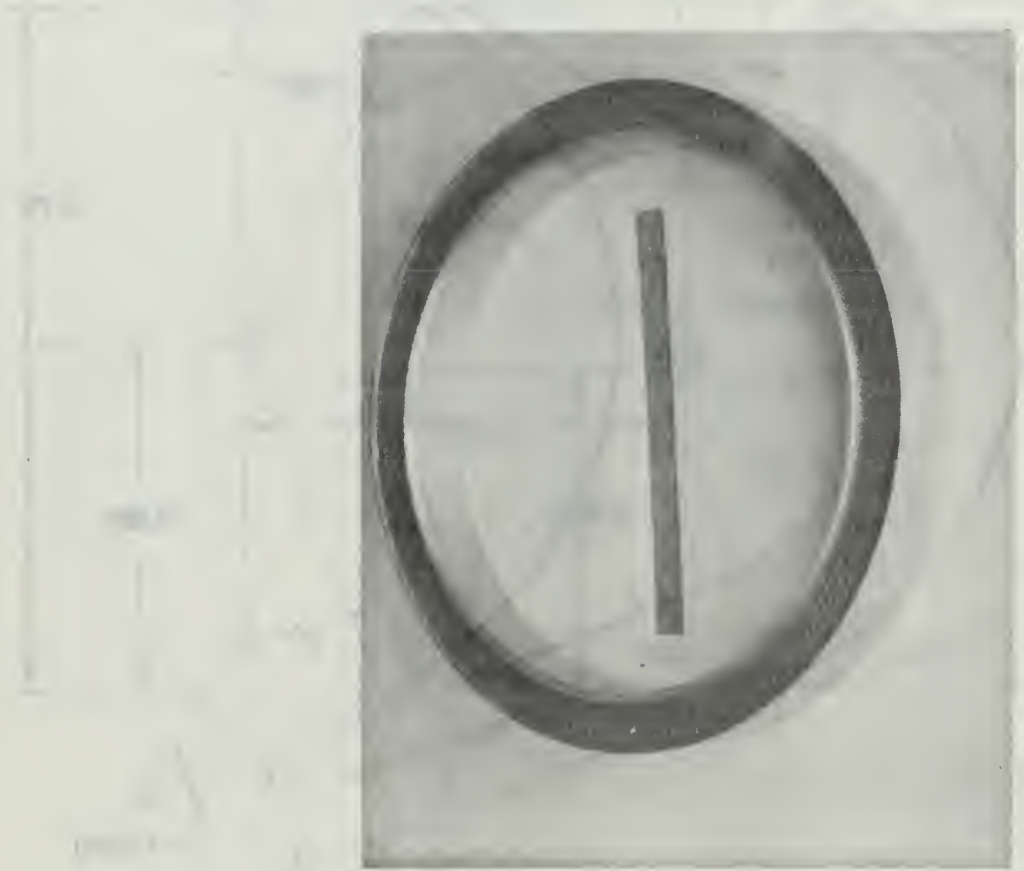


FIGURE 9
HONEYCOMB FLOW STRAIGHTENER

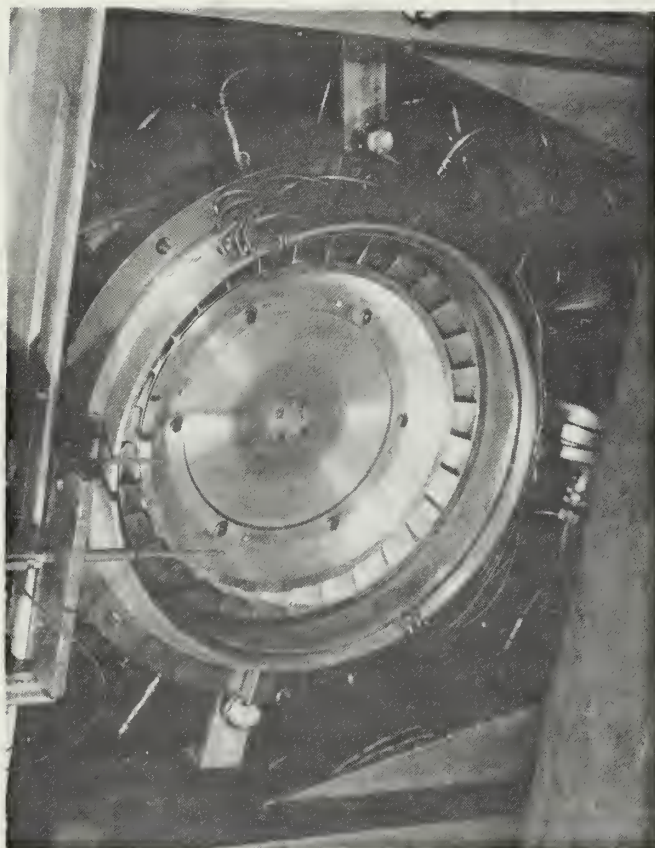


FIGURE 10
STATOR ROLLER BEARING SUPPORTS

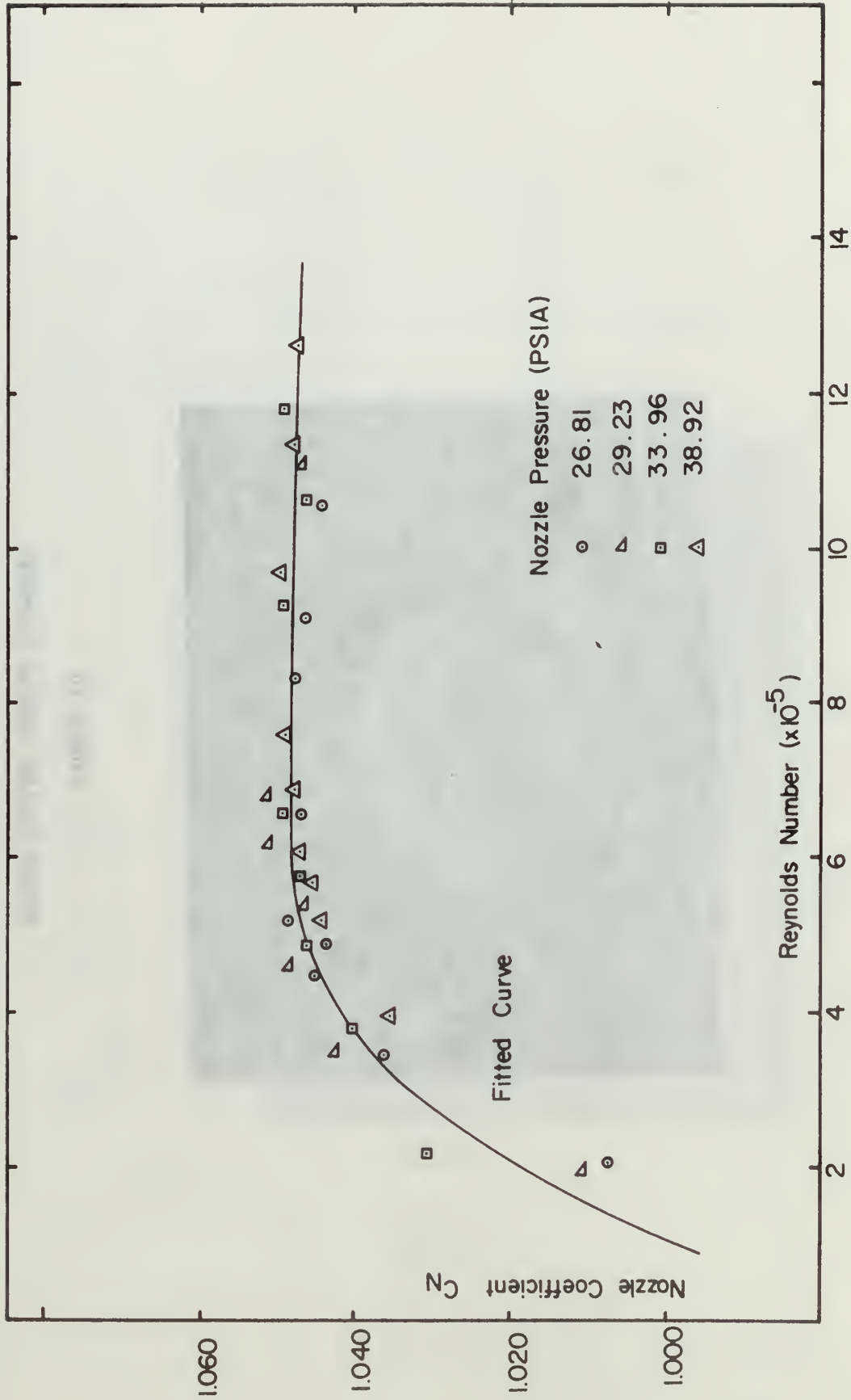


FIGURE 11
NOZZLE COEFFICIENT VS. NOZZLE REYNOLDS NUMBER

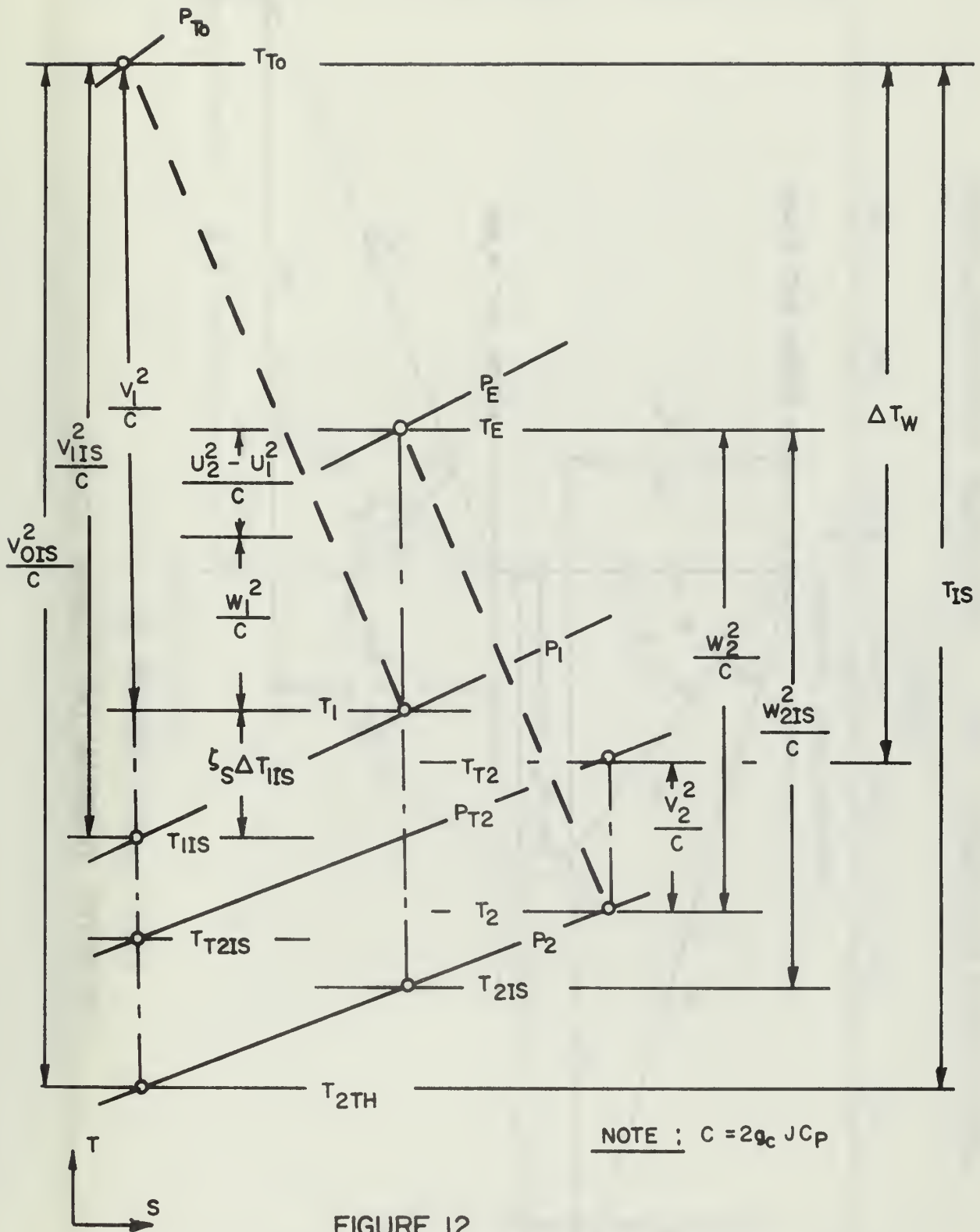


FIGURE 12

THERMODYNAMIC PROCESS FOR AN AXIAL
TURBOMACHINE

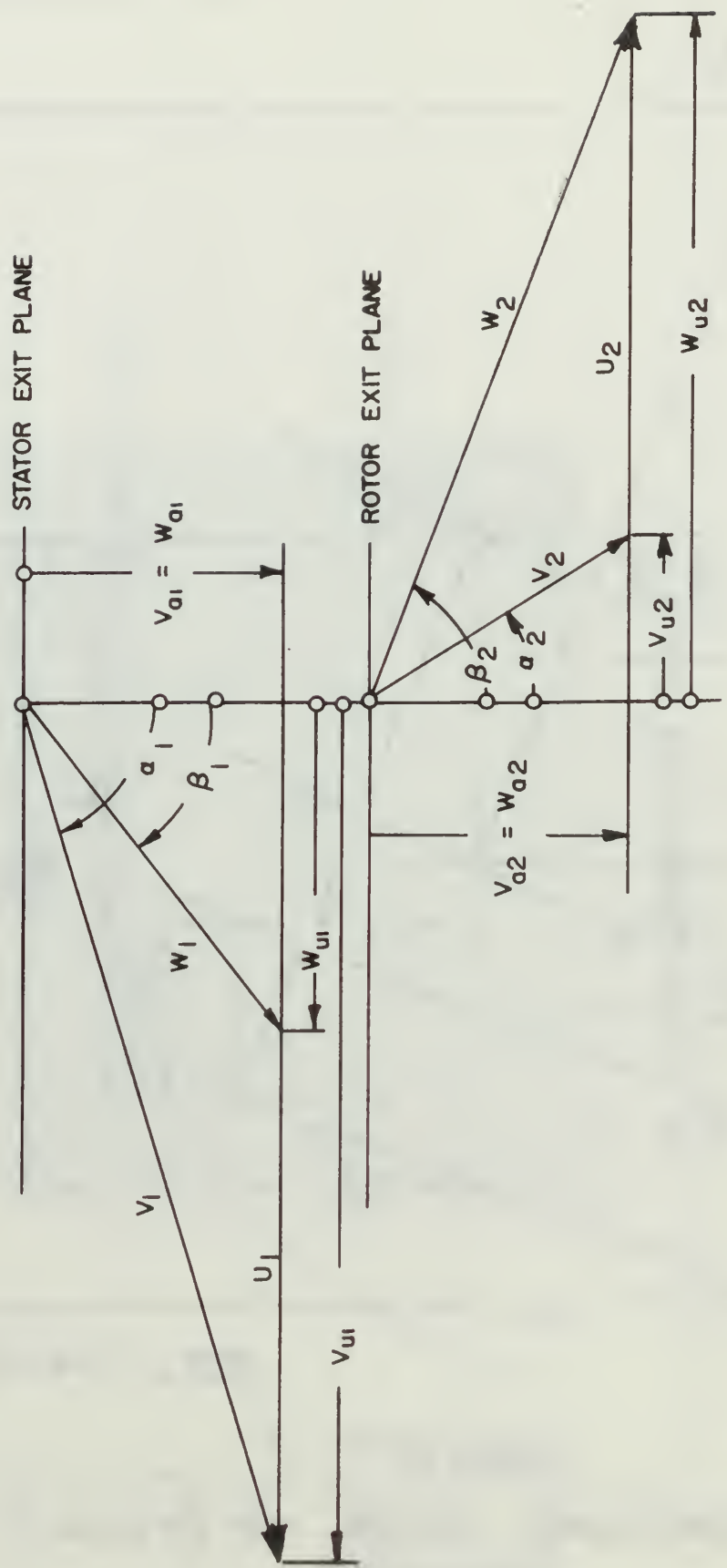


FIGURE 13
VELOCITY DIAGRAM OF TURBINE STAGE

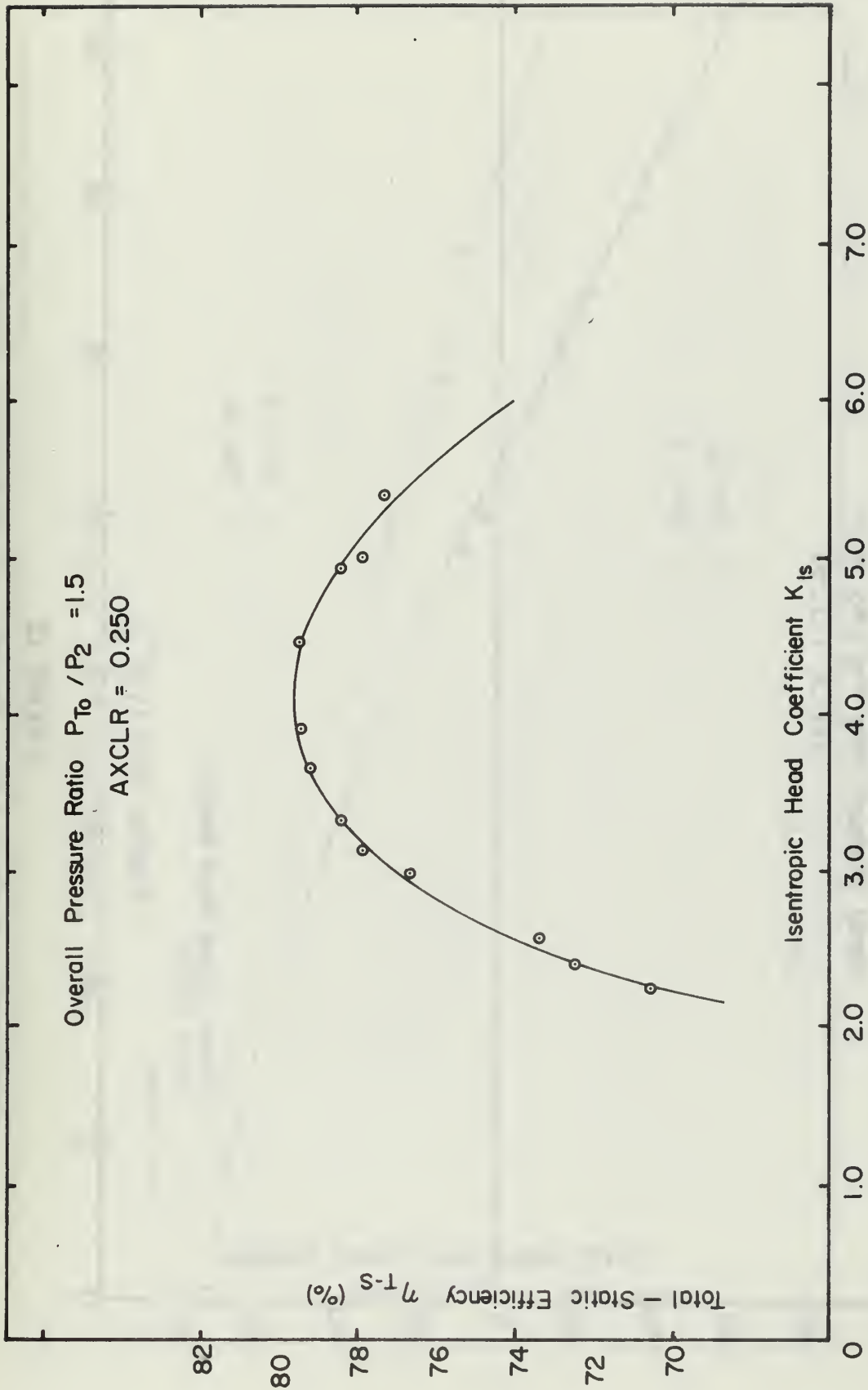


FIGURE 14
 TOTAL - STATIC EFFICIENCY VS. ISENTROPIC HEAD COEFFICIENT

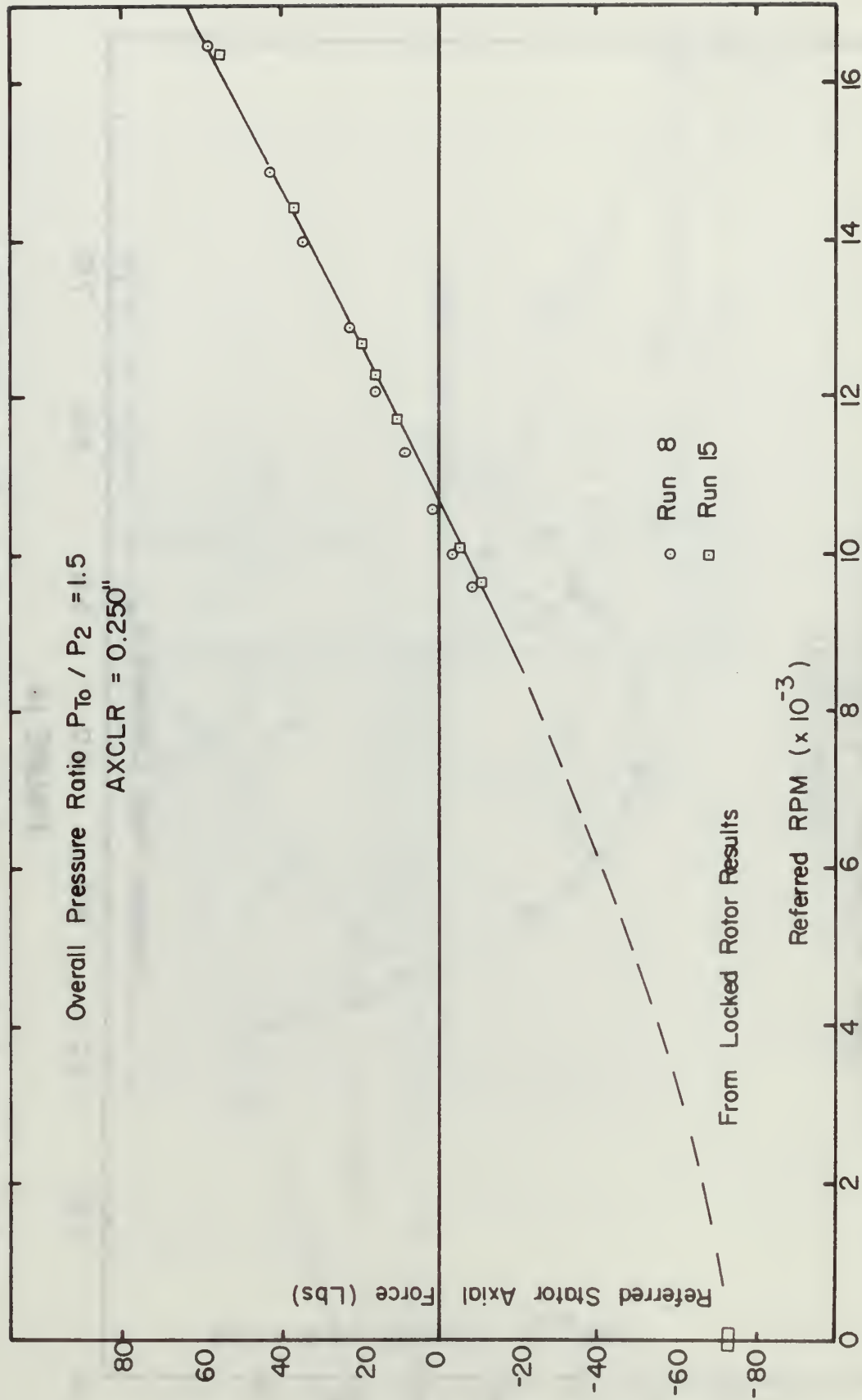


FIGURE 15
 REFERRED STATOR AXIAL FORCE VS. REFERRED RPM

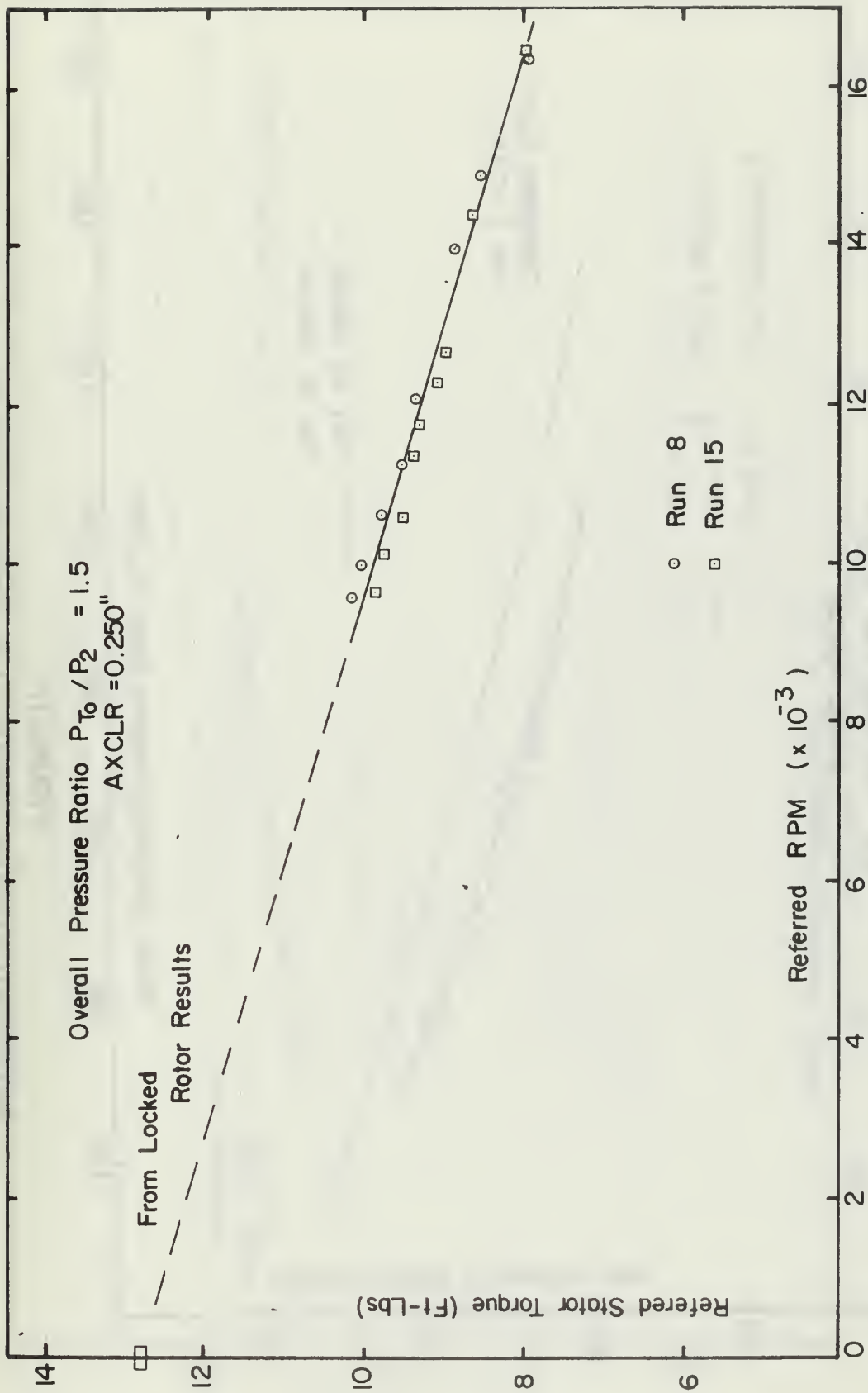


FIGURE 16
 REFERRED STATOR TORQUE VS. REFERRED RPM

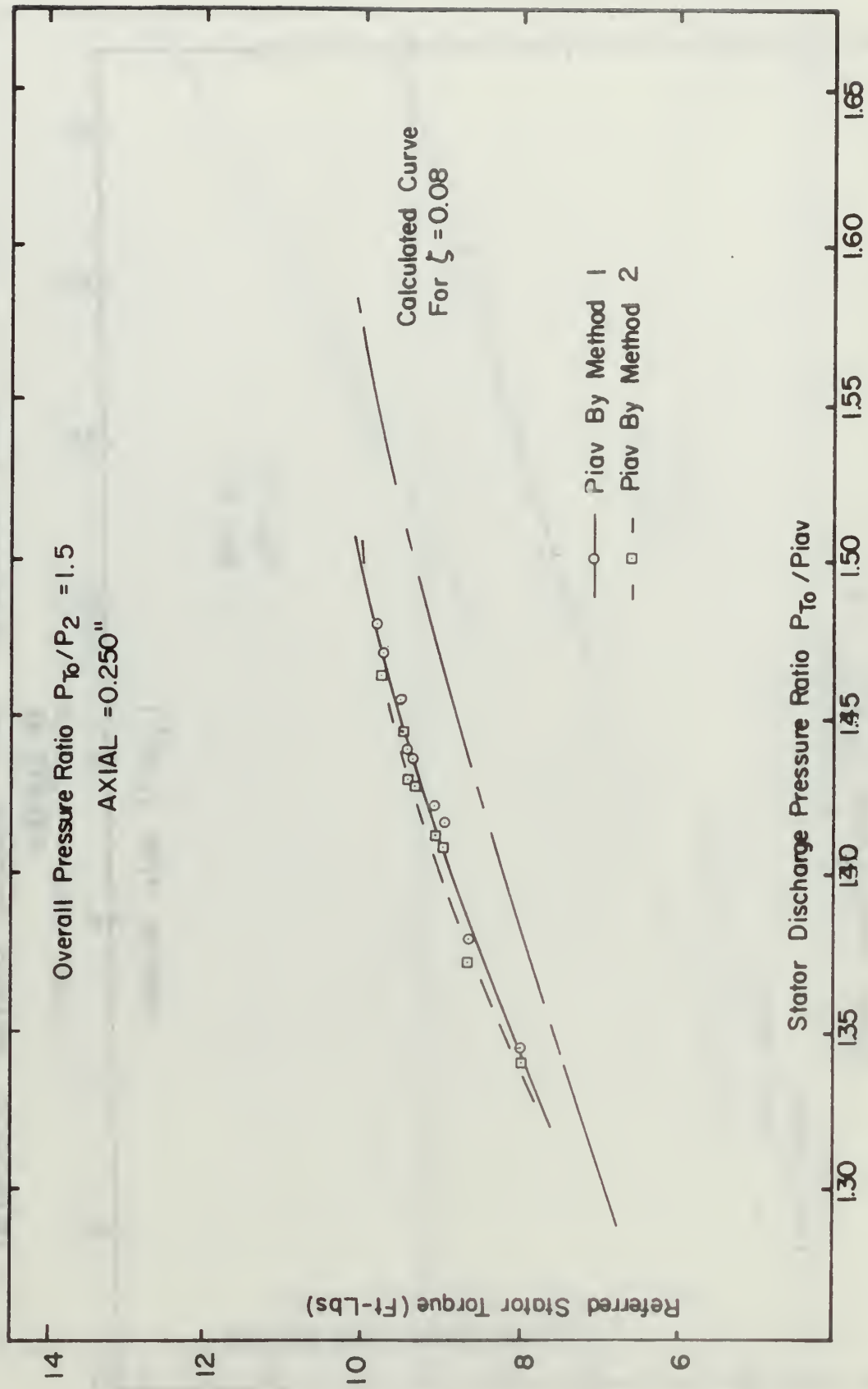


FIGURE 17

REFERRED STATOR TORQUE VS. STATOR PRESSURE RATIO

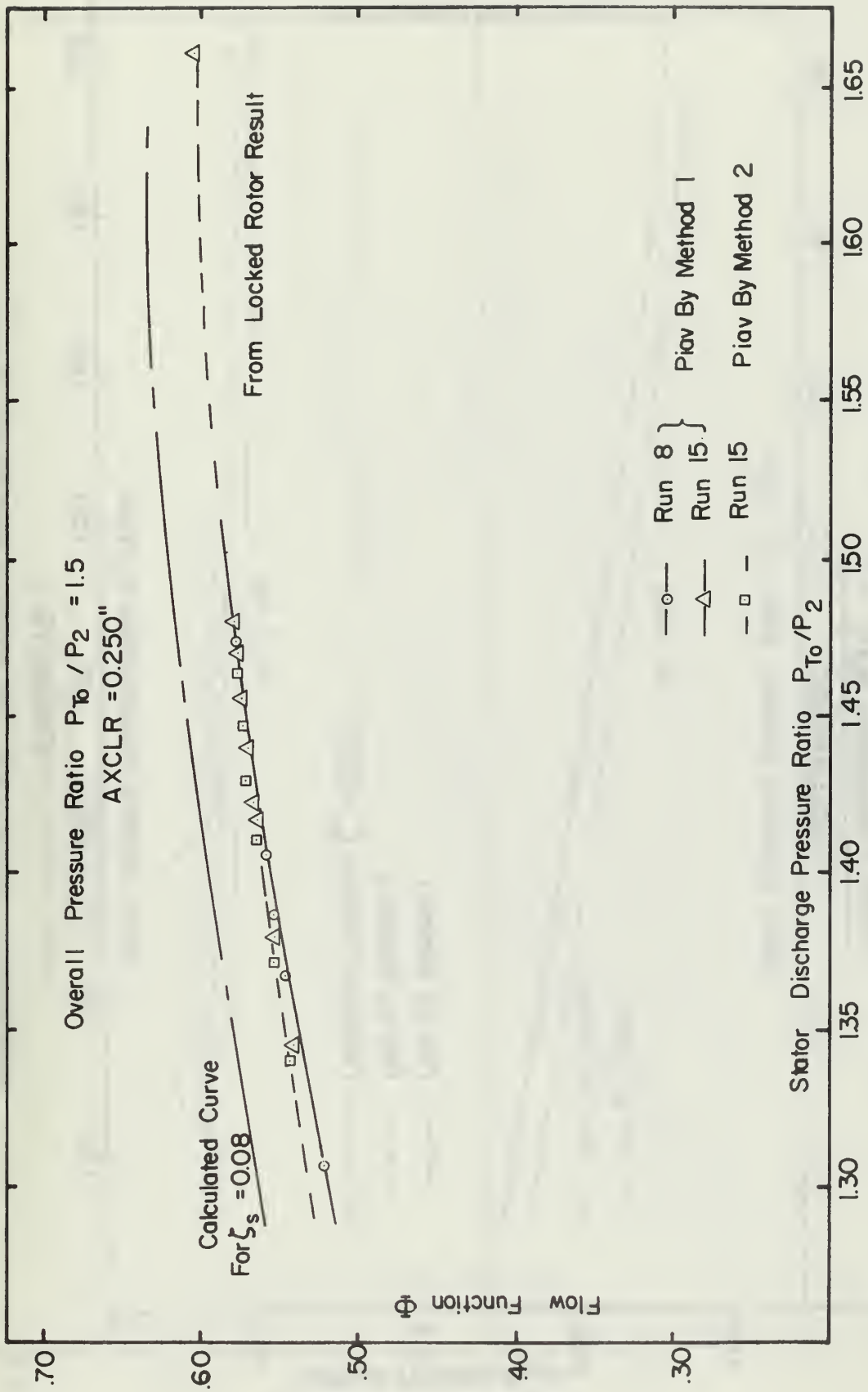


FIGURE 18

FLOW FUNCTION VS. STATOR PRESSURE RATIO

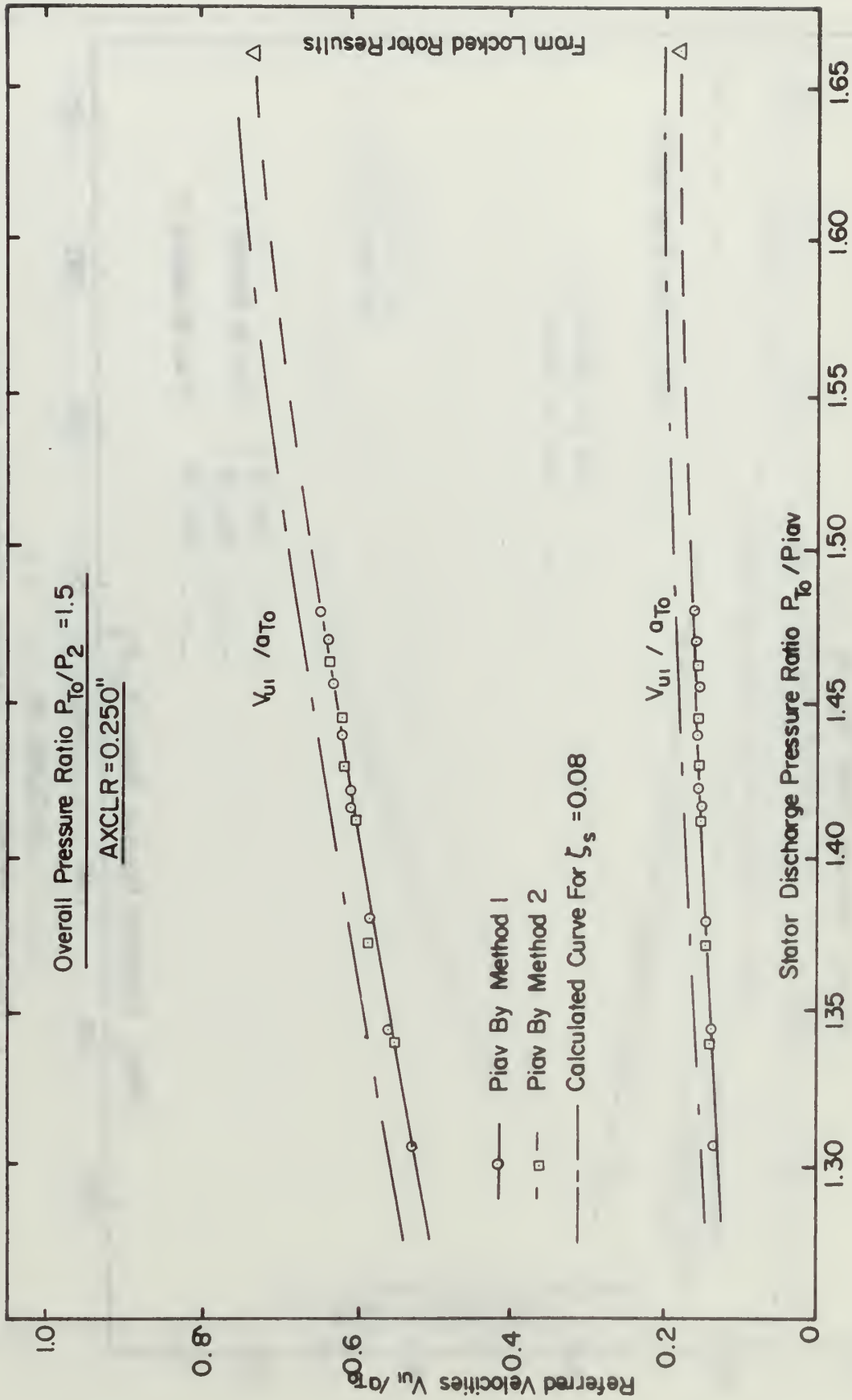


FIGURE 19

REFERRED VELOCITIES VS. STATOR PRESSURE RATIO

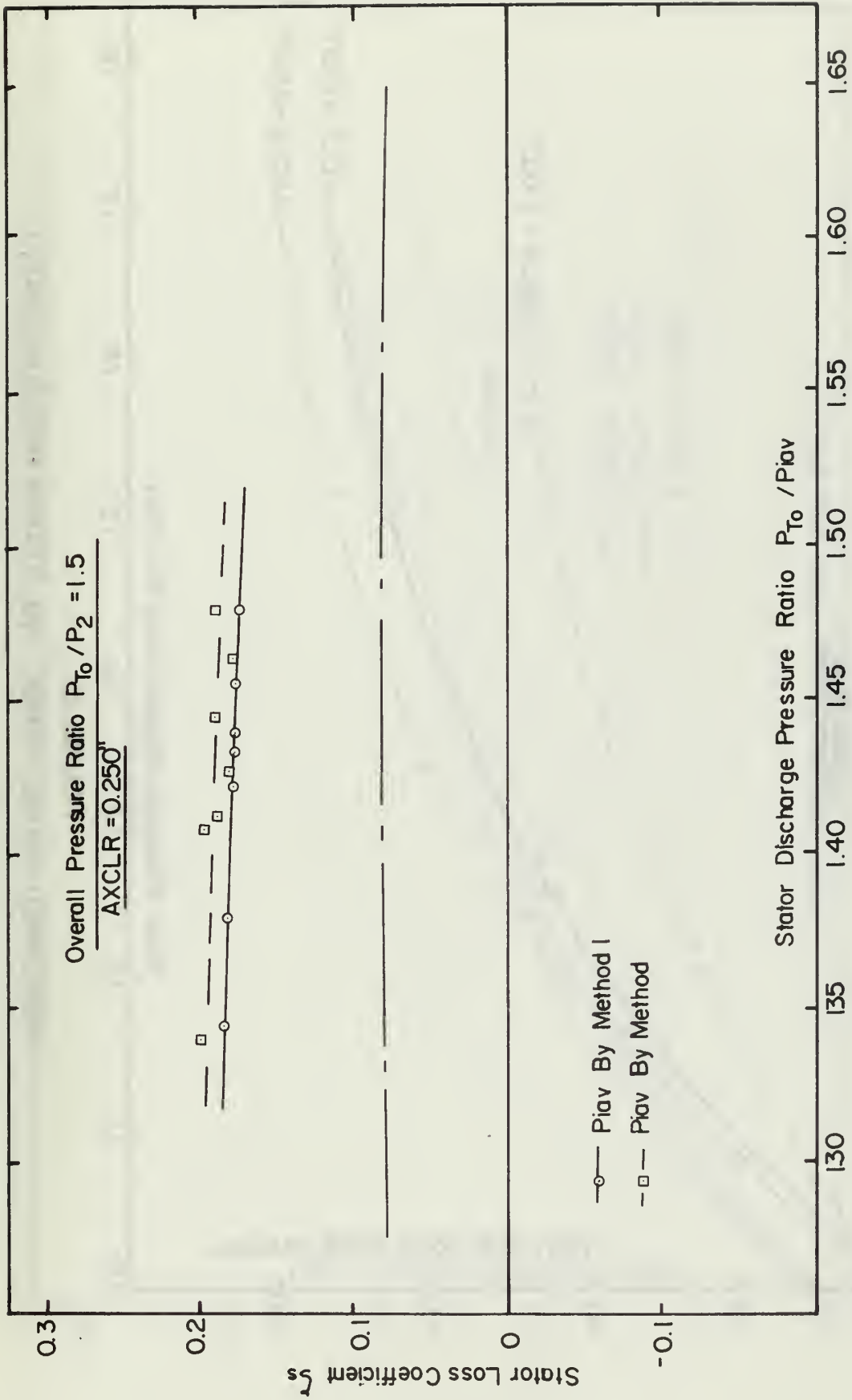


FIGURE 20

STATOR LOSS COEFFICIENT VS. STATOR PRESSURE RATIO

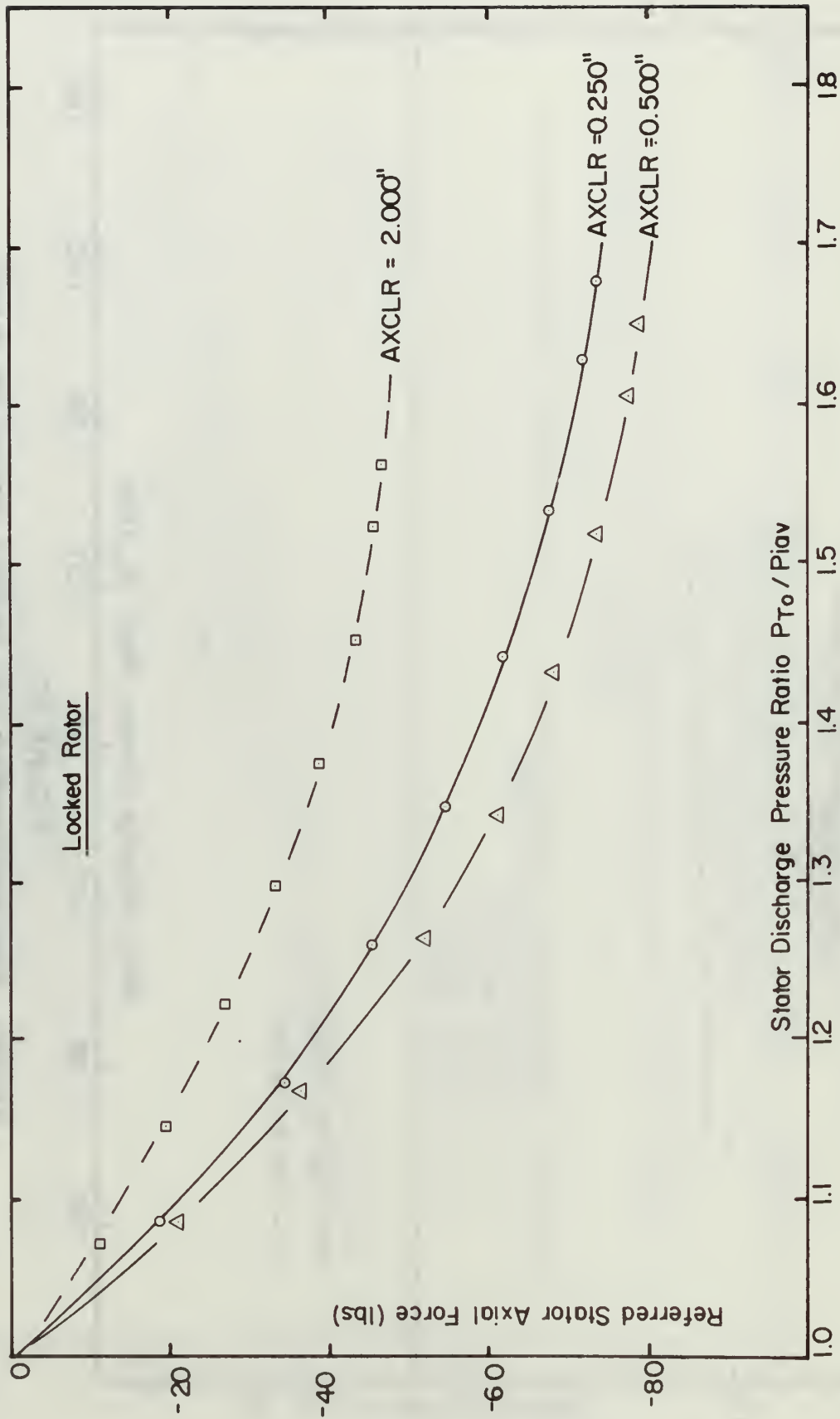


FIGURE 21
REFERRED AXIAL FORCE VS. STATOR PRESSURE RATIO

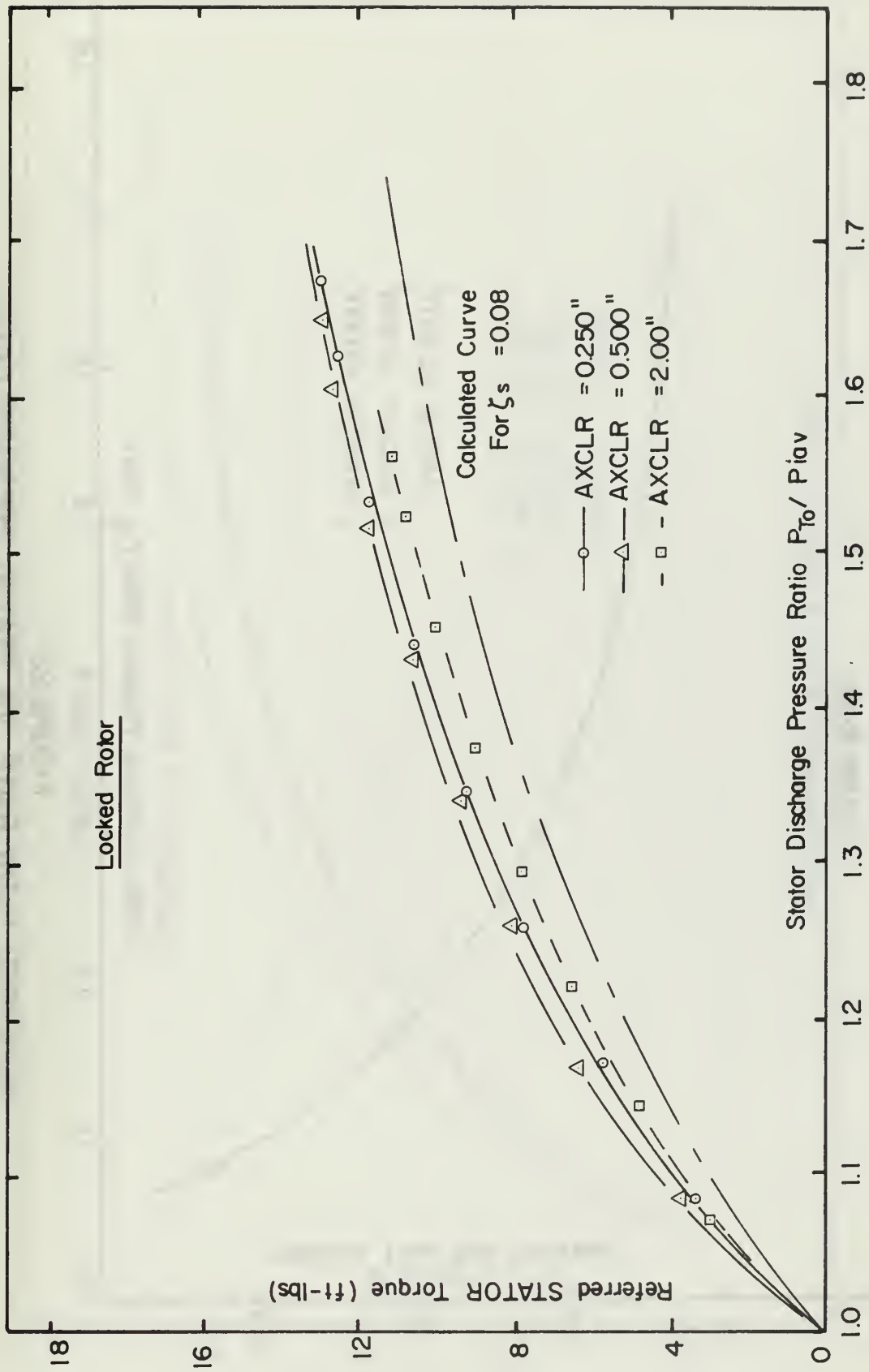


FIGURE 22

REFERRED STATOR TORQUE VS. STATOR PRESSURE RATIO

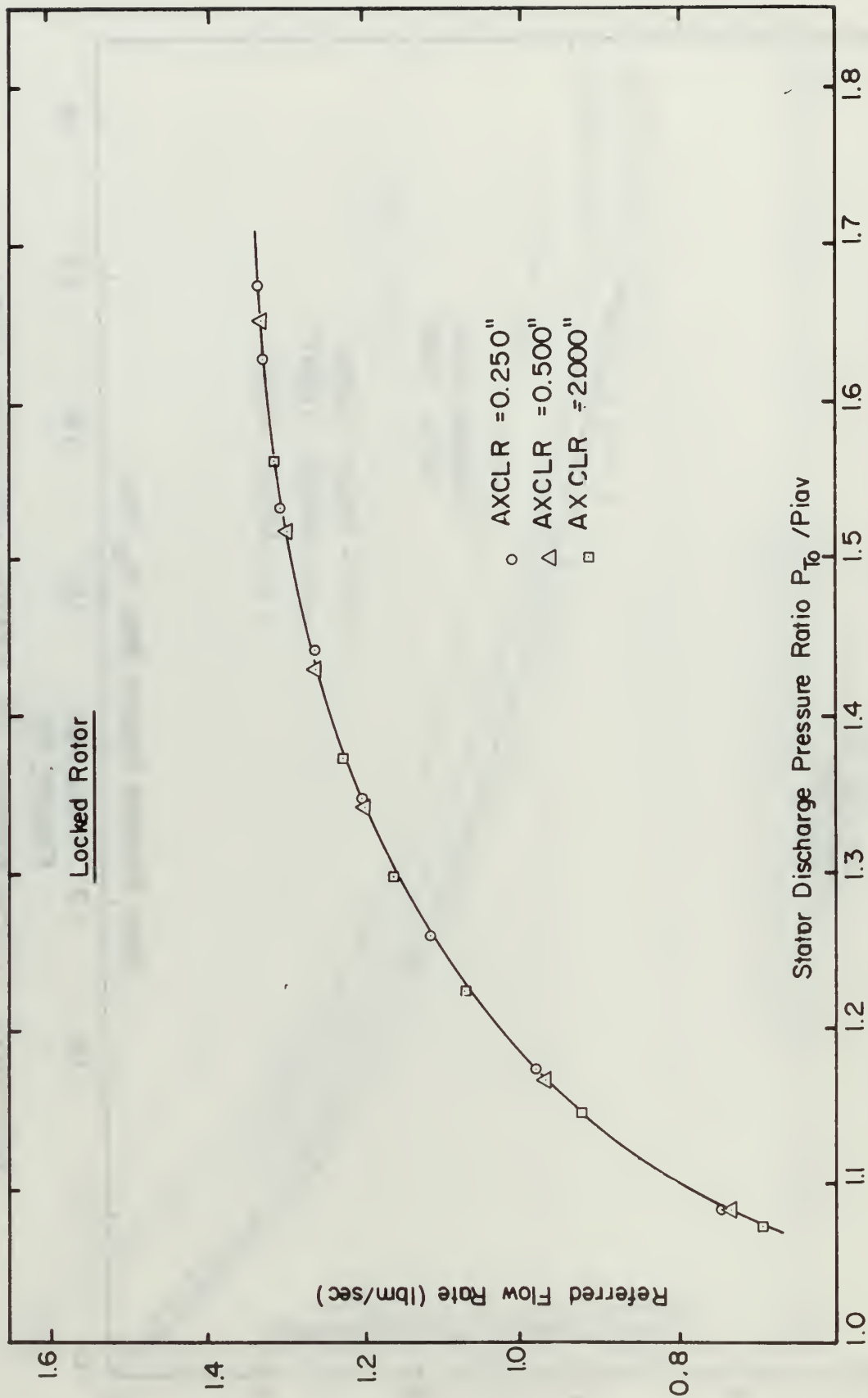


FIGURE 23
REFERRED FLOW RATE VS. STATOR PRESSURE RATIO

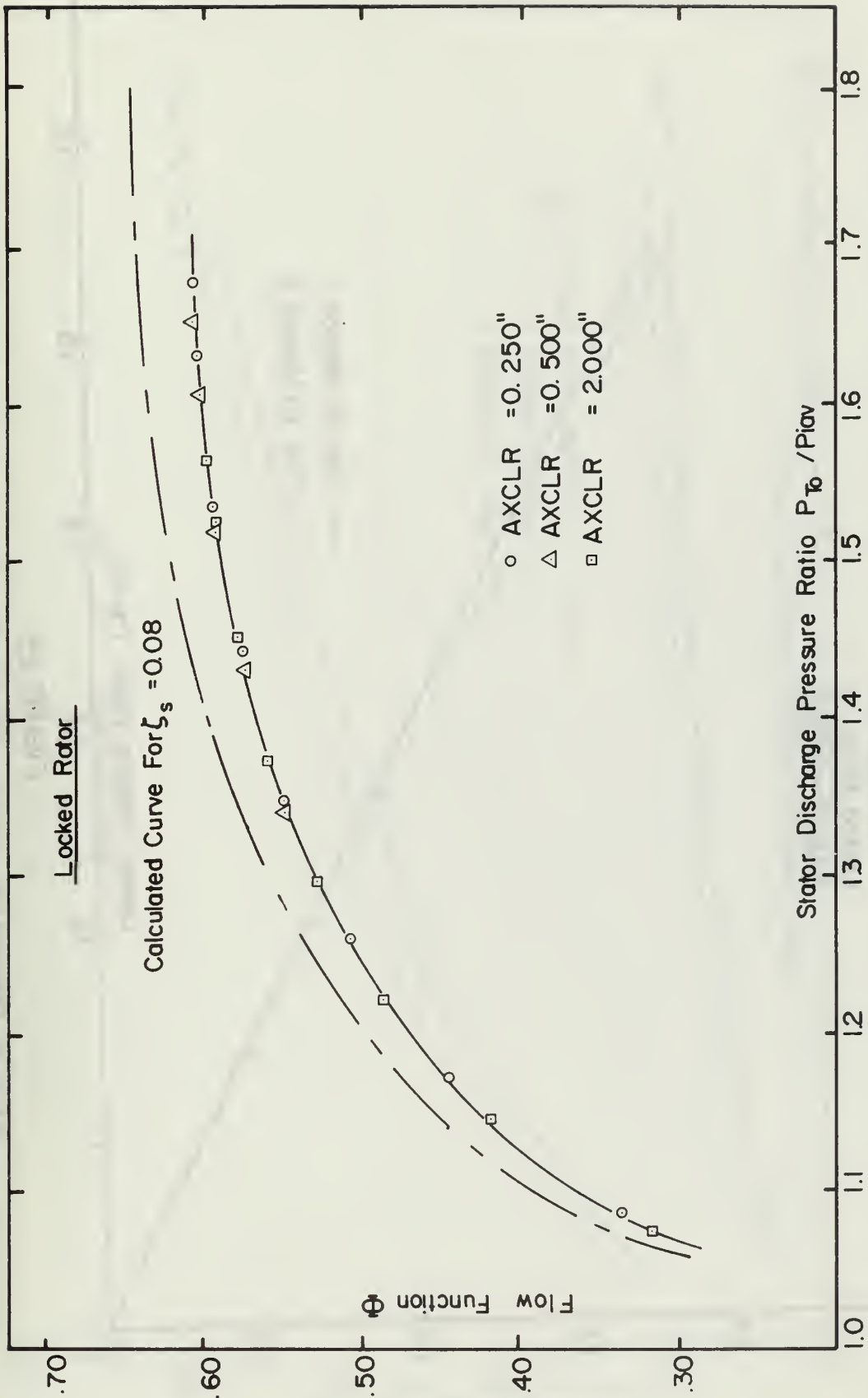


FIGURE 24
FLOW FUNCTION VS. STATOR PRESSURE RATIO

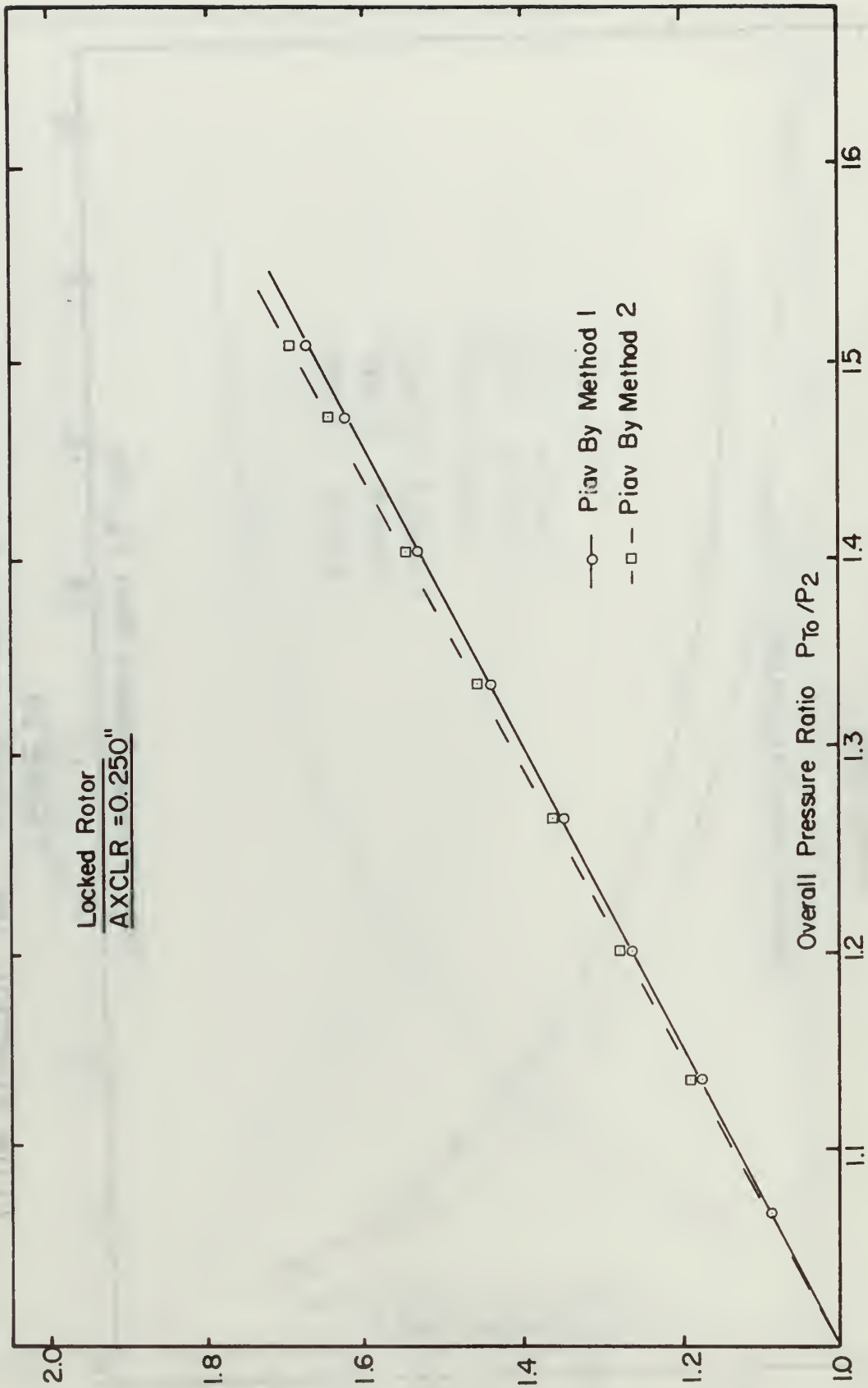


FIGURE 25

STATOR PRESSURE RATIO VS. OVERALL PRESSURE RATIO

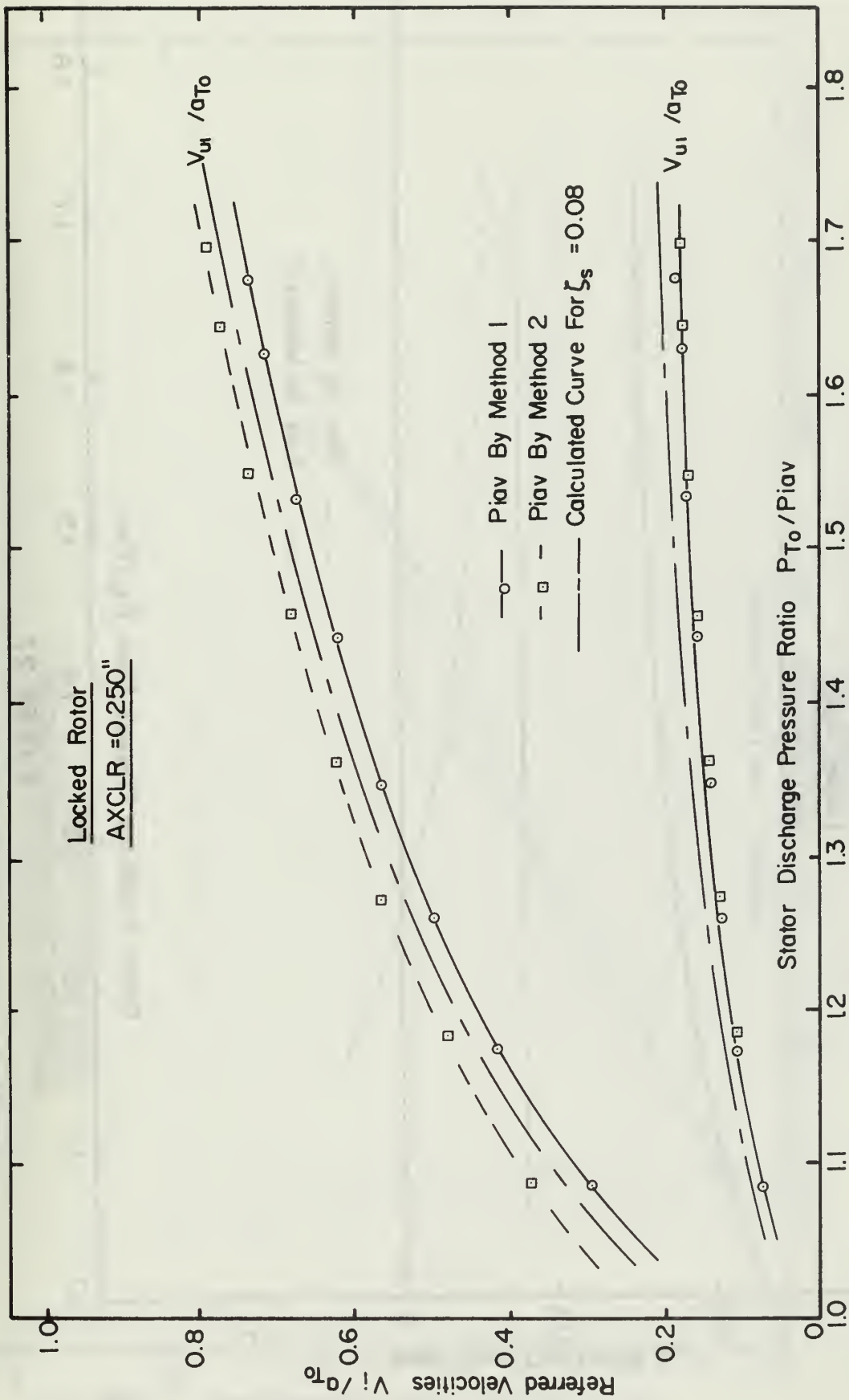


FIGURE 26

REFERRED VELOCITIES VS. STATOR PRESSURE RATIO

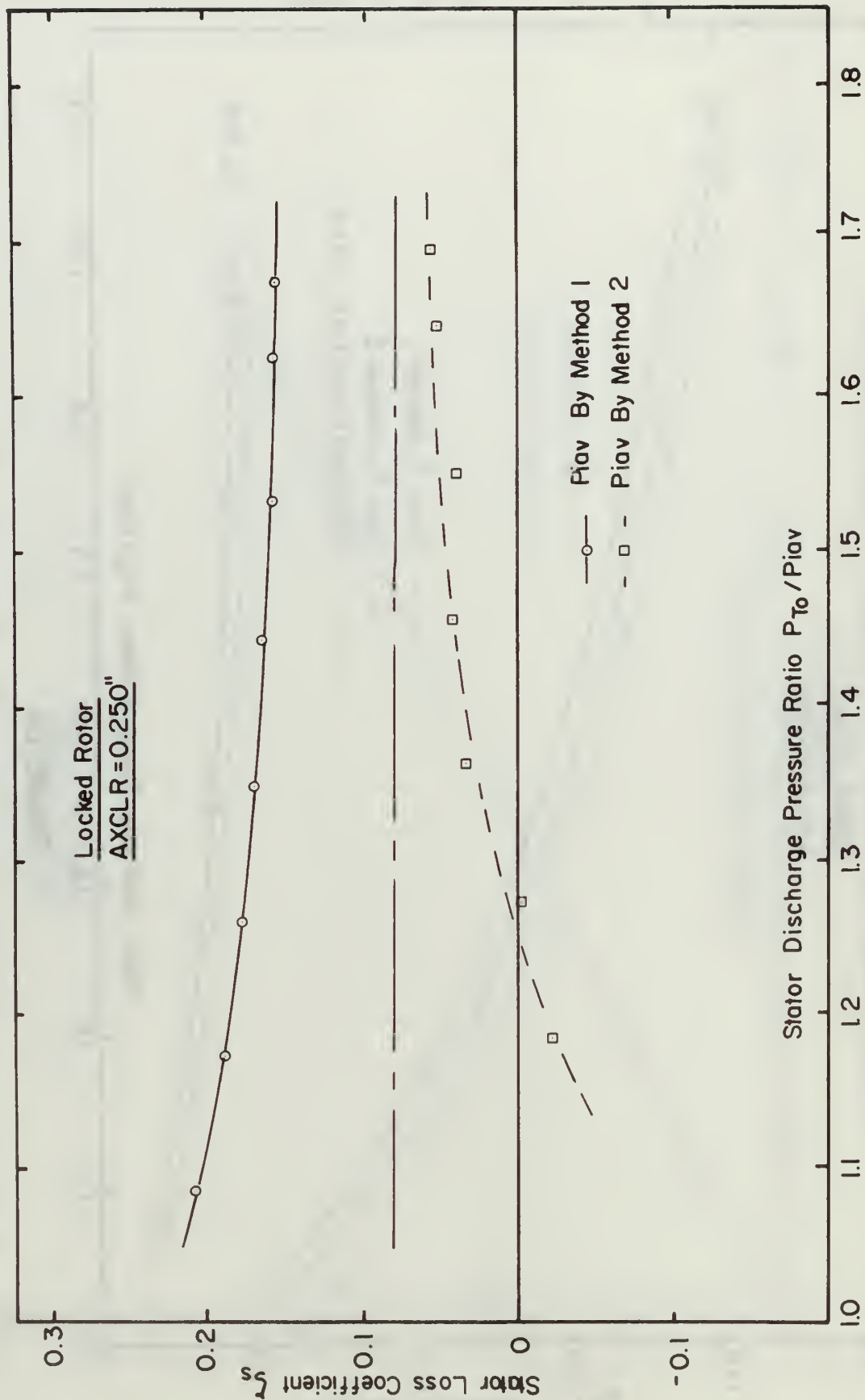


FIGURE 27

STATOR LOSS COEFFICIENT VS. STATOR PRESSURE RATIO

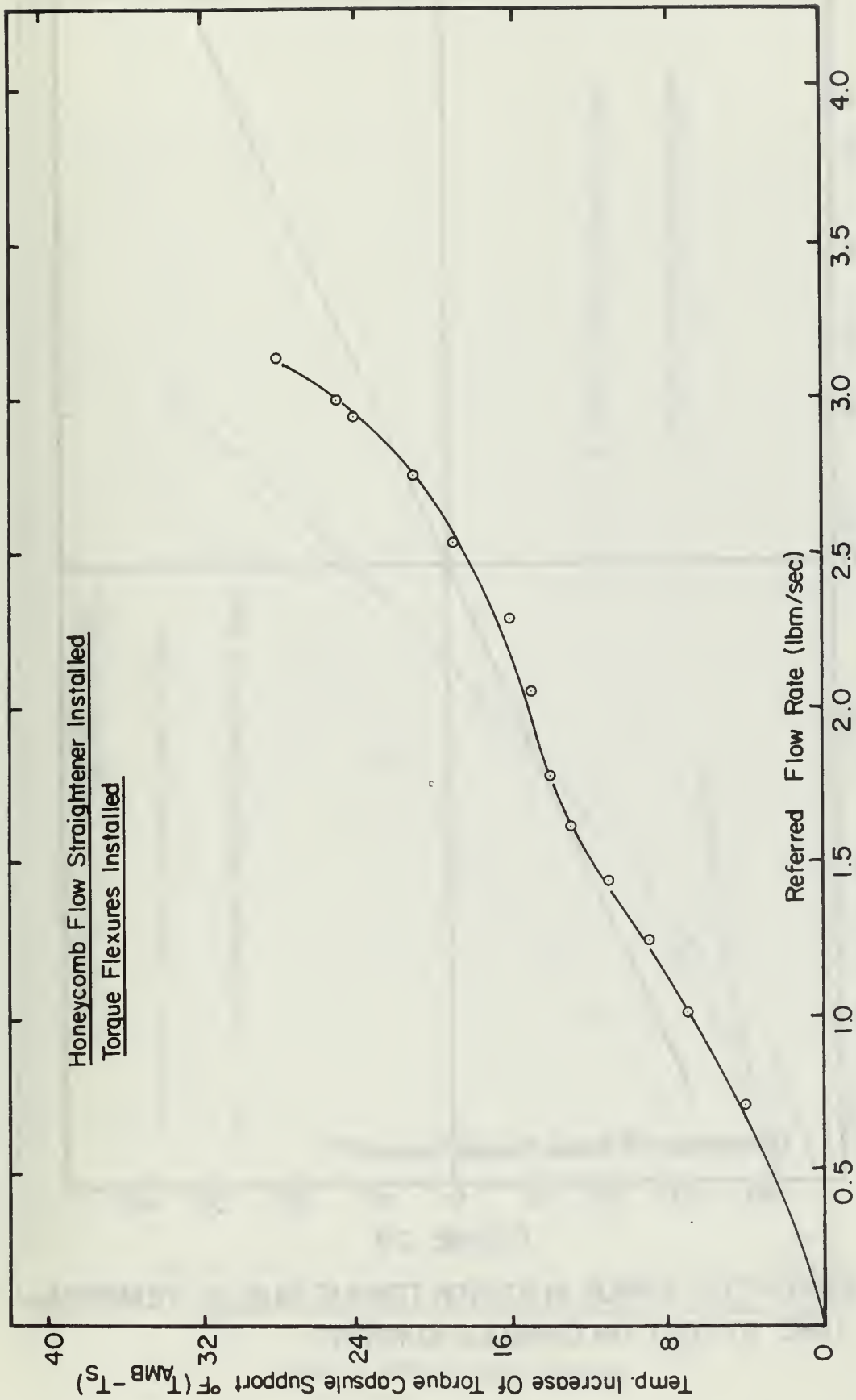


FIGURE 28

TEMPERATURE INCREASE OF CAPSULE SUPPORT VS. REFERRED FLOW RATE

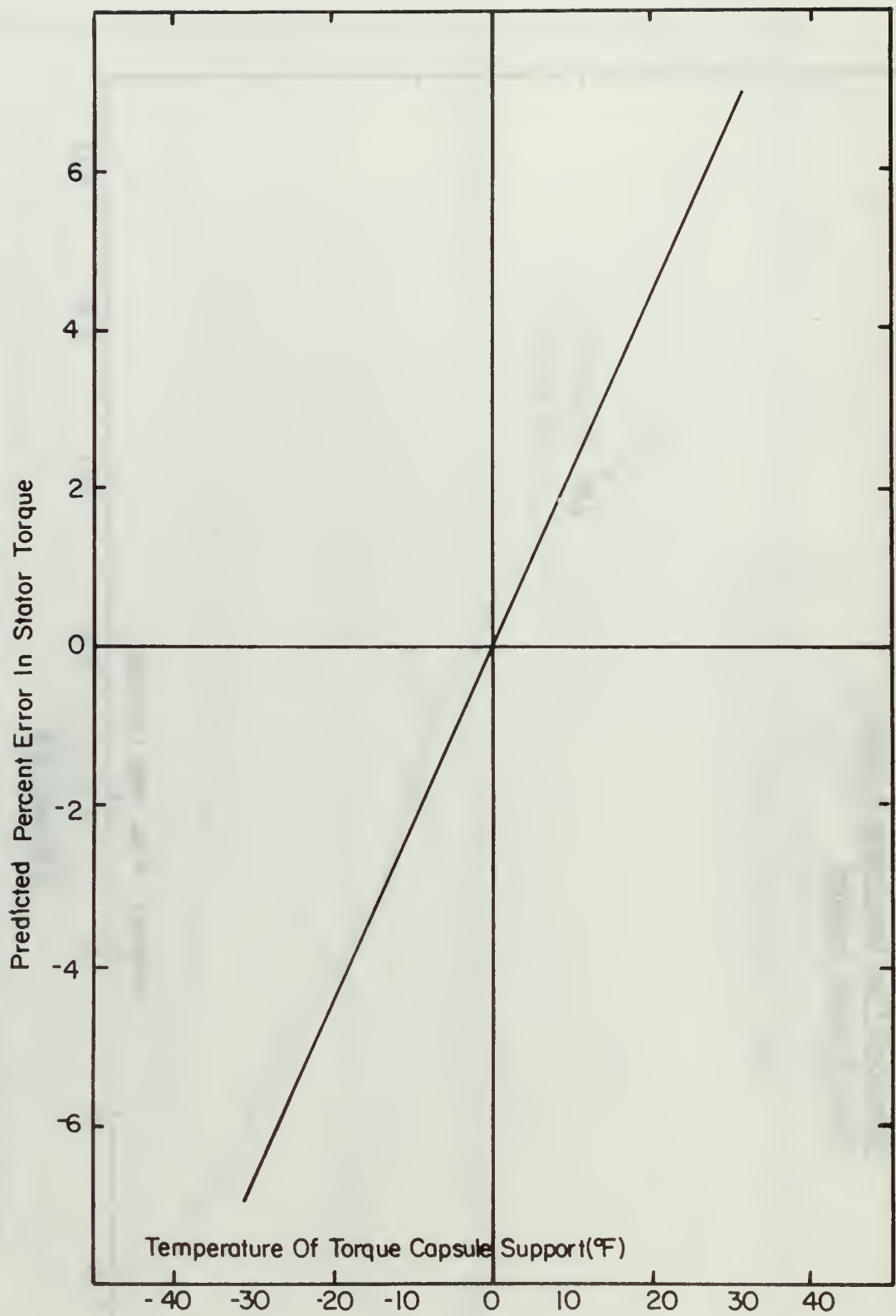


FIGURE 29

PREDICTED ERROR IN STATOR TORQUE DUE TO TEMPERATURE EFFECT ON CAPSULE SUPPORT.

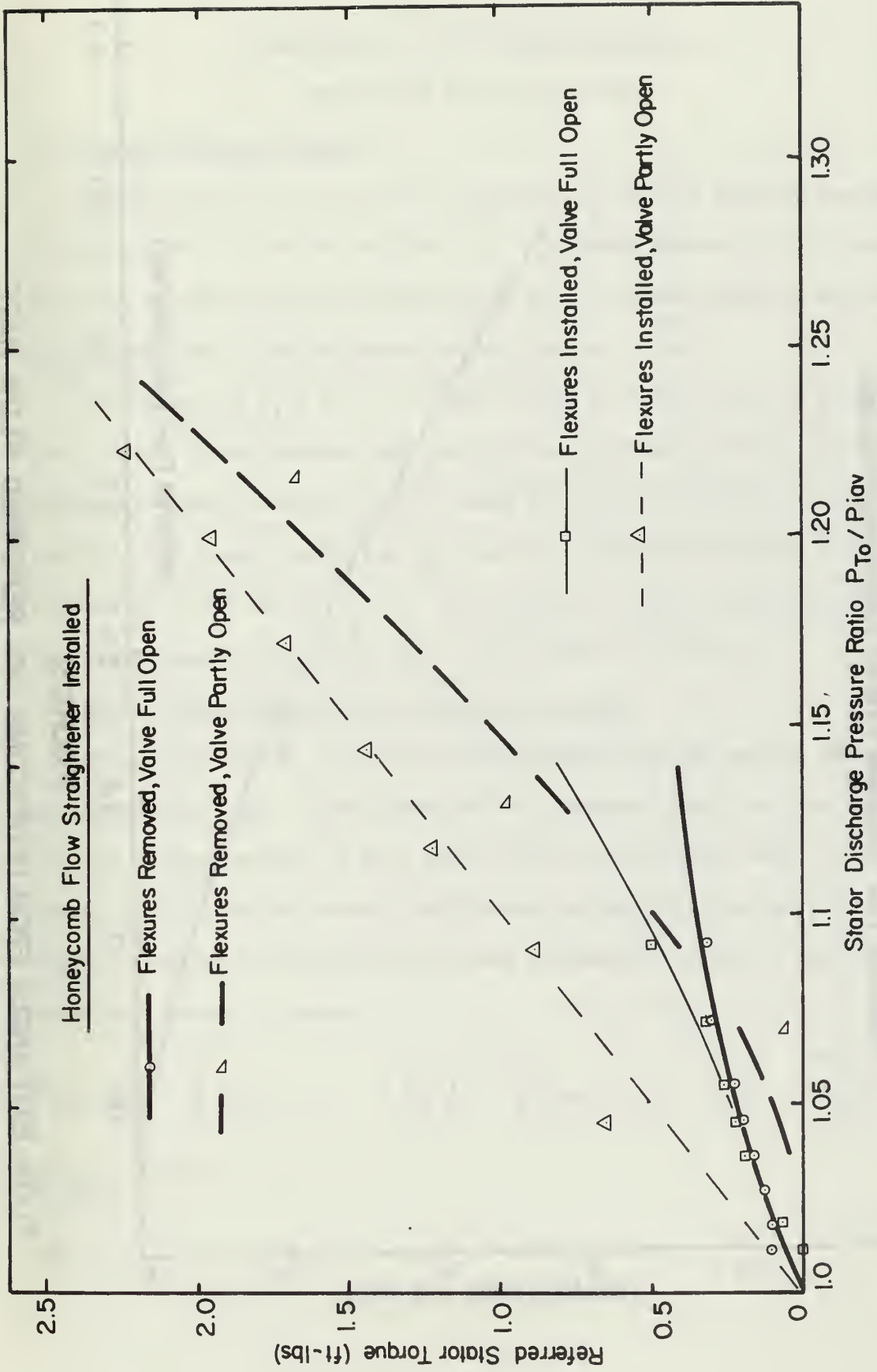


FIGURE 30

REFERRED STATOR TORQUE VS. STATOR PRESSURE RATIO

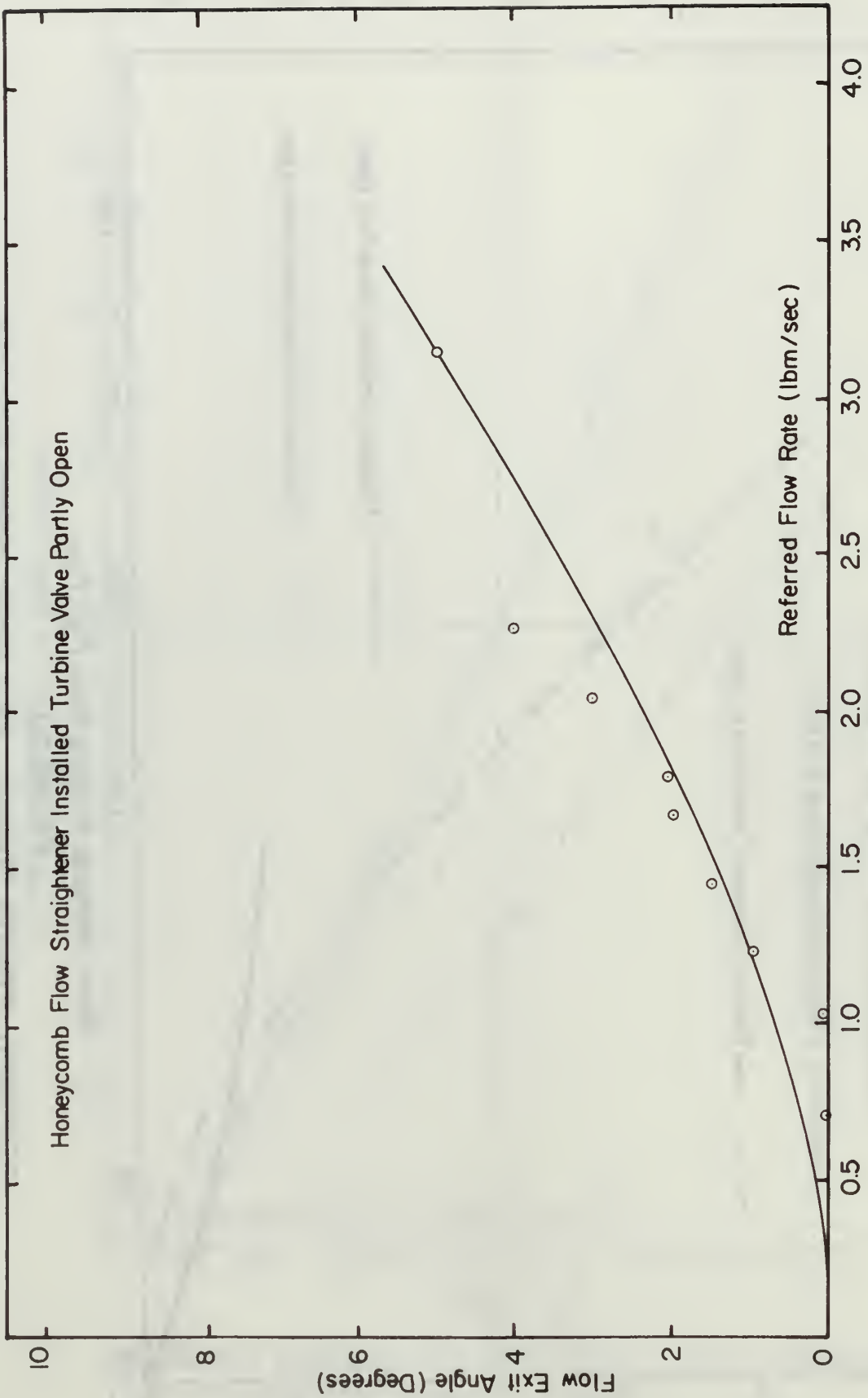


FIGURE 31

FLOW EXIT ANGLE FROM HONEYCOMB VS. REFERRED FLOW RATE

APPENDIX A

PREDICTION OF STATOR DISCHARGE ANGLE AND STATOR LOSS COEFFICIENT

1. Stator Discharge Angle

The prediction of the stator discharge angle uses methods described by Vavra [Ref. 8] and Ainley [Ref. 2]. In these methods, it is assumed that the discharge angle is influenced only by blade geometry and Mach number, and that flow incidence angles have no effect.

For values of $M_1 \leq 0.5$, a formula given by Vavra [Ref. 8] is used for a first approximation, and the effects of blade geometry and Mach number are then accounted for by using the method described by Ainley [Ref. 2]. A linear variation of α is then assumed for values of M_1 between $M_1 = 0.5$ and $M_1 = 1.0$. The results of these calculations for the blade geometry shown in Fig. 7 are listed in Table III.

2. Stator Loss Coefficient By Method of Ainley

The prediction of stator loss coefficient uses the method described by Ainley [Ref. 2]. In this method it is assumed that the loss coefficient is independent of Mach number and is influenced only by blade geometry and flow incidence. The losses are divided into profile losses Y_ρ which include mixing losses, secondary losses Y_s , and tip clearance losses Y_k , where

$$Y_{\rho(i=0)} = \left\{ Y_{\rho(\alpha_1=0)} + \left(\frac{\alpha_1}{\alpha_2} \right)^2 \left[Y_{\rho(\alpha_1=\alpha_2)} - Y_{\rho(\alpha_1=0)} \right] \right\} \times \left(\frac{t/C}{0.2} \right)^{\alpha_1/\alpha_2}$$

and

$$Y_s + Y_K = \left[\lambda + B \left(\frac{K}{h} \right) \right] \left(\frac{C_L}{s/C} \right)^2 \left(\frac{\cos^2 \alpha_2}{\cos^3 \alpha_m} \right)$$

Values of $Y_\rho = f(s/C)$ are given in Fig. 4 of Ref. 2 and values for

$$\lambda = f \left[\frac{(A_2/A_1)^2}{(1 + I.D./O.D.)} \right]$$

are given in Fig. 8. A relation given by Vavra [Ref. 9] is then used to relate the stator loss coefficient to the pressure loss coefficient. The results of these calculations are listed in Table IV.

3. Loss Coefficient By Method of Traupel

The method of Traupel⁵ is one of the most complete methods used and takes into account a large number of variables considered to have an influence on the loss coefficient.

$$\zeta = \zeta_\rho + \zeta_w + \zeta_r + \zeta_{zus}$$

where ζ = Total loss coefficient
 ζ_ρ = Profile loss coefficient
 ζ_w = Wall loss coefficient
 ζ_r = Secondary loss coefficient
 ζ_{zus} = Damping wire loss coefficient

The profile loss coefficient is given by:

$$\zeta_\rho = \zeta_{\rho 0} \cdot \chi_{\rho 0} \cdot \chi_M \cdot \chi_s + \zeta_m + \zeta_F$$

where $\zeta_{\rho 0}$ = Basic loss coefficient
 $\chi_{\rho 0}$ = Reynolds number correction

⁵Traupel, W., "Thermische Turbomaschinen, Erster Band," Springer Verlag, Berlin/Goettingen, Heidelber, 1958, pg. 269-298.

χ_M = Mach number correction

χ_s = Trailing edge thickness correction

ζ_m = Mixing loss correction

ζ_F = Correction for straight blades

The wall loss coefficient, which is due to the friction loss at the annulus of the hub and tip, is given by:

$$\zeta_w = \zeta_{p0} \cdot \chi_{p0} \frac{s \cdot \sin \alpha_1}{h}$$

The secondary loss coefficient is given by:

$$\zeta_r = \psi_\ell \zeta_{r0} + \zeta_s$$

where ψ_ℓ = Aspect ratio correction

ζ_{r0} = Basic secondary loss

ζ_s = Tip leakage loss

A summary of the calculations is listed in Table V.

4. Loss Coefficient Method By Soderberg

The method of Soderberg is taken from a paper by Horlock.⁶

Soderberg bases the loss on blade geometry, aspect ratio, thickness ratio, and Reynolds Number, and then relates the loss coefficient to the gas deflection angle through the aspect ratio only. He ignores such parameters as Mach number and certain non-dimensional gas properties.

The results of a calculation for the converging TTTR nozzles is listed in Table VI.

⁶Horlock, J. H., "Losses and Efficiencies in Axial Flow Turbines," Ins. J. Mech. Sci., Vol. 2, 1960, pg. 59-60.

TABLE III

Prediction of Stator Discharge Angle

$$s = 0.8594 \text{ in}$$

$$a = 0.2050 \text{ in}$$

$$t = 0.0240 \text{ in}$$

$$a/s = 0.2385 \text{ in}$$

$$t/s = 0.0279 \text{ in}$$

For $M_1 \leq 0.5$:

$$\alpha^* = \cos^{-1} \left(\frac{a/s}{K_t} \right) \quad [\text{Ref. 8}]$$

$$\begin{aligned} \text{where } K_t &= 1 - \frac{27}{10^3} \left(\frac{t}{s} 100 \right)^{3.3} \frac{a}{s} \\ &= 0.9809 \end{aligned}$$

$$\text{Hence } \alpha^* = \cos^{-1} (0.24318) = 75.92^\circ$$

$$\alpha = \alpha^* + 4 \left(\frac{s}{e} \right)$$

$$\text{where } e = \frac{J^2}{8Z} \quad [\text{Ref. 2}]$$

$$= 4.5338$$

$$4(s/e) = 0.76^\circ$$

$$\text{Hence } \alpha = 76.68^\circ$$

For $M_1 = 1.0$

$$\alpha (M_1 = 1.0) = \cos^{-1} \left(\frac{a}{s - t/\cos \alpha^*} \right) = \cos^{-1} (0.27152) = 74.25^\circ$$

$$\text{For } M_1 \text{ (average)} = 0.65 \quad \alpha_1 \text{ (average)} = 75.90^\circ$$

TABLE IV

Loss Coefficient by Method of Ainley

$$\alpha_1 = 0^\circ$$

$$\alpha_2 = -75.90^\circ$$

$$t = 0$$

$$c = 1.4313$$

$$s = 0.8594$$

$$s/c = 0.6004$$

$$Y_p(\alpha_1 = 0) = 0.0490$$

Fig. 4

$$Y_s + Y_K = \left[\lambda + B \left(\frac{K}{h} \right) \right] \left(\frac{C_L}{s/C} \right)^2 \left(\frac{\cos^2 \alpha_2}{\cos^3 \alpha_m} \right)$$

$$\text{where } \tan \alpha_m = \frac{\tan \alpha_1 + \tan \alpha_2}{2} = -1.9906$$

$$\alpha_m = -63.33^\circ$$

$B = 0.5$ For non-shrouded wheels

$$\frac{C_L}{s/C} = 2 (\tan \alpha_1 - \tan \alpha_2) \cos \alpha_m = 3.5720$$

$$\lambda = f \left[\frac{\left(\frac{A_2}{A_1} \right)^2}{\left(1 + \text{I.D./O.D.} \right)} \right]$$

$$\frac{A_2}{A_1} = \frac{A_{02} \cos \alpha_2}{A_{01} \cos \alpha_1} = \frac{\pi D_{m2} h_2 \cos \alpha_2}{\pi D_{m1} h_1 \cos \alpha_1}$$

$$h_1 = h_2, \quad D_{m1} = D_{m2}$$

$$\text{Hence } \lambda = f \left[\frac{\cos^2 \alpha_2 / \cos^2 \alpha_1}{\left(1 + R_{\text{hub1}} / R_{\text{tip1}} \right)} \right] = f (0.0321) = 0.0056$$

Fig. 8

$$K = 0$$

$$Y_s + Y_K = 0.0056 (3.5720)^2 \frac{\cos^2(-75.90)}{\cos^3(-63.33)} = 0.0471$$

$$\text{Hency } Y = Y_\rho + Y_s + Y_k = 0.0961$$

$$t/s = 0.0279$$

$$\text{Trailing edge correction factor } F = 1.02$$

$$\text{Hence } Y = 1.02 (0.0961) = 0.0980$$

$$\zeta_s = \frac{\left[\frac{1+Y}{1+Y\left(\frac{P_1}{P_{T0}}\right)} \right]^{\frac{Y-1}{Y}} - 1}{\left(\frac{1}{P_1/P_{T0}}\right)^{\frac{Y-1}{Y}} - 1}$$

[Ref. 9]

page 99

$$\text{With } M_1 \text{ (average)} = 0.65, \left(\frac{P_1}{P_{T0}}\right)_{\text{average}} = 0.7055 \text{ (Run 15)}$$

$$\zeta_s = 0.0756$$

TABLE V

Loss Coefficient By Method of Traupel

$$\zeta_{\rho 0} = f(\alpha_0, \alpha_1) = 0.0040$$

Fig. B3

$$\psi_{\rho 0} = f_1\left(\text{Re}, \frac{KS}{C}\right)$$

$$\text{Re} = \frac{V_1 C}{\nu} = \frac{750 \times 1.4313/12}{1.564 \times 10^{-4}} = 5.72 \times 10^5$$

$$K = 0$$

$$\text{Hence } \chi_{\rho 0} = 0.92$$

Fig. B5

$$\psi_M = f(M_1) = 0.075 \text{ for } M_1 = 0.65$$

Fig. B4

$$\psi_s = f(1-K)$$

$$1 - K = 1 - \left(s - \frac{t}{\cos \alpha_1}\right) = 1 - \left(0.8594 - \frac{0.0240}{\cos 75.9^\circ}\right) = 0.2392$$

$$\text{Hence } \psi_s = 1.60$$

Fig. B6

$$\zeta_M = f(1 - K) = 0.0700$$

Fig. B6

$$\zeta_F = f(h/D_m)$$

$$h/D_m = \frac{0.690}{8.48} = 0.0814$$

$$\text{Hence } \zeta_F = 0.0250$$

Fig. B7

$$\text{Thus } \zeta_\rho = 0.0040 \times 0.92 \times 0.075 \times 1.60 + 0.0700 + 0.0250$$

$$\text{or } \zeta_\rho = 0.0954$$

$$\zeta_w = 0.0040 \times 0.92 \times \frac{0.8594 \times \sin 75.9}{0.690} = 0.0044$$

$$\psi_\ell / \psi_{\rho 0} = f(c/h)$$

$$c/h = \frac{1.4313}{0.690} = 2.078$$

$$\text{Hence } \psi_\ell / \psi_{\rho 0} = 1.70$$

Fig. B9

$$\text{and } \psi_\ell = 1.70 (0.92) = 1.563$$

$$\zeta_{r0} = f\left(\frac{V_{u1}}{U_1}\right)$$

$$\frac{V_{u1}}{U_1} = \frac{725}{555} = 1.306$$

From point 8 Run 15

$$\text{Hence } \zeta_{r0} = 0.0350$$

Fig. B8

$$\zeta_s = f(h_s/h) = 0$$

Not applicable to stator

$$\text{Hence } \zeta_r = 1.563 \times 0.0350 = 0.0547$$

$$\zeta_{zus} = 0$$

Not applicable to stator

$$\text{Hence } \zeta_s = 0.0954 + 0.0044 + 0.0547 = 0.1545$$

TABLE VI

Loss Coefficient By Method of Soderberg

$$\xi^1 = (1 + \xi^*) \left[0.975 + 0.075 \frac{b}{h} \right] - 1$$

$$\alpha_0 = 0$$

$$\alpha_1^\dagger = 75.90^\circ$$

$$b = 0.975 \quad \text{Blade axial chord}$$

$$h = 0.690 \quad \text{Blade height}$$

$$t/c = 0.248 \quad \text{Thickness/chord}$$

$$\xi^* = f(\Delta\alpha) = 0.0700$$

Fig. 5

$$\text{Hence } \xi' = 0.1580$$

$$\text{And } \zeta_s = \frac{\left[\frac{1 + \xi}{1 + \xi \left(\frac{P_1}{P_{T0}} \right)} \right]^{\frac{\gamma - 1}{\gamma}} - 1}{\left(\frac{1}{\frac{P_1}{P_{T0}}} \right)^{\frac{\gamma - 1}{\gamma}} - 1}$$

$$\text{With } M_1 \text{ (average)} = 0.65, \quad \left(\frac{P_1}{P_{T0}} \right)_{\text{average}} = 0.7055 \text{ (Run 15)}$$

$$\zeta_s = 0.1022$$

APPENDIX B

PREDICTION OF TORQUE ON CLOSURE

PLATE AND SHROUD

1. Torque on Closure Plate

Because of the proximity of the rotor and its high speed rotation, a core of rotating fluid will be set up between the rotor and closure plate, and friction will thus transmit some torque to the closure plate.

Schlichting⁷ gives a formula for the torque transmitted to a stationary flat plate by a rotating parallel plate, assuming the core of fluid rotates at one-half the speed of the wheel.

For turbulent flow:

$$M = 0.037 \rho \omega^2 R^5 \left(\frac{\nu}{\omega R^2} \right)^{1/5}$$

Using values of ρ and ν for air at 520°R and one atmosphere,

with $R = 3.87$ in

$$M = 0.037 \times 0.002378 \left(\frac{\pi N}{60} \right)^2 \left(\frac{3.87}{12} \right)^5 \left[\frac{173 \times 10^{-6} \times 60 \times 144}{\pi N \times 3.87^2} \right]^{1/5}$$

This results in a moment of 0.007 ft-lbs at 10,000 RPM and 0.023 ft-lbs at 20,000 RPM.

2. Torque on Shroud

A torque will be transmitted to the rotor shroud by the tangential component of V_1 and by the scrubbing of rotor at the tip. A

⁷Schlichting, H., "Boundary Layer Theory," pg. 607

formula given by Schlichting⁸ for the torque transmitted between two rotating cylinders is:

$$u(r) = \frac{1}{r_2^2 - r_1^2} \left[r \left(\omega_2 r_2^2 - \omega_1 r_1^2 \right) - \frac{r_1^2 r_2^2}{r} \left(\omega_2 - \omega_1 \right) \right]$$

$$\frac{du}{dr} = \frac{1}{r_2^2 - r_1^2} \left[\left(\omega_2 r_2^2 - \omega_1 r_1^2 \right) + \frac{r_1^2 r_2^2}{r^2} \left(\omega_2 - \omega_1 \right) \right]$$

$$T = \mu \frac{du}{dr}$$

With $\omega_2 = 0$ and $r = r_2$,

$$M = T A_2 r_2 = \mu \left(\frac{du}{dr} \right) \left(2\pi r_2 h \right) r_2$$

$$\text{or } M = 4\pi\mu h \frac{r_1^2 r_2^2 \omega_1}{r_2^2 - r_1^2}$$

As before, with the core assumed to rotate at one-half the rotor speed, and the values for air at standard conditions, the moment transmitted is 0.018 ft-lbs at 10,000 RPM and 0.037 ft-lbs at 20,000 RPM.

⁸Schlichting, H., "Boundary Layer Theory," pg. 81

APPENDIX C

PREDICTION OF STATOR DISCHARGE

PRESSURE DISTRIBUTION

The equation of motion for absolute flow through a stator, as given by Vavra [Ref. 9] is:

$$\frac{\partial \bar{V}}{\partial t} + \nabla H = \bar{V} \times (\nabla \times \bar{V}) + T \nabla s + \bar{f}_f \quad (C.1)$$

If steady, frictionless flow is assumed, the equation reduces to:

$$\nabla H = \bar{V} \times (\nabla \times \bar{V}) + T \nabla s \quad (C.2)$$

Each variable in the above equation may then be expressed in an axisymmetric coordinate system, where

$$\nabla H = \bar{i}_m \frac{\partial H}{\partial m} + \frac{\bar{i}_\theta}{R} \frac{\partial H}{\partial \theta} + \bar{i}_n \frac{\partial H}{\partial n}$$

$$T \nabla s = T \left(\bar{i}_m \frac{\partial s}{\partial m} + \frac{\bar{i}_\theta}{R} \frac{\partial s}{\partial \theta} + \bar{i}_n \frac{\partial s}{\partial n} \right)$$

$$\begin{aligned} \text{and } \bar{V} \times (\nabla \times \bar{V}) = & \bar{i}_m \left\{ \frac{V_\theta}{R} \left[\frac{\partial (RV_\theta)}{\partial m} - \frac{\partial V_m}{\partial \theta} \right] - V_n \left[\frac{\partial V_m}{\partial n} + V_m K_m \right] \right. \\ & \left. + V_n \left[\frac{\partial V_n}{\partial m} + V_n K_n \right] \right\} + \frac{\bar{i}_\theta}{R} \left\{ V_m \left[\frac{\partial V_m}{\partial \theta} - \frac{\partial (RV_\theta)}{\partial m} \right] \right. \\ & \left. + V_n \left[\frac{\partial V_n}{\partial \theta} - \frac{\partial (RV_\theta)}{\partial n} \right] \right\} + \bar{i}_n \left\{ \frac{V_\theta}{R} \left[\frac{\partial (RV_\theta)}{\partial n} - \frac{\partial V_n}{\partial \theta} \right] \right. \\ & \left. + V_m \left[\frac{\partial V_m}{\partial n} + V_m K_m \right] - V_m \left[\frac{\partial V_n}{\partial m} + V_n K_n \right] \right\} \end{aligned}$$

Equating components:

$$\bar{i}_m: \frac{\partial H}{\partial m} = \left\{ \frac{V_\theta}{R} \left[\frac{\partial (RV_\theta)}{\partial m} - \frac{\partial V_m}{\partial \theta} \right] - V_n \left[\frac{\partial V_m}{\partial n} + V_m K_m \right] + \right.$$

$$V_n \left[\frac{\partial V_n}{\partial m} + V_n K_n \right] + \frac{\partial s}{\partial m} \quad (C.3)$$

$$\begin{aligned} \bar{i}_\theta: \frac{1}{R} \frac{\partial H}{\partial \theta} &= \frac{V_m}{R} \left[\frac{\partial V_m}{\partial \theta} - \frac{\partial (RV_\theta)}{\partial m} \right] + \frac{V_n}{R} \left[\frac{\partial V_n}{\partial \theta} - \frac{\partial (RV)}{\partial n} \right] \\ &+ \frac{1}{R} \frac{\partial s}{\partial \theta} \quad (C.4) \end{aligned}$$

$$\begin{aligned} \bar{i}_n: \frac{\partial H}{\partial n} &= \left\{ \frac{V_\theta}{R} \left[\frac{\partial (RV_\theta)}{\partial n} - \frac{\partial V_n}{\partial \theta} \right] + V_m \left[\frac{\partial V_m}{\partial n} + V_m K_m \right] \right. \\ &\left. - V_n \left[\frac{\partial V_n}{\partial m} + V_n K_n \right] \right\} + \frac{\partial s}{\partial n} \quad (C.5) \end{aligned}$$

where m = streamline coordinate
 n = coordinate normal to streamline
 K_m = curvature of streamline
 K_n = curvature of normal

If axisymmetric flow is assumed, all terms with $\partial/\partial \theta$ vanish and since the equation is written along a streamline where $V_n = 0$

$$\frac{1}{R} \frac{\partial H}{\partial \theta} = 0 = \frac{V_m}{R} \frac{\partial (RV_\theta)}{\partial m} \quad (C.6)$$

Since V_m is not zero, $\frac{\partial (RV_\theta)}{\partial m} = 0$ (C.7)

Then $\frac{\partial H}{\partial m} = \frac{\partial s}{\partial m}$ and if adiabatic flow is assumed then $\frac{\partial H}{\partial m} = 0$ means H is constant along a streamline. In addition, $\frac{\partial s}{\partial m} = 0$ means the flow is isentropic along a streamline. A consequence of these last two statements results in isentropic flow or $\bar{V} \times (\nabla \times \bar{V}) = 0$. The remaining

equation is then:

$$\frac{\partial H}{\partial n} = \frac{V_\theta}{R} \frac{\partial (RV_\theta)}{\partial n} + V_m \frac{\partial V_m}{\partial n} + V_m^2 K_m + \frac{\partial s}{\partial n} \quad (C.8)$$

or

$$\frac{\partial}{\partial n} \left(\frac{V_m^2}{2} \right) + V_m^2 K_m + \frac{V_\theta}{R} \frac{\partial (RV_\theta)}{\partial n} - \frac{\partial H}{\partial n} + T \frac{\partial s}{\partial n} = 0$$

Employing the relation $H = C_\rho T + \left(\frac{V_\theta^2 + V_m^2}{2} \right)$ the following important equation results:

$$\begin{aligned} \frac{\partial}{\partial n} \left(V_m^2 \right) + V_m^2 \left(2K_m - \frac{1}{C_\rho} \frac{\partial s}{\partial n} \right) + 2 \frac{V_\theta}{R} \frac{\partial (RV_\theta)}{\partial n} - 2 C_\rho \frac{\partial T}{\partial n} \\ + \left(2T - \frac{V_\theta^2}{C_\rho} \right) \frac{\partial s}{\partial n} = 0 \end{aligned} \quad (C.9)$$

Equation (C.9) is known as the Radial Equilibrium Equation and is a linear differential equation with variable coefficients.

If three additional important assumptions are made, namely that there is no temperature or entropy gradient at the stator entrance, and that $\frac{\partial (RV_\theta)}{\partial n} = 0$ or free vortex flow exists ahead of the stator, and finally that the streamlines are cylindrical surfaces with $K_m = 0$, then $\frac{\partial}{\partial n} \left(V_m^2 \right) = 0$, which means V_m is not a function of radius. If $\frac{\partial}{\partial n} (RV_\theta) = 0$ can be maintained in the stator, the same conclusion can be made for V_m at the stator discharge.

The consequence of the above series of assumptions results in a set of velocity profiles as shown in Fig. 32. Also imposed on the profiles shown in Fig. 32 are the effects of annulus friction and secondary flow.

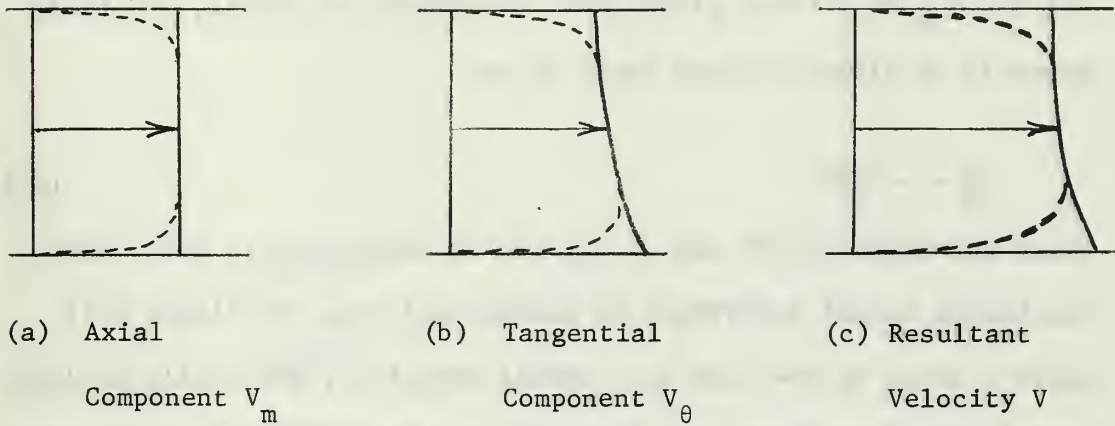


Figure 32

Predicted Velocity Profiles at Stator Discharge

The unequal pressure between the convex and concave sides of a blade cause trailing vortices to be formed and are the origin of the secondary flow. The vortices cause a reduction in the tangential component near the hub and tip radii. It is evident from the above velocity profile in Fig. 32C that the pressure distribution must necessarily be a complicated one and not linear.

When the assumption that $\frac{\partial(RV_\theta)}{\partial n} = 0$ is put in cylindrical coordinates, so that:

$$\frac{\partial(RV_u)}{\partial R} = \frac{\partial(RV_a \tan\alpha)}{\partial R} = 0$$

or

$$V_a R \frac{\partial(\tan\alpha)}{\partial R} + V_a \tan\alpha = 0$$

hence

$$\frac{\partial(\tan\alpha)}{\partial R} = \frac{\partial\alpha}{\partial R} = -\frac{\tan\alpha}{R} \quad (C.10)$$

But for $\frac{\partial(RV_u)}{\partial R} = 0$ the blades must themselves be radial, and their geometry is given by Vavra [Ref. 9] as

$$\frac{\partial \alpha}{\partial R} = + \frac{\tan \alpha}{R} \quad (C.11)$$

Since equations (C.10) and (C.11) are in opposition to each other, the blades cannot everywhere be radial, and thus the blades will exert a force on the flow in a radial direction, which will produce curved stream surfaces. As a result, the assumption of axisymmetric stream surfaces is in error, and in addition $\frac{\partial(RV_u)}{\partial R} = 0$ cannot be maintained in the stator, so free vortex flow is not possible. Thus $\frac{\partial V_a^2}{\partial R} = -2 \frac{V_u}{R} \frac{\partial(RV_u)}{\partial R}$ and this can be solved if it is assumed there is constant total enthalpy and flow angle ahead of the stator. The solution is given by Vavra [Ref. 8] which is:

$$V_a = V_{am} \left(\frac{R_m}{R} \right)^{\sin^2 \alpha_1}$$

where V_{am} = axial velocity at the mean radius. Thus $V_a = f(R)$ and the resulting velocity or pressure distribution becomes extremely complicated.

APPENDIX D

STACK RESULTS

CONFIGURATION- CONVERGING NOZZLES, SHROUD P/N 1-57, INSERT P/N 2-05-3(STRAIGHT)

RUN NUMBER 15 DATE 1 AUG 64

METHOD J=1

POINT	FAX(+)	CLFAX(+)	FC(+)	F1(-)	F2(-)	F3(-)	F4(-)	F5(-)	F6A(-)	FNET	TOR(+)	CLTOR(+)	KFAX	RTORO
1	-15.62	9.23	1261.90	56.34	49.13	50.55	89.75	66.72	10.67	10.67	18.73	0.23	-10.46	9.98
2	-0.28	10.78	1201.90	56.34	46.13	56.27	88.91	67.49	12.27	12.27	18.07	0.23	-10.54	9.01
3	17.38	11.73	1201.90	56.34	46.13	56.43	88.91	68.36	11.91	11.91	18.03	0.04	18.11	9.42
4	50.66	12.23	1201.90	56.34	46.13	56.43	88.91	69.49	11.90	11.90	18.07	0.04	11.61	9.42
5	50.66	13.56	1201.90	56.34	46.13	56.43	88.91	70.28	11.44	11.44	18.20	0.04	20.12	8.58
6	56.66	14.56	1201.90	56.34	45.60	55.73	94.15	72.78	10.63	10.63	18.04	0.04	20.12	8.57
8	84.40	17.02	1201.90	56.34	45.60	55.73	94.15	74.22	9.75	9.75	11.90	0.04	37.90	7.59

FLOW RATES(LBM/SEC), RE(NUZ), FLOW FNC, AND STATOR BLOCKAGE FACTOR

POINT	NOZZLE FLOW	TURRINE FLOW	LABLEAK	RE	PHI	XI
1	1.8637	1.8122	0.0335	5117.0	0.5798	0.8905
2	1.8382	1.8648	0.0334	5104.0	0.5746	0.8913
3	1.8241	1.7804	0.0338	5062.0	0.5709	0.8905
4	1.8776	1.7778	0.0340	5076.0	0.5693	0.8897
5	1.8088	1.7711	0.0338	5010.0	0.5681	0.8884
6	1.7685	1.7344	0.0341	4907.0	0.5537	0.8889
8	1.7332	1.6950	0.0343	4808.0	0.5420	0.8886

PRESSURES(PSTIA) AND PRESSURE RATIOS

PAMB=14.57

POINT	PNOZ	PTPL	PTC	PIAV	PHC	PLENUM PR(PTPL/PHD)	STATOR PR(PTO/PIAV)
1	36.03	22.12	21.81	14.81	14.57	1.2186	1.4793
2	35.07	22.17	21.87	14.81	14.57	1.2156	1.4790
3	36.02	22.18	21.87	14.20	14.57	1.2156	1.4350
4	36.15	22.17	21.86	14.28	14.57	1.2119	1.4350
5	36.13	22.18	21.86	14.40	14.57	1.2102	1.4267
6	36.03	22.18	21.86	14.85	14.57	1.2149	1.3779
8	36.03	22.17	21.88	16.27	14.57	1.2149	1.3446

TEMPERATURES(DEC F)

POINT	TTL	TTO	T1	T11	T111
1	567.93	567.93	508.15	507.99	507.99
2	567.93	567.93	515.21	515.16	515.16
3	568.23	568.23	518.39	518.39	518.39
4	568.23	568.23	520.46	520.46	520.46
5	568.53	568.53	520.48	520.48	520.48
6	568.77	568.77	521.51	521.51	521.51
8	568.96	568.96	521.51	521.51	521.51

ANGLE, VELOCITY, ALPHA, BETA, GAMMA, DELTA, EPSILON, ZETA, THETA, AND MACH NOS

POINT	VAI	VUI	VI	V:VS	ALPHA I	VCHEFS	MVI	MVAI	MVAL	MVUI
1	185.74	781.74	768.76	441.50	75.81	0.140	2.0421	0.1683	0.1683	0.0913
2	184.71	777.22	765.16	437.49	76.24	0.137	2.0452	0.1690	0.1693	0.0935
3	183.68	772.69	761.76	433.29	76.67	0.134	2.0483	0.1697	0.1697	0.0957
4	182.64	768.16	758.41	429.25	77.10	0.131	2.0514	0.1704	0.1704	0.0979
5	181.61	763.64	755.01	425.41	77.53	0.127	2.0545	0.1711	0.1711	0.1001
6	180.57	759.11	751.68	421.76	77.96	0.124	2.0576	0.1718	0.1718	0.1023
7	179.54	754.59	748.41	418.29	78.39	0.121	2.0607	0.1725	0.1725	0.1045
8	178.51	750.06	745.16	414.99	78.82	0.118	2.0638	0.1732	0.1732	0.1067
9	162.97	697.71	675.13	747.74	79.25	0.115	2.0669	0.1739	0.1739	0.1089

RELATIVE VELOCITY, ALPHA, BETA, GAMMA, DELTA, EPSILON, ZETA, THETA, AND MACH NOS

POINT	MAI	MUI	M1	UI	BETA I	MVI
1	185.74	371.74	41.71	376.01	69.26	0.1762
2	184.71	367.22	41.26	371.96	69.69	0.1784
3	183.68	362.69	40.81	367.88	70.12	0.1806
4	182.64	358.16	40.36	363.76	70.55	0.1828
5	181.61	353.64	39.91	359.73	70.98	0.1850
6	180.57	349.11	39.46	355.76	71.41	0.1872
7	179.54	344.59	39.01	351.84	71.84	0.1894
8	178.51	340.06	38.56	347.97	72.27	0.1916
9	162.97	181.74	16.60	631.61	6.44	0.1657

EFFICIENCIES

POINT	ZETA	STATOR	ETA	STAT	MU	ZETA
1	0.1764	0.8230	0.8230	0.8230	0.8230	0.8230
2	0.1756	0.8244	0.8244	0.8244	0.8244	0.8244
3	0.1761	0.8239	0.8239	0.8239	0.8239	0.8239
4	0.1743	0.8217	0.8217	0.8217	0.8217	0.8217
5	0.1806	0.8194	0.8194	0.8194	0.8194	0.8194
6	0.1820	0.8190	0.8190	0.8190	0.8190	0.8190
7	0.1820	0.8190	0.8190	0.8190	0.8190	0.8190
8	0.1820	0.8190	0.8190	0.8190	0.8190	0.8190
9	0.1820	0.8190	0.8190	0.8190	0.8190	0.8190

ACTOR RESULTS

CONFIGURATION- CIRCULAR ARC, SHARPLE MOTOR, P/N 1044-A, AXIAL (INC 0.250 IN, RADIAL CLNC 0.009 IN

RUN NUMBER 15 DATE 1 AUG 69

METHOD J= 1

PRESSURES(PST1) AND PRESSURE RATIOS

PAMB=14.57
 POINT PTO P1AV P1Z P2=PHO OVERALL PR(P10/P2)

1	21.91	14.83	14.76	14.57	1.5041
2	21.87	15.03	14.75	14.57	1.5014
3	21.87	15.20	14.76	14.57	1.5014
4	21.96	15.27	14.78	14.57	1.5014
5	21.91	15.47	14.84	14.57	1.5041
6	21.88	15.85	15.64	14.57	1.5008
7	21.88	16.27	15.35	14.57	1.5021

TEMPERATURES(TEG R)

POINT	TT0	T1	TE	TT2	T2	T215	T21H	TT215	DELTA T15	DELTA T1H
1	506.83	509.15	525.83	518.38	507.84	505.74	495.54	497.43	61.35	47.45
2	506.83	515.21	527.06	518.09	512.08	510.66	500.47	503.53	61.63	48.43
3	504.00	518.97	528.26	518.10	513.06	511.64	501.45	504.51	61.90	48.21
4	504.04	520.03	527.70	518.77	513.72	512.30	502.11	505.17	62.08	48.27
5	504.71	520.89	527.83	518.29	513.27	511.85	501.66	504.72	62.17	48.43
6	504.89	524.31	528.67	522.41	517.49	516.07	505.88	508.94	62.86	49.85
7	504.85	527.37	530.67	525.41	519.84	518.42	508.23	511.31	62.08	49.45

POINT	VA2	VU2	V2	V-15	ALPHA-2	MV2	STAGE LIFTING FACTOR	STAGE FLOW FACTOR
1	15.35	-2.817	152.57	18.19	-1.61	1.185	2.72	0.44
2	15.35	-1.317	150.72	16.31	-5.81	1.154	1.71	0.44
3	15.35	4.317	148.87	14.43	11.61	1.124	1.44	0.44
4	15.35	0.317	147.02	12.55	17.41	1.094	1.44	0.44
5	15.35	0.317	145.17	10.67	23.21	1.064	1.44	0.44
6	15.35	1.317	143.32	8.79	29.01	1.034	1.44	0.44
7	15.35	1.317	141.47	6.91	34.81	1.004	1.44	0.44
8	15.35	1.317	139.62	5.03	40.61	0.974	1.44	0.44
9	15.35	1.317	137.77	3.15	46.41	0.944	1.44	0.44

RELATIVE VELOCITIES(F/SEC), ANGLES(DEG), AND REL VEL COEFFS

POINT	WAZ	WUZ	N2	U2	M215	BETA 2	DBETA	WCOEFS	MW2
1	15.35	-602.59	435.64	374.77	453.12	-59.74	17.87	0.9491	0.3915
2	15.35	-392.59	424.13	412.24	443.84	-64.37	17.85	0.9648	0.3915
3	15.35	-302.59	412.64	438.33	434.56	-68.99	17.83	0.9805	0.3915
4	15.35	-212.59	401.15	464.42	425.28	-73.62	17.81	0.9962	0.3915
5	15.35	-122.59	389.66	490.51	416.00	-78.24	17.79	1.0119	0.3915
6	15.35	-32.59	378.17	516.60	406.72	-82.87	17.77	1.0276	0.3915
7	15.35	-382.59	418.58	492.44	435.53	-87.50	17.75	1.0433	0.3915
8	15.35	-382.59	430.16	522.90	446.34	-92.12	17.73	1.0590	0.3915
9	15.35	-382.59	441.74	553.36	457.15	-96.74	17.71	1.0747	0.3915

EFFICIENCIES, RPM, WCHK OUTPUT(HPI), AND ENTHALPY DRIP(TU/LHM)

POINT	ZETA	POTCR	ETA	RLT(CEL-ZETA)	RPM	HP	DELTA H5	DELTA H6	PERCENT FACTOR	EFF	DEGREE OF REACTION
1	0.0991	0.0991	0.0991	10.000	29.51	14.71	11.48	1.0205	0.0645		
2	0.0888	0.0888	0.0888	11.000	29.67	14.84	11.62	1.0199	0.0622		
3	0.0785	0.0785	0.0785	12.000	29.83	14.97	11.76	1.0193	0.0600		
4	0.0682	0.0682	0.0682	13.000	29.99	15.10	11.89	1.0187	0.0578		
5	0.0579	0.0579	0.0579	14.000	30.15	15.23	12.02	1.0181	0.0556		
6	0.0476	0.0476	0.0476	15.000	30.31	15.36	12.15	1.0175	0.0534		
7	0.0373	0.0373	0.0373	16.000	30.47	15.49	12.28	1.0169	0.0512		
8	0.0270	0.0270	0.0270	17.000	30.63	15.62	12.41	1.0163	0.0490		
9	0.0167	0.0167	0.0167	18.000	30.79	15.75	12.54	1.0157	0.0468		

GENERAL RESULTS

RUN NUMBER 15 DATE 1 AUG 69

POINT	PRESSURE RATIO	REFERRED SPEED RPM	ISENTROPIC HEAD COEFF	EFFICIENCY TOT-STATIC PERCENT	EFFICIENCY TOT-TOT PERCENT	REFERRED FLOW RATE LBM/SEC	REFERRED MOMENT FT-LB	REFERRED PCMR HP	DEGREE OF REACTION (HUB)	DEGREE OF REACTION (MEAN)	DEGREE OF REACTION (TIP)
1	1.5041	9651.	5.3795	77.40	79.89	1.2728	10.393	19.098	-0.0288	0.0395	0.1648
2	1.5055	10100.	4.8229	78.51	80.93	1.2620	10.549	19.323	-0.0251	0.0552	0.1805
3	1.5018	10564.	4.4740	78.50	80.92	1.2620	10.549	19.323	-0.0251	0.0552	0.1805
4	1.5018	11323.	3.8946	79.50	82.09	1.2541	8.632	18.766	-0.0249	0.0724	0.1949
5	1.5075	11741.	3.6538	79.30	82.09	1.2541	8.632	18.766	-0.0249	0.0724	0.1949
6	1.5035	12299.	3.2145	78.41	81.63	1.2440	8.072	18.488	-0.0277	0.0724	0.2212
7	1.5041	12670.	3.1216	77.89	81.45	1.2391	7.755	18.709	-0.0201	0.1396	0.2505
8	1.5022	14372.	2.8064	72.50	78.39	1.2163	6.205	17.004	-0.0377	0.1989	0.2569
9	1.5021	16336.	1.8673	63.62	72.62	1.1905	4.700	14.636	-0.1564	0.2608	0.3621

STATOR RESULTS

CONFIGURATION= CONVERGING NOZZLES, SHROUD P/A 10.92, INSERT P/N 20003-3(STRAIGHT)

RUN NUMBER 15 DATE= 1 AUG 69

M(THRO) J= 3

FORCE AND MOMENT BALANCE(LBS AND FT-LBS)														
POINT	FAX(+)	CLFAX(+)	F(-)	F1(-)	F2(-)	F3(-)	F4(-)	F5(-)	F6A(-)	FNT	TOPQ(+)	CLTORQ(+)	RFAX	RTORQ
1	-15.60	9.37	1201.90	272.33	56.54	46.19	58.55	86.75	666.72	10.59	14.73	3.03	-10.46	6.98
2	-0.86	10.79	1201.90	278.23	56.54	46.19	58.47	87.91	671.91	10.23	14.07	3.04	-0.54	6.50
3	12.04	11.77	1201.90	281.33	56.54	46.19	58.43	88.91	686.30	10.01	14.53	3.04	18.71	9.52
4	17.36	12.87	1201.90	282.62	56.54	46.19	58.24	89.23	696.49	10.03	13.97	3.04	17.61	9.10
7	25.44	13.15	1201.90	285.02	56.54	46.19	56.19	90.14	696.55	9.79	13.57	3.04	20.12	8.98
8	30.00	14.56	1201.90	282.93	56.54	45.80	55.71	92.02	720.28	9.11	12.90	3.04	37.09	8.67
9	84.40	17.02	1201.90	300.25	56.54	45.76	55.79	94.15	742.22	8.01	11.90	3.04	56.07	7.99

FLOW RATES(LHM/SEC), HE(NOZ), FLOW FNC, AND STATOR BLOCKAGE FACTOR

POINT	NOZZLE FLOW	TURBINE FLOW	LBLEAK	HE	PHI	X1
1	1.8657	1.8322	0.3335	521710.	0.5795	0.8906
2	1.8532	1.8193	0.3339	516144.	0.5768	0.8915
3	1.8382	1.8048	0.3334	510943.	0.5746	0.8939
4	1.8371	1.8044	0.3338	506216.	0.5709	0.8942
5	1.8315	1.7974	0.3339	502867.	0.5699	0.8930
6	1.8110	1.7774	0.3340	501011.	0.5683	0.8930
7	1.8048	1.7711	0.3338	497720.	0.5531	0.8925
8	1.7985	1.7644	0.3341	490832.	0.5420	0.8917
9	1.7332	1.6590	0.3343	480832.		

PRESSURES(P5IA) AND PRESSURE RATIOS

POINT	PN0Z	PTPL	PTC	PIAV	PHO	PLENUM	PR(PTPL/PHO)	STATOR	PR(PTO/PIAV)
1	36.00	22.12	21.51	14.81	14.57	1.5186	1.4789		
2	36.00	22.07	21.87	15.14	14.57	1.5196	1.4633		
3	36.02	22.08	21.87	15.30	14.57	1.5182	1.4453		
4	36.15	22.17	21.90	15.37	14.57	1.5190	1.4293		
7	36.00	22.08	21.86	15.50	14.57	1.5182	1.4424		
8	36.00	22.07	21.86	15.69	14.57	1.5189	1.4200		
9	36.00	22.07	21.88	16.33	14.57	1.5189	1.3395		

TEMPERATURES(DEG R)

POINT	TTPL	TTG	TI	TIIS
1	557.93	556.83	519.13	497.93
2	561.70	560.60	523.15	502.89
3	565.52	562.35	516.87	506.22
4	568.23	564.30	518.68	509.56
5	568.60	564.65	519.88	509.98
6	568.26	564.44	521.42	511.41
7	568.53	564.71	522.40	512.11
8	568.67	564.85	524.67	516.06
9	568.55	564.95	528.67	519.66

ABSOLUTE VELOCITIES(FT/SEC), ANGLES(DEG), VEL COEFF, AND MACH NOS

PCINT	VAL	VUI	VI	VUIS	ALPHA I	VCDEFS	MVI	MVAI	RVAI	PVUI
1	185.96	733.87	757.67	841.20	75.79	0.9000	0.6845	0.1681	0.1608	0.6344
2	184.52	732.57	755.39	832.98	75.46	0.9069	0.6933	0.1662	0.1590	0.6311
3	182.63	716.57	739.48	821.50	75.77	0.9002	0.6635	0.1639	0.1571	0.6164
4	179.83	713.92	733.98	814.71	75.82	0.9098	0.6608	0.1611	0.1545	0.6146
5	177.95	690.81	718.97	794.20	75.92	0.9077	0.6223	0.1508	0.1527	0.6104
6	176.19	690.84	712.99	794.96	75.69	0.9169	0.6323	0.1523	0.1533	0.5993
7	169.07	679.21	699.94	765.67	76.52	0.9142	0.6237	0.1507	0.1451	0.5830
8	163.01	639.85	660.29	737.45	75.71	0.9454	0.5858	0.1446	0.1369	0.5492

RELATIVE VELOCITIES(FT/SEC), ANGLES(DEG), AND MACH NOS

POINT	MW	MUI	M	UI	BETA I	MWI
1	185.96	363.86	408.63	370.01	62.93	0.3694
2	184.52	343.99	390.26	388.51	61.79	0.3515
3	182.63	308.56	359.41	407.01	59.46	0.3225
4	179.83	278.63	331.68	436.98	57.15	0.2970
5	177.95	252.76	284.53	452.26	55.12	0.2811
6	176.19	224.72	267.84	489.12	48.86	0.2491
7	169.07	172.46	209.35	551.70	36.16	0.1866
8	163.01	124.24	163.21	621.61	2.89	0.1448

EFFICIENCIES

PCINT	ZETA STATOR	EIA STATOR(L-ZETAS)
1	0.1900	0.8100
2	0.1776	0.8224
3	0.1897	0.8103
4	0.1722	0.8278
5	0.1811	0.8189
6	0.1887	0.8113
7	0.1729	0.8054
8	0.1983	0.8017

MOTOR RESULTS

CONFIGURATION- CIRCULAR APC, SHARP LE MOTOR, P/F 1034-A, AXIAL CINC 0.257 IN, RADIAL CINC 0.000 IN

RUN NUMBER 15 DATE 1 AUG 69

METHOD J=7

PRESSURES(P5IA) AND PRESSURE RATIOS

PAMB=14.57

POINT	P10	P1AV	P12	P2=PHM	OVERALL P1(P10/P2)
1	21.91	14.81	14.77	14.57	1.2041
2	21.93	14.99	14.76	14.57	1.5055
3	21.87	15.14	14.75	14.57	1.5018
4	21.87	15.30	14.76	14.57	1.5075
5	21.90	15.37	14.77	14.57	1.5035
6	21.91	15.50	14.80	14.57	1.5041
7	21.91	15.56	14.82	14.57	1.5004
8	21.88	15.73	15.00	14.57	1.5021

TEMPERATURES(DEG R)

POINT	T10	T1	T1F	T2	T2IS	T2TH	TT2IS	DELTA T1S	DELTA T1M
1	566.83	509.13	523.32	507.38	506.67	495.53	497.47	61.80	47.45
2	566.99	512.15	529.98	512.10	510.24	500.71	502.65	61.89	48.26
3	564.30	518.98	528.55	513.15	511.70	502.40	504.35	61.90	48.21
4	564.65	519.88	528.55	513.02	511.91	502.16	504.20	62.48	48.55
5	564.44	521.42	528.63	515.77	512.19	502.37	504.65	62.08	48.67
6	564.71	522.47	528.89	516.29	512.64	502.54	505.04	62.17	48.43
7	564.85	524.00	528.39	515.00	512.80	502.99	505.63	61.86	44.85
8	564.95	528.07	531.74	518.14	511.64	502.95	510.13	62.00	39.45

ABSOLUTE VELOCITIES(FT/SEC) AND ANGLES(DEG)									
PCINT	VAZ	VUZ	V2	V-1S	ALPHA 2	MV2	STAGE LOADING FACTOR	STAGE FLOW FACTOR	
1	150.29	-36.02	154.55	858.19	-13.48	0.1402	2.35	C.49	
2	150.29	-1.79	151.14	862.91	C.68	0.1347	1.91	C.38	
3	149.42	38.67	149.47	862.37	C.59	0.1382	1.73	C.36	
4	148.52	53.67	151.13	866.41	19.84	0.1424	1.43	C.34	
5	147.56	79.43	161.58	863.59	28.29	0.1509	1.29	C.32	
6	147.10	94.86	172.09	864.25	32.85	0.1576	1.22	C.31	
7	144.52	191.53	243.25	862.12	52.04	0.2159	0.87	C.30	
8	142.52	261.52	251.56	863.09	61.43	0.2667	0.59	C.26	

RELATIVE VELOCITIES(FT/SEC), ANGLES(DEG), AND REL COEFS									
PCINT	MAZ	MUZ	M2	U2	MZIS	BETA 2	DBETA	MCDEFS	MW2
1	150.29	-411.78	437.41	374.77	447.27	-69.90	12.83	0.9700	0.3061
2	150.29	-411.78	437.41	391.50	447.27	-70.97	12.83	0.9739	0.3038
3	149.42	-411.78	437.41	412.24	448.50	-70.00	12.83	0.9739	0.3038
4	148.52	-403.93	431.37	442.69	448.50	-69.81	12.83	0.9564	0.3076
5	147.56	-405.42	431.85	459.09	446.97	-69.85	12.83	0.9662	0.3090
6	147.10	-401.02	427.31	480.45	444.39	-69.83	11.27	0.9616	0.3040
7	144.52	-372.92	426.64	495.44	441.82	-68.72	11.27	0.9656	0.3040
8	144.52	-372.92	398.06	562.90	459.63	-68.72	104.86	0.8660	0.3078
9	142.52	-378.41	404.28	639.73	491.45	-69.39	72.28	0.8226	0.3623

EFFICIENCIES, RPM, WORK OUTPUT(HPI), AND ENTHALPY DROP(BTU/LBM)										
POINT	ZETA	ROTOR	ETA	ROTUR(1.-ZETA)	RPM	HP	DELTA HIS	DELTA HW	REHEAT FACTOR	EFF DEGREE OF REACTION
1	C.0426	C.9564	0.2993	0.0220	10020.	29.51	14.71	11.38	1.0225	0.0350
2	C.0426	C.9564	0.2993	0.0220	10020.	29.99	14.84	11.65	1.0204	0.0387
3	C.0426	C.9564	0.2993	0.0220	10020.	29.67	14.82	11.67	1.0211	0.0343
4	C.0426	C.9564	0.2993	0.0220	10020.	29.67	14.82	11.67	1.0211	0.0343
5	C.0426	C.9564	0.2993	0.0220	10020.	29.67	14.82	11.67	1.0211	0.0343
6	C.0426	C.9564	0.2993	0.0220	10020.	29.67	14.82	11.67	1.0211	0.0343
7	C.0426	C.9564	0.2993	0.0220	10020.	29.67	14.82	11.67	1.0211	0.0343
8	C.0426	C.9564	0.2993	0.0220	10020.	29.67	14.82	11.67	1.0211	0.0343
9	C.0426	C.9564	0.2993	0.0220	10020.	29.67	14.82	11.67	1.0211	0.0343

GENERAL RESULTS

RUN NUMBER 15 DATE 1 AUG 69

POINT	PRESSURE RATIO	REFERRED SOUND RPM	ISENTROPIC HEAT. COEFF	EFFICIENCY TOT-STATIC PERCENT	EFFICIENCY TOT-TOT PERCENT	REFERRED FLOW RATE LBM/SEC	REFERRED MOMENT FT-LB	REFERRED PCWEP HP	DEGREE OF REACTION (HOUR)	DEGREE OF REACTION (MEAN)	DEGREE OF REACTION (TIP)
1	1.5041	5651.	5.3795	77.40	79.84	1.2729	10.293	19.099	-0.0228	0.0392	0.1648
2	1.5055	10100.	4.6225	78.51	80.49	1.2621	8.072	19.353	-0.0751	0.0662	0.1805
3	1.5018	10554.	4.4740	79.50	80.43	1.2521	8.072	19.353	-0.0249	0.0894	0.1949
4	1.5018	11223.	3.8946	79.50	82.05	1.2519	8.072	19.353	-0.0249	0.1156	0.2212
5	1.5075	11741.	3.6538	79.30	81.98	1.2449	8.072	19.353	-0.0249	0.1457	0.2405
6	1.5035	12019.	3.3145	78.41	81.41	1.2391	7.755	18.888	0.0277	0.1539	0.2549
7	1.5035	12019.	3.1216	77.89	81.16	1.2391	7.755	18.888	0.0277	0.1539	0.2549
8	1.5004	14353.	2.8064	72.50	78.50	1.2163	6.205	17.004	0.0277	0.1112	0.2369
9	1.5021	16566.	1.8673	63.62	72.04	1.1905	4.700	14.636	0.01564	0.2699	0.3621

Printout of Programs FLOCAL and TTTR for use of IBM 360/67

computer.

```

C PROGRAM FLOCAL. THIS PROGRAM CALCULATES THE NOZZLE DISCHARGE COEFFICIENT(KN)
C OF THE TTR BY MATCHING THE FLOW THROUGH THE NOZZLE WITH THAT OF THE FLOW
C THROUGH A STANDARD SHARP-EDGED ORIFICE. INPUT DATA-PBAR(IN HG), TBAR(DEG F),
C TCR(DEG F), DH(IN H2O), PREF1,PNOZ(IN HG), TNOZ(MV), DPFL(CM H2O), PREF, POR(IN
C HG), TOR(MV), L(NO OF DATA SETS), N(NO OF DATA POINTS IN EACH SET)
C
C DIMENSION DH(100), PREF1(100), PNOZ(100), TORR(100), TNOZ(100), TNOZR(100), DPFL(
1 100), PREF(100), POR(100), TOR(100), TORR(100), WFL(100), QKN(100),
2 RE(100)
C
C READ INPUT DATA
WRITE(6,14)
READ(5,15) L
DO 13 M=1, L
READ(5,15) N
READ(5,16) PBAR, TBAR, TCR
READ(5,16) (DH(I), I=1, N)
READ(5,16) (PREF1(I), I=1, N)
READ(5,16) (PNOZ(I), I=1, N)
READ(5,16) (TNOZ(I), I=1, N)
READ(5,16) (DPFL(I), I=1, N)
READ(5,16) (PREF(I), I=1, N)
READ(5,16) (POR(I), I=1, N)
READ(5,16) (TOR(I), I=1, N)
C
C INPUT CONSTANTS
D10=6.065
D20=4.2425
D1N=7.975
D2N=4.25
BETA0=D20/D10
BETAN=D2N/D1N
GAM=1.4
EX1=GAM/(GAM-1.)
EX2=(GAM-1.)/GAM
EX3=2./GAM
A=D20*(830.-5000.*BETA0+9000.*BETA0**2-4200.*BETA0**3+530./SQRT(
1 D10))
B=0.5993+C.007/D10
C=0.364C+C.076/SQRT(D10)
QKE=B+C*BETA0**4
QKINF=QKE/(1.+A*(0.15E-04/D20))
C
C COMPUTE CCRRECTED PRESS AND TEMPS
GHGBR=13.63905-0.00136303*TBAR
GHGCR=13.63905-0.00136303*TCR
CHGBR=C.4891585*GHGBR/13.54
CHGCR=C.4891585*GHGCR/13.54

```

```

GW68=C.9983763+68.*0.106058E-03-(68.**2)*0.159319E-05
GWCR=0.9983763+TCR*0.106058E-03-(TCR**2)*0.159319E-05
PAMB=PBAR*CHGBR

```

C CALCULATIONS FOR ORIFICE FLOW RATE

```

DO 12 I=1,N
QDPFL=DPFL(I)
DPFL(I)=QDPFL/2.54*GWCR*62.42732/1728.
PCR(I)=CHGCR*(PREF(I)-POR(I))+PAMB
TOR(I)=33.252+34.86*TOR(I)-0.1855*TOR(I)**2
TORR(I)=TOR(I)+459.69
ALPHA0=1.+1.93*(TOR(I)-68.)*0.1E-04
YO=1.0-(C.41+0.35*BETA0**4)*DPFL(I)/(GAM*POR(I))
ZO=1.9+2.4*(TOR(I)-100.)*0.1E-02
HW680=QDPFL/2.54*GWCR/GW68
FR=1.0
WFL(I)=0.1638427*D20**2*ALPHA0*QKINF*FR*YO*SQRT(POR(I))*HW680/
1 TORR(I))
10 XO=2.27376*WFL(I)/(D20*ZO)
FR=1.+(A/XO)*0.1E-05
WFLC=0.1638427*D20**2*ALPHA0*QKINF*FR*YO*SQRT(POR(I))*HW680/
1 TORR(I))
IF(ABS(WFLC-WFL(I)).LE.0.0001) GO TO 11
WFL(I)=WFLC
GO TO 10
11 WFL(I)=WFLC

```

C CALCULATIONS FOR NOZZLE DISCHARGE COEFFICIENT

```

QDH=DH(I)
DH(I)=QDH*GWCR*62.42732/1728.
PNCZ(I)=CHGCR*(PREF(I)-PNOZ(I))+PAMB
TNOZ(I)=33.252+34.86*TNOZ(I)-0.1855*TNOZ(I)**2
TNOZR(I)=TNOZ(I)+459.69
ALPHAN=1.+2.52*(TNOZ(I)-68.)*0.1E-04
R=1.-(DH(I)/PNOZ(I))
YN=SQRT(R**EX3*EX1*((1.-R**EX2)/(1.-R))*((1.-BETAN**4)/(1.-R**EX3*
1 BETAN**4)))
ZN=1.9+2.4*(TNOZ(I)-100.)*0.1E-02
HW68N=QDH*GWCR/GW68
QKN(I)=6.10342*WFL(I)*SQRT(TNOZR(I)/(HW68N*PNOZ(I)))/(D2N**2*YN*
1 ALPHA)
RE(I)=2.27376*WFL(I)/(D2N*ZN)*0.1E+07
12 CONTINUE

```

C WRITE OUTPUT DATA
WRITE(6,17)
WRITE(6,18)M,PNOZ(I)
WRITE(6,19)


```

WRITE(6,20)PAMB,N,GAM
WRITE(6,21)
DO 13 I=1,N
WRITE(6,22)I,WFL(I),QKN(I),RE(I)
13 CONTINUE
C
14 FORMAT (1H1,32X,'FLCW NOZZLE CALIBRATION FOR THE TRANSONIC TURBINE
1 TEST RIG')
15 FORMAT (I3)
16 FORMAT (8F10.0)
17 FORMAT (// // 32X,'TEST SERIES',25X,'NOZZLE SUPPLY PRESSURE')
18 FORMAT (/35X,I3,38X,F5.2)
19 FORMAT (/32X,'ATMOS. PRESS.',11X,'DATA POINTS',11X,'GAMMA')
20 FORMAT (/35X,F6.2,19X,I2,17X,F3.1)
21 FORMAT (/34X,'POINT',8X,'FLOW RATE',8X,'DISCHARGE',8X,'REYNOLDS',/
1 47X,'(LBM/SEC)',7X,'COEFFICIENT',8X,'NUMBER',//)
22 FORMAT (36X,I2,9X,F8.4,8X,F9.5,7X,F11.2)
STOP
END

```

```

C CHARACTERISTICS OF THE TRANSSONIC TURBINE TEST RIG, USING ONE-DIMENSIONAL
C ANALYSIS, AT THE MEAN RADIUS.
C
C INPUT DATA AXCLR, RADCLR(IN), PBAR(IN HG), TBAR, TCR(DEG R), DH(IN H2O), PREF1
C PNOZ,PTPL,PTO,PREF2,PHUB,PTIP,P13-P21,PHD,PCLI-PCL3(IN HG), TNOZ,TTPL,TTD,
C THD(MV), AXIL,TORQR,DYNAR(COUNTS-10,000),RPM,CLAXIL,CLTRQR(COUNTS),
C MM(NG OF RUNS), NRUN(RUN NO), N(ND OF DATA POINTS IN EACH RUN)
C
C REAL*4 MVALM,MVA1,MVIM,MVIC,MV1,MW1,MV2,MW2
C
C DIMENSION DH(50),PREF1(50),PNOZ(50),PTPL(50),PTO(50),PREF2(50),
C 1PHUB(50),PTIP(50),P13(50),P14(50),P15(50),P16(50),P17(50),P18(50),
C 2P19(50),P20(50),P21(50),PHD(50),PCL1(50),PCL2(50),PCL3(50),
C 3TNOZ(50),TTPL(50),TTD(50),THD(50),AXIL(50),TORQR(50),DYNAR(50),
C 4RPM(50),CLAXIL(50),CLTRQR(50)
C
C DIMENSION FAX(50),CLFAX(50),FO(50),F1(50),F2(50),F3(50),F4(50),
C 1F5(50),F6A(50),FNET(50),TORQ(50),X1(50),X2(50),X3(50),X4(50),X5(50),
C 2FLOWL(50),RE(50),PHI(50),PIAV(50),PRPL(50),PRS(50),TI(50),
C 3T1IS(50),VA1(50),VU1(50),V1(50),V1IS(50),ALPH1(50),VCOFS(50),
C 4MV1(50),MVA1(50),WAL(50),WU1(50),W1(50),UI(50),BETA1(50),MW1(50),
C 5ZETAS(50),ETAS(50),PT2(50),PR(50),WIE(50),TT2(50),T2IS(50),
C 6T2TH(50),TT2IS(50),DELTW(50),DELTIS(50),DELHW(50),DELHIS(50),
C 7VA2(50),VU2(50),V2(50),VOIS(50),ALPH2(50),WA2(50),WU2(50),W2(50),
C 8UZ(50),W2IS(50),BETA2(50),DBETA(50),WCOFS(50),ZETAR(50),ETAR(50),
C 9REFRPM(50),XKIS(50),ETATS(50),ETATT(50),REFLOW(50),REFMOM(50),
C *HP(50),REFHP(50),REACHB(50),REACMN(50),REACTP(50),F(50),MV2(50),
C *MW2(50),REACEF(50),QNOZ(50),QTPL(50),PTC(50),QHD(50),TTPQ(50),
C *TTO(50),SLF(50),SFF(50),RFAX(50),RTORQ(50),RVAL(50),RVUI(50)
C
C READ(5,10) MM
C FFORMAT(I3)
C CALL CANCEL (2)
C
C DO 13 M=1,MM
C CALL
C INPUT(NRUN,N,AXCLR,RADCLR,PBAR,TBAR,TCR,DH,PREF1,PNOZ,
C 1PTPL,PTO,PREF2,PHUB,PTIP,P13,P14,P15,P16,P17,P18,P19,P20,P21,PHD,
C 2PCL1,PCL2,PCL3,TNOZ,TTPL,TTD,THD,AXIL,TORQR,DYNAR,RPM,CLAXIL,
C 3CLTRQR,DA,T,E)
C
C SETCON(DIN,D2N,BETAN,RG,GAM,GC,CP,CJ,C,EX1,EX2,EX3,PI,
C 1ZNS,TETS,RTIPL,RHUB1,RTIP2,RHUB2,AAXS,AAXR,ATHS,RM1,RM2,SKT,RKT,
C 2RADCLR,B1,B2,B3,B4,B5,D1,D2,D3,D4,D5,D6,CL1,CL2,CL3)
C DO 12 J=1,2
C DO 11 I=1,N
C QDH=DH(I)
C QPREF1=PREF1(I)
C CPNOZ=PNOZ(I)

```

0028
0029

QPTPL=PTPL(I) 0031
 QPTO=PTO(I)
 QPREF2=QREF2(I) 0032
 QPHUB=PHUB(I) 0033
 QPTIP=PTIP(I)
 QP13=PI3(I)
 QP14=PI4(I)
 QP15=PI5(I)
 QP16=PI6(I)
 QP17=PI7(I)
 QP18=PI8(I)
 QP19=PI9(I)
 QP20=PI10(I)
 QP21=PI11(I)
 QPHD=PHD(I)
 QTNZ=TNZ(I) 0041
 QTTPL=TTPL(I) 0030
 QTHD=THD(I) 0035
 QAXIL=AXIL(I)
 QTORQR=TORQR(I) 0039
 QDYNAR=DYNAR(I) 0038
 QRPM=RPM(I) 0040
 QLAXIL=CLAXIL(I) 0037
 QLTRQR=CLTRQR(I) 0045

C

CALL CONVERT(PBAR, TBAR, TCR, PAMB, HW68, QDH, QPREF1, QPNOZ, QPTPL, QPTO,
 1 QPREF2, QPHUB, QPTIP, QP13, QP14, QP15, QP16, QP17, QP18, QP19, QP20, QP21,
 2 QPHD, QPCL1, QPCL2, QPCL3, QTNZ, TNOZR, QTTPL, TTPLR, QTTT, TTOR, QTHD,
 3 QAXIL, QFAX, QTCRQR, QTORQR, QDYNAR, DYNA, QLAXIL, QLFAX, QLTRQR, QLTORQR,
 4 CL1, CL2, CL3)

C

CALL FLORAT(D2N, RG, GC, EX1, EX2, EX3, HW68, QDH, QPNCZ, QPTPL, QPHD, PRP,
 1 QTNZ, TNOZR, QTTPL, TTPLR, QTHD, B1, B2, B3, B4, B5, D1, D2, D3, D4, D5, D6,
 2 NRUN, I, QRE, QFLCWN, QFLOWL, QFLOWT, BETAN)

C

CALL STATOR(RG, GAM, GC, C, PI, EX1, EX2, EX3, EPS, RTIPI, RHUB1, RM1, QPHUB,
 1 QPTIP, QP1AV, QPTO, QP13, QP18, QP19, QP20, QP21, QPHD, QPRS, QFLOWT, AAXS,
 2 ATHS, SKT, J, TTOR, TIRM, TII SR, QZETAS, QETAS, QPHI, QXI, QRP, M, VALM,
 3 QVU1, VIM, QV1IS, VCOEFS, ALPHIM, MVALM, QUL, QWAI, QWU1, QWU1, QBETA1,
 4 QMW1, QTORQR, QLTORQR, QFAX, QLFAX, QF0, QF1, QF2, QF3, QF4, QF5, QF6A, QFNET,
 5 QRFAX, QRTORQR, QRVA1, QRVU1)

C

CALL ROTOR(RG, GC, CJ, CP, C, PI, EX1, EX2, RM1, RM2, AAXR, RKT, QPTO,
 1 QP1AV, QPHD, QPT2, PRM, DYNA, QFLOWT, TTOR, TIRM, T2R, QDEL TW, T2ISR,
 2 TER, QVU1, QW1, QW1, QBETA1, QVU2, QVA2, QV2, QALPH2, QU2, QWU2, QWA2, QW2,
 3 QW2IS, QBETA2, QDBETA, WCOEFS, QZETAR, QETAR, QMV2, QMW2, GAM, QRP, M, QSLF,
 4 QSFF)

C

```
PERFRM(C,PI,EX2,QPT0,QPHUB,QTIIP,QPHD,QPT2,DYNA,QRPM,  
CALL QVLIIS, QUL, QV2, QETATS, QETATT, QEACMN, QEACHB, QEACTP, QXKIS, QEFLOW,  
1 QVLIIS, QUL, QV2, QETATS, QETATT, QEACMN, QEACHB, QEACTP, QXKIS, QEFLOW,  
2 QEFPRM, QEFMOM, QHP, QEFHP, T2ISR, QF, VIM, QW1, QW2, QEACEF, CP)  
3 FAX(I)=QFAX  
CLFAX(I)=QLFAX  
FO(I)=QF0  
F1(I)=QF1  
F2(I)=QF2  
F3(I)=QF3  
F4(I)=QF4  
F5(I)=QF5  
F6A(I)=QF6A  
FNET(I)=QFNET  
TORQ(I)=QTORQ  
CLTORQ(I)=QLTORQ  
FLOWN(I)=QFLOWN  
FLOWT(I)=QFLOWT  
FLOWL(I)=QFLOWL  
RE(I)=QRE  
PHI(I)=QPHI  
XI(I)=QXI  
QNCZ(I)=QPN0Z  
QTPPL(I)=QPTPL  
P0(I)=QPT0  
PIAV(I)=QPIAV  
QHD(I)=QPHD  
PRPL(I)=QPRP  
PRSP(I)=QPRS  
TTPQ(I)=TTPLR  
TI(I)=TIRM  
TIIIS(I)=TIISR  
VAI(I)=VAIM  
VUI(I)=QVUI  
VI(I)=VIM  
VIIS(I)=QVLIIS  
ALPH1(I)=ALPH1M  
VCOFS(I)=VCOEFS  
MVA1(I)=MVA1M  
MVAI(I)=MVAI  
WUI(I)=QWUI  
WUI(I)=QWUI  
WI(I)=QWI  
UI(I)=QUI  
BETAI(I)=QBETAI  
MWI(I)=QMWI
```

ZETAS(I)=QZETAS
ETAS(I)=QETAS
PT2(I)=QPT2
PR(I)=PRM
TE(I)=TER
TT2(I)=TT2R
T2(I)=T2R
T2IS(I)=T2ISR
T2TH(I)=T2THSR
TT2IS(I)=TT2ISR
DELTW(I)=QDELTW
DELTIS(I)=QDLTIS
DELHW(I)=QDELHW
DELHIS(I)=QDLHIS
VA2(I)=QVA2
VU2(I)=QVU2
V2(I)=QV2
VOIS(I)=QVOIS
ALPH2(I)=QALPH2
MV2(I)=QMV2
WA2(I)=QWA2
WU2(I)=QWU2
W2(I)=QW2
MW2(I)=QMW2
U2(I)=QU2
W2IS(I)=QW2IS
BETA2(I)=QBETA2
DBETA(I)=QDBETA
WCOFS(I)=WCOWFS
ZETAR(I)=QZETAR
ETAR(I)=QETAR
REFRPM(I)=QEFRPM
XKIS(I)=QXKIS
ETATS(I)=QETATS
F(I)=QF
ETATT(I)=QETATT
EFLOW(I)=QEFLOW
REFMOM(I)=QEFMOM
HP(I)=QHP
REFHP(I)=QEEHP
REACEF(I)=QEACEF
REACHB(I)=QEACHB
REACMN(I)=QEACMN
REACTP(I)=QEACTION
SLF(I)=QSLF
SFAX(I)=QSFAX
RTORQ(I)=QRTORQ

```

11 C
RVAl(I)=QRVA1
RVU1(I)=QRVU1
CONTINUE

12 C
CALL          OUTPTS(NRUN,N,FAX,CLFAX,F0,F1,F2,F3,F4,F5,F6A,FNET,J,
1 TORQ,CLTORQ,FLOWN,FLOWT,RE,PHI,XI,QNOZ,QTPL,PTO,PIAV,QHD,
2 PRPL,PRS,TTPO,TT0,T1,TTIS,VA1,VU1,V1,V1IS,ALPH1,VCOFS,MV1,MVA1,
3 WA1,WU1,W1,U1,BETA1,MW1,ZETAS,ETAS,PAMB,DA,T,E,RFAX,RTORQ,RVA1,
4 RVU1)

13 C
CALL          OUTPTR(NRUN,N,AXCLR,RADCLR,PAMB,PTO,PIAV,PT2,QHD,PR,
1 TT0,T1,TE,TT2,T2,T2IS,TT2IS,DELTIIS,DELTW,VA2,VU2,V2,VOIS,
2 ALPH2,WA2,WU2,U2,W2IS,BETA2,DBETA,WCOFS,ZETAR,ETAR,RPM,HP,
3 DELHIS,DELHW,REFRPM,XKIS,ETATS,ETATT,REFLOW,REFMOM,REFHP,J,
4 REACHB,REACMN,REACTP,DA,T,E,F,REACEF,MV2,MW2,SLF,SFF)
CONTINUE

12 C
STOP
END

SUBROUTINE  INPUT(NRUN,N,AXCLR,RADCLR,PBAR,TBAR,TCR,DH,PREF1,PNOZ,
1 PTPL,PTO,PREF2,PHUB,PTIP,PI3,PI4,PI5,PI6,PI7,PI8,PI9,P20,P21,PHD,
2 PCL1,PCL2,PCL3,TNOZ,TTPL,TT0,THD,AXIL,TORQR,DYNAR,RPM,CLAXIL,
3 CLTRQR,DA,T,E)
DIMENSION  DH(50),PREF1(50),PNOZ(50),PTPL(50),PTO(50),PREF2(50),
1 PHUB(50),PTIP(50),PI3(50),PI4(50),PI5(50),PI6(50),PI7(50),PI8(50),
2 PI9(50),P20(50),P21(50),PHD(50),PCL1(50),PCL2(50),PCL3(50),
3 TNOZ(50),TTPL(50),TT0(50),THD(50),AXIL(50),TORQR(50),DYNAR(50),
4 RPM(50),CLAXIL(50),CLTRQR(50)
READ (5,101)NRUN,N,DA,T,E
READ (5,102)AXCLR,RADCLR
READ (5,102)PBAR,TBAR,TCR
READ (5,102)(DH(I),I=1,N)
READ (5,102)(PREF1(I),I=1,N)
READ (5,102)(PNOZ(I),I=1,N)
READ (5,102)(PTPL(I),I=1,N)
READ (5,102)(PTO(I),I=1,N)
READ (5,102)(PHUB(I),I=1,N)
READ (5,102)(PTIP(I),I=1,N)
READ (5,102)(PI3(I),I=1,N)
READ (5,102)(PI4(I),I=1,N)
READ (5,102)(PI5(I),I=1,N)
READ (5,102)(PI6(I),I=1,N)
READ (5,102)(PI7(I),I=1,N)
READ (5,102)(PI8(I),I=1,N)
READ (5,102)(PI9(I),I=1,N)
READ (5,102)(P20(I),I=1,N)
READ (5,102)(P21(I),I=1,N)
READ (5,102)(PHD(I),I=1,N)
READ (5,102)(PCL1(I),I=1,N)
READ (5,102)(PCL2(I),I=1,N)
READ (5,102)(PCL3(I),I=1,N)
READ (5,102)(RPM(I),I=1,N)
READ (5,102)(CLAXIL(I),I=1,N)
READ (5,102)(CLTRQR(I),I=1,N)
READ (5,102)(TORQR(I),I=1,N)
READ (5,102)(DYNAR(I),I=1,N)

```

```

0123
0124
0126
0136
0134
0138
0128
0130
0131
0132
0129

```

```

101 READ (5,102)(P19 (I), I=1,N)
102 READ (5,102)(P20 (I), I=1,N)
      READ (5,102)(P21 (I), I=1,N)
      READ (5,102)(PHD (I), I=1,N)
      READ (5,102)(TNOZ (I), I=1,N)
      READ (5,102)(TTPL (I), I=1,N)
      READ (5,102)(TTC (I), I=1,N)
      READ (5,102)(THD (I), I=1,N)
      READ (5,102)(AXIL (I), I=1,N)
      READ (5,102)(TORQR (I), I=1,N)
      READ (5,102)(DYNAR (I), I=1,N)
      READ (5,102)(RPM (I), I=1,N)
      READ (5,102)(CLAXIL (I), I=1,N)
      READ (5,102)(CLTRQR (I), I=1,N)
      FORMAT(2I3,4X,3A3)
      RETURN
      END

```

```

101
102

```

```

SUBROUTINE SETCON(DIN,D2N,BETAN,RG,GAM,GC,CP,CJ,C,EX1,EX2,EX3,PI,
1 ZNS,TETS,RTIPI,RHUB1,RTIP2,RHUB2,AAXS,AAXR,ATHS,RM1,
2 RADCLR,B1,B2,B3,B4,B5,D1,D2,D3,D4,D5,D6,CL1,CL2,CL3)

```

```

DIN=7.975
D2N=4.25C
BETAN=D2N/DIN
RG=53.3448
GAM=1.4
GC=32.174
CJ=778.16
EX1=GAM/(GAM-1.)
EX2=(GAM-1.)/GAM
EX3=2./GAM
CP=EX1*RG/CJ
PI=3.1416
ZNS=31.205
DTHS=0.594
TETS=0.0244
DTHR=0.1314
SR=0.4495
TETR=0.020
RTIPI=4.585
RHUB1=3.895
RTIP2=4.763
RHUB2=3.826

```

C

```

0139
0140

```

```

0142
0143
0144
0145
0146
0147

```

```

0178
0179

```

```

0212
0213
0215
0218
0219
0220

```

```

0221
0224
0225
0226
0227
0238
0239
0228
0229
0240
0241

```

0231
0243
0232
0230
0242

```

AAXS=PI*((RTIP1)**2-(RHUB1)**2)
AAXR=PI*((RTIP2)**2-(RHUB2)**2)
ATHS=DTHS*(RTIP1-RHUB1)*ZNS
RM1=(RTIP1+RHUB1)/2.
RM2=(RTIP2+RHUB2)/2.
SKT=1.-(2.7/1000.)*((TETS/SS*100.)**3.3)*DTHS/SS
RKT=(1.-(2.7/1000.))*((TETR/SR*100.)**3.3)*DTHR/SR)*((AAXR+PI*
1 RADCLR*(RTIP2+RADCLR/2.))/AAXR)
SKT=0.95
ATHS=ATHS/1.06
WRITE(6,200) BETAN,AAXS,AAXR,ATHS,RM1,RM2
WRITE(6,201) SKT,RKT
FORMAT(//,10F12.7)
B1=9.5208828E-01
B2=4.4891640E-07
B3=-7.5810743E-13
B4=5.5023778E-19
B5=-1.4571314E-25
D1=-1.004586E-01
D2=2.122579E-01
D3=-1.081851E-01
D4=2.767576E-02
D5=-3.489933E-03
D6=1.726733E-04
CL1=-2.7923457E-03
CL2=5.1056171E-04
CL3=9.1106005E-08
RETURN
END

```

0212A
0212B

200
201

```

SUBROUTINE CNVERT(PBAR,TBAR,TCR,PAMB,HM68,DH,PREF1,PNOZ,PTPL,PTO,
1 PREF2,PHUB,PTIP,P13,P14,P15,P16,P17,P18,P19,P20,P21,PHD,PCLI,
2 PCL2,PCL3,TNOZ,TNOZR,TTPL,TTPLR,TTOR,THD,AXIL,FAX,TORQR,TORQ,
3 DYNAR,DYNA,CLAXIL,CLFAX,CLTRQR,CLTORQ,CLI,CL2,CL3)
TEMP(X)=32.+35.98*X-.435*X**2
GHGBR=13.63905-C.00136303*TBAR
GHGCR=13.63905-C.00136303*TCR
CHGBR=0.4891585*GHGBR/13.54
CHGCR=0.4891585*GHGCR/13.54
GW68=0.9983763+68.*0.106058E-03-(68.**2)*0.159319E-05
GWCR=C.9983763+TCR*0.106058E-03-(TCR**2)*0.159319E-05
PAMB=PBAR*CHGBR
HM68=CH*GWCR/GW68
DH=DH*GWCR*62.42732/1728.
PNOZ=CHGCR*(PREF1-PNOZ)+PAMB

```

C


```

PTPL=CHGCR*(PREF1-PTPL)+PAMB
PTO=CHGCR*(PREF1-PTO)+PAMB
PHUB=CHGCR*(PREF2-PHUB)+PAMB
PTIP=CHGCR*(PREF2-PTIP)+PAMB
P13=CHGCR*(PREF2-P13)+PAMB
P14=CHGCR*(PREF2-P14)+PAMB
P15=CHGCR*(PREF2-P15)+PAMB
P16=CHGCR*(PREF2-P16)+PAMB
P17=CHGCR*(PREF2-P17)+PAMB
P18=CHGCR*(PREF2-P18)+PAMB
P19=CHGCR*(PREF2-P19)+PAMB
P20=CHGCR*(PREF2-P20)+PAMB
P21=CHGCR*(PREF2-P21)+PAMB
PHC=CHGCR*(PREF2-PHD)+PAMB
TNOZ=TEMP(TNOZ)
TNCZR=TNOZ+459.69
TTPL=TEMP(TTPL)
TTPLR=TTPL+459.69
TTC=TEMP(TTC)
TTTO=TTTO+459.69
THD=TEMP(THD)
FAX=0.08*AXIL
TCRQ=TORQR/30.
DYNA=DYNAR/30.
CLFAX=0.01*CLAXIL
CLTORQ=(CL1+CL2*CLTRQR+CL3*CLTRQR**2)/12.
PHUB=PHUB/1.05
TORQ=TORQ/1.05
WRITE(6,300) PAMB,HW68,DH,PNOZ,PTPL,PTO,PHUB,PTIP
WRITE(6,301) P13,P14,P15,P16,P17,P18,P19,P20,P21,PHD
WRITE(6,301) TNOZ,TNOZR,TTPL,TTPLR,TTTO,TTOR,THD
WRITE(6,301) FAX,TORQ,DYNA,CLFAX,CLTORQ
FORMAT(1H1,10F10.3)
FORMAT(///,10F10.3)
RETURN
END
300
301

```

```

SUBROUTINE FLORAT(D2N,RG,GC,EX1,EX2,EX3,HW63,DH,PNOZ,PTPL,PHD,PR,
1 TNOZ,TNOZR,TTPL,TTPLR,THD,B1,B2,B3,B4,B5,B1,D2,D3,D4,D5,D6,NRUN,
2 I,RE,FLOWN,FLOWL,FLOWT,BETAN)

```

C

```

ALPHAN=1.+2.52*(TNOZ-68.)*0.1E-04
R=1.-(DH/PNOZ)
Y1=R**EX3
Y2=EX1
Y3=1.-R**EX2
Y4=1.-R

```

```

Y5=1.-BETAN**4
Y6=1.-R**EX3*BETAN**4
ARG=Y1*Y2*(Y3/Y4)*(Y5/Y6)
YN=SQRT(ARG)
ZN=1.9+2.4*(TNOZ-100.)*0.1E-02
WRITE(6,402) ALPHAN,R,YN,ZN
CN=1.0400
WN=0.1638427*D2N**2*ALPHAN*YN*CN*SQRT(PNOZ**HW68/TNOZR)
RE=2.27376*WN/(D2N*ZN)*0.1E+07
CN=B1+RE*(B2+RE*(B3+RE*(B4+B5*RE)))
WNC=0.1638427*D2N**2*ALPHAN*YN*CN*SQRT(PNOZ**HW68/TNOZR)
IF(ABS(WNC-WN).LE.0.0001) GO TO 401
WN=WNC
GO TO 400
400 FLOWN=WNC
401 RE=2.27376*FLOWN/(D2N*ZN)*0.1E+07
PR=PTPL/PHD
WREF=D1+PR*(D2+PR*(D3+PR*(D4+PR*(D5+D6*PR))))
CORR=(1.+C.32*((TTPL-THD)/TTPL))*1.2
FLOWL=WREF*PTPL/SQRT(TTPLR*RG/GC)/CORR
FLOWT=FLOWN-FLOWL
WRITE(6,403) FLOWN, FLOWL, FLOWT, CN, RE
FORMAT(///,10F10.7)
402 FORMAT(///,4F10.4,F20.2)
403 GO TO 406
404 WRITE(6,405) NRUN,I
405 FORMAT(/33X,I4,7X,36HFLOW RATE TOO HIGH, CHECK INPUT DATA/)
406 RETURN
END

SUBROUTINE STATOR(RG,GAM,GC,C,PI,EX1,EX2,EX3,EPS,RTIPI,RHUB1,RMI,
1 PHUB,PTIP,PIAV,PTO,P13,P18,P19,P20,P21,PHD,PRS,FLOWT,AAXS,AFHS,
2 SKT,J,ITCR,TIRM,MV1M,MVA1M,MV1C,MV1,MV2,MW1,MV2,MW2
3 VCOEFS,ALPHM,MVA1M,MVA1,MV1,MV1C,MV1,MV2,MW1,MV2,MW2
4 CLFAX,FO,F1,F2,F3,F4,F5,F6A,FNET,RFAX,RTORQ,RVAI,RVUI)
REAL*4 MVA1M,MVA1,MV1M,MV1C,MV1,MV2,MW1,MV2,MW2
IF(J.GE.2) GO TO 500
PIAV=(PHUB+PTIP)/2.
THIS SECTION, M SUBSCRIPT REPRESENTS VALUES COMPUTED BY CONTINUITY BELOW
C2=(C*PIAV*ATHS)/(RG*FLOWT)
V1M=SQRT(C*TTOR+(C2/2.))**2)-C2/2.
TIRM=TTOR-V1M**2/C
V1M=(FLOWT*RG*TIRM)/(PIAV*AAXS*SKT)
VR=V1M/V1M
IF(ABS(VR).GE.1.0) VR=1.0
AN=ARCOS(VR)

```

```

VUI=VIM*SIN(AN)
ALPHIM=AN*180./PI
MVIM=VIM/SQRT(GAM*GC*RG*TIRM)
MVAIM=VAIM/SQRT(GAM*GC*RG*TIRM)
CALL FORCE(PI,RTIPI,RHUB1,AAXS,PHUB,PIAV,PTIP,P13,P18,P19,
1 P20,P21,PHD,FAX,CLFAX,FO,F1,F2,F3,F4,F5,F6A,FNET)
GO TO 506
500 WRITE(6,501)
501 FORMAT(//,9X,3HEPS8X,4HPIAV9X,3HTIM10X,3HTIC9X,4HVA1M9X,4HVA1C9X,
14HMV1M9X,4HMVIC7X,8HALPHA 1M5X,8HALPHA 1C/)
EPS=C.0
502 P1AV=PHUB/3.*(((1.+EPS)*(RTIPI)**2+(RHUB1)*(RTIPI)-(2.+EPS)*
1 (RHUB1)**2)/(RTIPI)**2-(RHUB1)**2))+PTIP/3.*(((2.+EPS)*(RTIPI)
2 **2-(RHUB1)*(RTIPI)-(1.+EPS)*(RHUB1)**2)/(RTIPI)**2-(RHUB1)**2))
CALL MOMENT(RG,GAM,GC,C,RM1,AAXS,TORQ,CLTORQ,FLOWT,PI,RTIPI,
1 RHUB1,FAX,CLFAX,PHUB,PTIP,PIAV,P13,P18,P19,P20,P21,PHD,TIOR,TIRM,
2 VUI,VAIM,VIM,ALPHA,MVAIM,FO,F1,F2,F3,F4,F5,F6A,FNET)
C1=FLOWT*RG/(PIAV*AAXS*SKT)
VAIC=SQRT(C*TIOR-VUI**2+(C/(2.*C1))**2)-C/(2.*C1)
ALPHIC=ATAN(VUI/VAIC)
ALPHIC=ALPHIC*180./PI
VIC=SQRT(VAIC**2+VUI**2)
TIRC=TIOR-(VIC**2)/C
MVIC=VIC/SQRT(GAM*GC*RG*TIRC)
WRITE(6,503)EPS,PIAV,TIRM,TIRC,VAIM,VAIC,MVIM,MVIC,ALPHIM,ALPHIC
503 FCRMAT(10F13.5)
DIFF=ABS(TIRM-TIRC)
IF(DIFF-0.01) 506,506,504
504 IF(TIRC.LT.TIRM) GO TO 505
EPS=EPS+DIFF/500.
GO TO 502
505 EPS=EPS-DIFF/500.
GO TO 502
506 PRS=PIAV/PTO
IF(PRS.GE.1.0) PRS=0.9990
T1ISR=TTOR*PRS**EX2
ZETAS=(TIRM-T1ISR)/(TTOR-T1ISR)
ETAS=1.0-ZETAS
V1IS=SQRT(C*(TTOR-T1ISR))
VCOEFS=VIM/V1IS
PHI=FLOWT/(PTO*ATHS)*SQRT(TTOR*RG/GC)
PRTHS=PRS
IF(PRTHS.LT.0.52828) PRTHS=0.52828
XI=(PHI/SQRT(2.*EX1*(PRTHS**EX3-PRTHS**((GAM+1.)/GAM))))
PRS=1./PRS
UI=PI*RPMM*RM1/360.
WUI=VUI-UI
WAI=VAIM

```

```

BETA1=ATAN(WU1/WA1)
W1=WAL/COS(BETA1)
BETA1=BETA1*180./PI
MW1=W1/SQRT(GAM*RG*GC*TIRM)
RFAX=FAF/(PTO/14.69)
RTORQ=TORQ/(PTO/14.69)
RVAL=VALM/SQRT(GAM*GC*RG*TTOR)
RVU1=VU1/SQRT(GAM*GC*RG*TTOR)
RETURN
END

```

```

SUBROUTINE MOMENT(RG,GAM,GC,C,RM1,AAXS,TORQ,CLTORQ,FLOWT,PI,RTIPI,
1 RHUB1,FAF,CLFAX,PHUB,PTIP,P1AV,P13,P18,P19,P20,P21,PHD,TTOR,TIRM,
2 VU1,VALM,V1M,ALPH1M,MV1M,MVA1M,F0,F1,F2,F3,F4,F5,F6A,FNET)

```

```

REAL*4 MVA1M,MVA1,MV1M,MV1C,MV1,MW1,MW2,MW2
VU1=(TORQ+CLTORQ)*12.*GC/(FLOWT*RM1)
A0=PI*5.125**2
A2=PI*(5.125**2-5.003**2)
A3=PI*(5.003**2-4.901**2)
A4=PI*(4.901**2-4.773**2)
A5=PI*(4.773**2-RTIPI**2)
A6A=PI*RHUB1**2
FC=A0*PHD
F1=AAXS*P1AV
F2=A2*P21
F3=A3*((P20+P19)/2.)
F4=A4*P18
F5=A5*((PTIP+P13)/2.)
F6A=A6A*PHUB
FNET=FAF+CLFAX+F0-F1-F2-F3-F4-F5-F6A
VALM=FNET*GC/FLOWT
ALPH1M=ATAN(VU1/VALM)
V1M=SQRT(VALM**2+VU1**2)
TIRM=TTOR-(V1M**2)/C
MV1M=V1M/SQRT(GAM*GC*RG*TTIRM)
MVA1M=VALM/SQRT(GAM*GC*RG*TTIRM)
RETURN
END

```

```

SUBROUTINE FORCE(PI,RTIPI,RHUB1,AAXS,PHUB,P1AV,PTIP,P13,P18,P19,
1 P20,P21,PHD,FAF,CLFAX,F0,F1,F2,F3,F4,F5,F6A,FNET)

```

```

A0=PI*5.125**2
A2=PI*(5.125**2-5.003**2)

```

```

A3=PI*(5.003**2-4.901**2)
A4=PI*(4.901**2-4.773**2)
A5=PI*(4.773**2-RTIP1**2)
A6A=PI*RHUB1**2
FC=A0*PHD
F1=AA*SS*P1AV
F2=A2*P21
F3=A3*((P20+P19)/2.)
F4=A4*P18
F5=A5*((PTIP+P13)/2.)
F6A=A6A*PHUB
FNET=FAX+CLFAX+FO-F1-F2-F3-F4-F5-F6A
RETURN
END

```

```

SUBROUTINE ROTOR(RG,GC,CJ,CP,C,PI,EX1,EX2,RM1,RM2,AA*XR,RKT,PTO,
1 P1AV,PHD,PT2,PRM,DYNA,FLOWT,TTOR,TT2R,DELTW,TTISR,TER,
2 VU1,U1,W1,BETA1,VU2,VA2,V2,ALPH2,U2,WU2,WA2,W2,W2IS,BETA2,DBETA,
3 WCDEF S,ZETAR,ETAR,MV2,MW2,GAM,RPM,SLF,SFF)

```

```

REAL*4 MVA1M,MVA1,MV1M,MVIC,MV1,MW1,MV2,MW2
VU2=RM1/RM2*VU1-(12.*DYNA*GC)/(RM2*FLOWT)
U2=U1*RM2/RM1
WU2=VU2-U2
DELTW=(DYNA*PI*RPM)/(30.*FLOWT*CJ*CP)
TTOR=TTOR-DELTW
TTISR=TTIRM*(PHD/P1AV)**EX2
TER=TTIRM*(W1**2-U1**2+U2**2)/C
C3=FLOWT*RG/(PHD*AA*XR*RKT)
VA2=SQRT(C*TT2R-VU2**2+(C/(2.*C3))**2)-C/(2.*C3)
V2=SQRT(VA2**2+VU2**2)
T2R=TT2R-(V2**2)/C
MV2=V2/SQRT(GAM*RG*GC*TT2R)
PT2=PHD*(TT2R/T2R)**EX1
PRM=PTO/PHD
WA2=VA2
MW2=SQRT(WA2**2+WU2**2)
ALPH2=W2/SQRT(GAM*RG*GC*TT2R)
ALPH2=ATAN(VU2/VA2)
BETA2=ALPH2*180./PI
BETA2=ATAN(WU2/WA2)
DBETA=BETA2*180./PI
ZETAR=(T2R-TTISR)/(TER-TTISR)
W2IS=SQRT(C*(TER-TTISR))
WCDEF S=W2/W2IS

```

C

```

IF(U2.LE.1.0) U2=0.001
SLF=(VU1-VU2)/U2
SFF=VA2/U2
RETURN
END

SUBROUTINE PERFRM(C,PI,EX2,PTO,PHUB,PTIP,PHD,PT2,DYNA,RPM,FLOWT,
1 TTOR,T2THR,T2ISR,DELHIS,DELHM,DELTIIS,DELTM,VOIS,V1IS,U1,V2,
2 ETATS,ETATT,REACMN,REACHB,REACTP,XKIS,REFLOW,REFRPM,REFMOM,HP,
3 REFHP,T2ISR,F,V1,W1,U2,W2,REACEF,CP)
DELTIIS=TTOR*(1.0-(PHD/PTO)**EX2)
T2THR=TTOR-DELTIIS
TT2ISR=TTOR*(PT2/PTO)**EX2
DELHIS=CP*(TTOR-T2THR)
DELHM=CP*(TTOR-T2R)
ETATS=DELTM/DELTIIS*100.
F=T2ISR/T2THR
ETATT=DELTM/(DELTIIS-(V2**2)/(C*F))*100.
VOIS=SQRT(C*DELTIIS)
REACEF=(W2**2-W1**2+U1**2-U2**2)/(V1**2+W2**2-W1**2+U1**2-U2**2)
REACMN=1.0-(V1IS/VOIS)**2
REACHB=((PHUB/PHD)**EX2-1.)/((PTO/PHD)**EX2-1.)
REACTP=((PTIP/PHD)**EX2-1.)/((PTO/PHD)**EX2-1.)
IF(U1.LE.1.0) U1=0.001
XKIS=(VCIS/U1)**2
DELTA=PTO/14.69
THETA=TTOR/518.69
REFLOW=FLOWT*SQRT(THETA)/DEL
REFRPM=RPM/SQRT(THETA)
REFMOM=DYNA/DEL
HP=(DYNA*PI*RPM)/(30.*550.)
REFHP=HP/(DEL*SQRT(THETA))
RETURN
END

SUBROUTINE OUTPTS(NRUN,N,FAX,CLFAX,F0,F1,F2,F3,F4,F5,F6A,FNET,J,
1 TORQ,CLTORQ,FLOWN,FLOWT,FLOWL,RE,PHI,XI,QNOZ,QTPL,PTO,PIAV,QHD,
2 PRPL,PRP,TTPQ,TT0,T1,T1IS,VA1,VU1,V1,V1IS,ALPHI,VCOFS,MV1,MVA1,
3 WAI,WU1,W1,U1,BETA1,MW1,ZETAS,ETAS,PAMB,DA,T,E,RFAX,RTORQ,RVAL,
4 RVU1)
REAL*4 MVA1M,MVA1,MV1M,MVIC,MV1,MV2,MW2
DIMENSION FAX(50),CLFAX(50),F0(50),F1(50),F2(50),F3(50),F4(50),
1 F5(50),F6A(50),FNET(50),TORQ(50),CLTORQ(50),FLOWN(50),FLOWT(50),
2 FLOWL(50),RE(50),PHI(50),XI(50),QNOZ(50),QTPL(50),PTO(50),
3 PIAV(50),QHD(50),PRPL(50),PRP(50),TTPQ(50),TT0(50),T1(50),

```

C

```

4 T1IS(50), VAL(50), VU1(50), V1(50), VLIS(50), ALPH1(50), VCOFS(50),
5 MVL(50), MVAL(50), WAI(50), WU1(50), W1(50), WI(50), UI(50), BETAI(50), MW1(50),
6 ZETAS(50), ETAS(50), RFAX(50), RTORQ(50), RVAL(50), RVU1(50)
WRITE(6,800) NRUN,DA,T,E,J
800 FORMAT(1H1,1X,STATOR RESULTS,///,1X,CONFIGURATION- CONVERGING
1 NOZZLES,SHROUD P/N 1050,INSERT P/N 2005-3(STRAIGHT),///,1X,RU
2 NUMBER,13,4X,DATE,3A3,///,44X,METHOD J=,12)
WRITE(6,801)
801 FORMAT(///,30X,FORCE AND MOMENT BALANCE(LBS AND FT-LBS),///,1X,
1 POINT,2X,FAX(+),1X,CLFAX(+),2X,FO(+),3X,FI(-),3X,F2(-),
2,3X,F3(-),3X,F4(-),3X,F5(-),2X,F6A(-),4X,FNET,2X,TORQ(+
3),1X,CLTORQ(+),2X,RFAX,5X,RTORQ,/)
DO 802 I=1,N
WRITE(6,803) I,FAX(I),CLFAX(I),FO(I),F1(I),F2(I),F3(I),F4(I),F5(I)
1,F6A(I),FNET(I),TORQ(I),CLTORQ(I),RFAX(I),RTORQ(I)
803 FORMAT(14,2X,9F8.2,2F9.2)
WRITE(6,804)
804 FORMAT(///,30X,FLOW RATES(LBM/SEC),RE(NOZ),FLOW FNC,AND STATO
1R BLOCKAGE FACTOR,///,1X,POINT,2X,NOZZLE FLOW,2X,TURBINE FLOW
2,3X,LABLEAK,8X,RE,9X,PHI,7X,XI,/)
DO 805 I=1,N
WRITE(6,806) I,FLOWN(I),FLOWT(I),FLOWL(I),RE(I),PHI(I),XI(I)
806 FORMAT(14,2X,F10.4,3X,F10.4,3X,F10.4,3X,F10.4,2F10.4)
WRITE(6,807) PAMB
807 FORMAT(///,30X,PRESSURES(PSIA) AND PRESSURE RATIOS,///,1X,PAMB=
1,F5.2,///,1X,POINT,2X,PNOZ,3X,PTPL,3X,PTO,3X,PIAV,4X,
2,PHD,3X,PLENUM PR(PTPL/PHD),2X,STATOR PR(PTO/PIAV),/)
DO 808 I=1,N
WRITE(6,809) I,QNOZ(I),QTPL(I),PTO(I),PIAV(I),QHD(I),PRPL(I),PRS(I)
809 FORMAT(14,1X,5F7.2,6X,F7.4,14X,F7.4)
WRITE(6,810)
810 FORMAT(///,30X,TEMPERATURES(DEG R),///,1X,POINT,3X,TTPL,4X,
1,TT0,5X,T1,5X,T1IS,/)
DO 811 I=1,N
WRITE(6,812) I,TTPQ(I),TTO(I),T1(I),T1IS(I)
812 FORMAT(14,1X,4F8.2)
WRITE(6,813)
813 FORMAT(1H1,30X,ABSOLUTE VELOCITIES(FT/SEC),ANGLES(DEG),VEL COEF
1,AND MACH NOS,///,1X,POINT,3X,VAL,6X,VU1,7X,V1,6X,VLIS,
2,3X,ALPHA,1,2X,VCOEFS,4X,MV1,4X,MVAL,4X,RVAL,4X,RVU1,/)
DC 814 I=1,N
WRITE(6,815) I,VAL(I),VU1(I),V1(I),VLIS(I),ALPH1(I),VCOFS(I),
815 MVL(I),MVAL(I),RVAL(I),RVU1(I)
FORMAT(14,1X,5F9.2,5F8.4)
WRITE(6,816)
816 FORMAT(///,30X,RELATIVE VELOCITIES(FT/SEC),ANGLES(DEG),AND MAC
1H NOS,///,1X,POINT,3X,WAI,6X,WU1,7X,W1,7X,UI,5X,BETA 1,
2,4X,MW1,/)

```

```

DO 817 I=1,N
817 WRITE(6,818) I, W1(I), W1(I), U1(I), BETA(I), MW1(I)
818 FORMAT(14,1X,5F9.2,F8.4)
WRITE(6,819)
819 FORMAT(///,30X,'EFFICIENCIES',//,1X,'POINT',2X,'ZETA STATOR',2X,
1 'ETA STATOR(1.-ZETAS)',/)
DO 820 I=1,N
820 WRITE(6,821) I,ZETAS(I),ETAS(I)
821 FORMAT(14,3X,F10.4,7X,F10.4)
RETURN
END

SUBROUTINE OUTPTR(NRUN,N,AXCLR,RADCLR,PAMB,PTO,PIAV,PT2,QHD,PR,
1 T1,TE,TT2,T2,T2IS,DELTTIS,DELTTIS,DELTTIS,VAR2,VU2,V2,VOIS,
2 ALPHA2,WA2,W2,U2,W2IS,BETA2,DBETA,WCOFS,ZETAS,ETAR,RPM,HP,
3 DELHIS,DELHW,REFRPM,XKIS,ETATS,ETATT,REFLOW,REFMOM,REFHP,J,
4 REACHB,REACMN,REACTP,DA,T,E,F,REACEF,MV2,MW2,SLF,SFF)
REAL*4 MVA1M,MVA1,MV1C,MV1,MW1,MW2,MW2
DIMENSION PTO(50),T2(50),PT2(50),QHD(50),PR(50),T1(50),
1 TE(50),TT2(50),T2(50),T2IS(50),T2TH(50),T2IS(50),DELTTIS(50),
2 DELTW(50),VA2(50),VU2(50),V2(50),VOIS(50),ALPHA2(50),WA2(50),
3 WU2(50),W2(50),U2(50),W2IS(50),BETA2(50),DBETA(50),WCOFS(50),
4 ZETAS(50),ETAS(50),RPM(50),HP(50),DELHIS(50),DELHW(50),REFRPM(50)
5, XKIS(50),ETATS(50),ETATT(50),REFLOW(50),REFMOM(50),REFHP(50),
6 REACHB(50),REACMN(50),REACTP(50),F(50),REACEF(50),MV2(50),MW2(50)
7,SLF(50),SFF(50)
WRITE(6,900) AXCLR,RADCLR,NRUN,DA,T,E,J
900 FORMAT(1H1,1X,'ROTOR RESULTS',//,1X,'CONFIGURATION- CIRCULAR ARC
1, 'SHARP IN',//,1X,'RUN NUMBER',I3,4X,'DATE',//,44X,'METHOD J
2, 'F6.3)
3=1,I2)
WRITE(6,901) PAMB
901 FORMAT(///,30X,'PRESSURES(Psia) AND PRESSURE RATIOS',//,1X,'PAMB=
1, 'F5.2',//,1X,'POINT',3X,'PT0',4X,'PIAV',3X,'PT2',3X,'P2=PHD',3X,
2, 'OVERALL PR(PTO/P2)',/)
DO 902 I=1,N
902 WRITE(6,903) I,PTO(I),PIAV(I),PT2(I),QHD(I),PR(I)
903 FORMAT(14,2X,4F7.2,6X,F7.4)
WRITE(6,904)
904 FORMAT(///,30X,'TEMPERATURES(DEG R)',//,1X,'POINT',4X,'T10',5X,
1 'T1',6X,'TE',6X,'TT2',5X,'T2',5X,'T2IS',4X,'T2TH',3X,'TT2IS',3X,
2 'DELTA TIS',2X,'DELTA TW',/)
DO 905 I=1,N
905 WRITE(6,906) I, T1(I),TE(I),TT2(I),T2(I),T2IS(I),T2TH(I),TT2
1 IS(I),DELTTIS(I),DELTW(I)
906 FORMAT(14,2X,8F8.2,2F10.2)
WRITE(6,907)

```



```

907 FORMAT(1H1,30X,'ABSOLUTE VELOCITIES(FT/SEC) AND ANGLES(DEG)',/,/,
1 1X,'POINT',3X,'VA2',6X,'VU2',7X,'V2',6X,'VOIS',3X,'ALPHA 2',3X,'M
2V2',4X,'STAGE LOADING FACTOR',2X,'STAGE FLCW FACTOR',/)
DO 908 I=1,N
908 WRITE(6,909) I,VA2(I),VU2(I),V2(I),VOIS(I),ALPH2(I),MV2(I),SLF(I),
1 SFF(I)
909 FORMAT(I4,1X,5F9.2,F8.4,F14.2,F21.2)
910 FORMAT(/,/,30X,'RELATIVE VELOCITIES(FT/SEC), ANGLES(DEG), AND REL
1 VEL COEFS',/,1X,'POINT',3X,'WA2',6X,'WU2',7X,'W2',7X,'U2',6X,
2 'W2IS',4X,'BETA 2',4X,'DBETA',2X,'WCOEFS',3X,'MW2',/)
DO 911 I=1,N
911 WRITE(6,912) I,WA2(I),WU2(I),U2(I),W2IS(I),BETA2(I),DBETA(I)
1,WCOFS(I),MW2(I)
912 FORMAT(I4,1X,7F9.2,2F8.4)
913 WRITE(6,913)
913 FORMAT(/,/,30X,'EFFICIENCIES, RPM, WORK OUTPUT(HP), AND ENTHALPY
1 DROP(BTU/LBM)',/,1X,'POINT',2X,'ZETA ROTOR',2X,'ETA ROTOR(1.-ZETA
2R)',2X,'RPM',6X,'HP',3X,'DELTA HIS',2X,'DELTA HW',2X,'REHEAT FACTO
3R',2X,'EFF DEGREE OF REACTION',/)
DO 914 I=1,N
914 WRITE(6,915) I,ZETAR(I),ETAR(I),RPM(I),HP(I),DELHIS(I),DELHW(I),F(
1),REACEF(I)
915 FORMAT(I4,4X,F8.4,8X,F8.4,6X,F8.0,F8.2,F8.2,F11.2,F13.4,F19.4)
916 FORMAT(1H1,1X,GENERAL RESULTS,/,1X,'RUN NUMBER',I3,4X,'DATE',
13A3,/,/,1X,'POINT',2X,'PRESSURE',2X,'REFERRED',2X,'ISENTROPIC',2X
2,'EFFICIENCY',2X,'EFFICIENCY',2X,'REFERRED',3X,'REFERRED',2X,'REFE
3RRED',2X,'DEGREE OF',2X,'DEGREE OF',/,10X,'RATIO',5
4X,'SPEED',3X,'HEAD COEFF',2X,'TOT-STATIC',4X,'TOT-TOT',3X,'FLOW RA
5TE',3X,'MOMENT',5X,'POWER',4X,'REACTION',3X,'REACTION',3X,'FT-LB',
6N,/,21X,'RPM',18X,'PERCENT',5X,'PERCENT',4X,'LBM/SEC',4X,'FT-LB',
77X,'HP',7X,'(HUB)')
DO 917 I=1,N
917 WRITE(6,918) I,PR(I),REFRPM(I),XKIS(I),ETATS(I),ETATT(I),REFLOW(I
1),REFMOM(I),REFHP(I),REACHB(I),REACMN(I),REACTP(I)
918 FORMAT(I4,F11.4,F10.0,F11.4,2F12.2,F11.4,F11.4,F11.3,F10.3,3F11.4)
RETURN
END

```

REFERENCES

1. Ainley, D. G. and Mathieson, G. C. R., An Examination of the Flow and Pressure Losses in Blade Rows of Axial-Flow Turbines, Aeronautical Research Council, R & M No. 2891, 1955
2. Ainley, D. G. and Mathieson, G. C. R., A Method of Performance Estimation for Axial-Flow Turbines, Aeronautical Research Council, R & M No. 2974, 1957
3. Brown, R. L., "An Investigation of the Secondary Flow Phenomena in a Cascade of High Deflection Axial-Flow Impulse Turbine Blades," Naval Postgraduate School Thesis, December 1966
4. Commons, P. M., "Instrumentation of the Transonic Turbine Test Rig to Determine the Performance of Turbine Inlet Guide Vanes through the Application of the Momentum and Moment of Momentum Equations," Naval Postgraduate School Thesis, September 1967
5. Harrison, R. G., "An Analysis of Single Stage Axial Flow Turbine Performance Using Three Dimensional Calculating Methods," Naval Postgraduate School Thesis, September 1967
6. Lenzini, M. J., "Calibration of Turbine Test Rig With Impulse Turbine at High Pressure Ratios," Naval Postgraduate School, June 1968
7. Messegee, J. A., "Influence of Axial and Radial Clearance on the Performance of a Turbine Stage With Blunt-Edge Non-Twisted Blades," Naval Postgraduate School Thesis, September 1967
8. Vavra, M. H., Aerothermodynamics and Flow in Turbomachines, New York, London: John Wiley and Sons, Inc., 1960
9. Vavra, M.H., Problems of Fluid Mechanics in Axial Turbomachines, Pts A, B, C, D and E, Von Karman Institute Course Note 556, Rhode-Saint-Genese, Belgium: Von Karman Institute for Fluid Dynamics, March 1969

INITIAL DISTRIBUTION LIST

	No. Copies
1. Defense Documentation Center Cameron Station Alexandria, Virginia 22314	20
2. Library, Code 0212 Naval Postgraduate School Monterey, California 93940	2
3. Commander, Naval Air Systems Command Attn: AIR 03C, 330B, 330 Navy Department Washington, D.C. 20360	1
4. Professor M.H. Vavra Department of Aeronautics Naval Postgraduate School Monterey, California 93940	1
5. Chairman, Department of Aeronautics Naval Postgraduate School Monterey, California 93940	1
6. Office of Naval Research (Power Branch) Attn: Mr. J.K. Patton, Jr. Navy Department Washington, D.C. 20360	1
7. Captain, Stewart G. Esdaile 38 Charkay Street Ottawa 5, Ontario Canada	5

DOCUMENT CONTROL DATA - R & D

(Security classification of title, body of abstract and indexing annotation must be entered when the overall report is classified)

1. ORIGINATING ACTIVITY (Corporate author) Naval Postgraduate School Monterey, California 93940		2a. REPORT SECURITY CLASSIFICATION Unclassified	
		2b. GROUP	
3. REPORT TITLE An Investigation of a Transonic Turbine Test Rig			
4. DESCRIPTIVE NOTES (Type of report and, inclusive dates) Master's Thesis; (October 1969)			
5. AUTHOR(S) (First name, middle initial, last name) Stewart G. Esdaile			
6. REPORT DATE October 1969		7a. TOTAL NO. OF PAGES 125	7b. NO. OF REFS 9
8a. CONTRACT OR GRANT NO.		9a. ORIGINATOR'S REPORT NUMBER(S)	
b. PROJECT NO.			
c.		9b. OTHER REPORT NO(S) (Any other numbers that may be assigned this report)	
d.			
10. DISTRIBUTION STATEMENT This document has been approved for public release and sale; its distribution is unlimited.			
11. SUPPLEMENTARY NOTES		12. SPONSORING MILITARY ACTIVITY Naval Postgraduate School Monterey, California 93940	
13. ABSTRACT The Transonic Turbine Test Rig installed in the Turbo-Propulsion Laboratory at the Naval Postgraduate School was designed such that losses in nozzle and rotor blading and overall performance characteristics can be determined for operation at several combinations of blade configurations, pressure ratios and speeds. This study relates the empirical data for stator loss coefficients to those determined for the converging-nozzle stator presently installed, and discusses reasons for some of the discrepancies. Also discussed are results of the flow nozzle calibration, locked rotor data, and temperature and inlet swirl effects. A method is proposed to reduce these effects for future work on the Turbine Test Rig.			

14. KEY WORDS	LINK A		LINK B		LINK C	
	ROLE	WT	ROLE	WT	ROLE	WT
Transonic Turbine Loss Coefficients						



thesE67

An investigation of a transonic turbine



3 2768 002 06228 3

DUDLEY KNOX LIBRARY